NACA TN 3918

NATIONAL ADVISORY COMMITTEE FOR AERONAUTICS

TECHNICAL NOTE 3918

WIND-TUNNEL INVESTIGATION OF EFFECT OF PROPELLER SLIPSTREAMS ON AERODYNAMIC CHARACTERISTICS OF A WING EQUIPPED WITH A 50-PERCENT-CHORD SLIDING FLAP AND A 30-PERCENT-CHORD SLOTTED FLAP

By Richard E. Kuhn and William C. Hayes, Jr.

Langley Aeronautical Laboratory
Langley Field, Va.

NACA

Washington
February 1957

1F

NATIONAL ADVISORY COMMITTEE FOR AERONAUTICS

TECHNICAL NOTE 3918

WIND-TUNNEL INVESTIGATION OF EFFECT OF PROPELLER SLIPSTREAMS ON AERODYNAMIC CHARACTERISTICS OF A WING EQUIPPED WITH A 50-PERCENT-CHORD SLIDING FLAP AND A 30-PERCENT-CHORD SLOTTED FLAP

By Richard E. Kuhn and William C. Hayes, Jr.

SUMMARY

An investigation of the aerodynamic characteristics of a wing equipped with a 50-percent-chord sliding flap and a 30-percent-chord slotted flap operating in the slipstreams of two large-diameter propellers has been conducted in the Langley 300 MPH 7- by 10-foot tunnel.

Large tunnel-wall effects for which there are no known correction methods were encountered in the tests. However, because of the current interest in and general scarcity of data applicable to aircraft designed for vertical take-off and landing (VTOL) and for short take-off and landing (STOL), the results (uncorrected) are presented herein with only limited discussion. It was observed, however, that stalling would occur in conditions approaching steady level flight at high-power conditions, but that a leading-edge slat effectively delayed this stall.

INTRODUCTION

An investigation of the aerodynamic characteristics of wing-propeller combinations that may be applicable to aircraft designed for vertical take-off and landing (VTOL) and short take-off and landing (STOL) is being conducted in the Langley 300 MPH 7- by 10-foot tunnel. The aerodynamic characteristics at low forward speed of a wing-propeller combination without flaps (tilting-wing configuration) at angles of attack up to 90° is reported in reference 1. References 2 and 3 report the characteristics of this same model equipped with plain and slotted flaps, respectively.

In the present investigation the aerodynamic characteristics of a semispan-wing model equipped with a 50-percent-chord sliding flap, a 30-percent-chord slotted flap, a 30-percent-chord leading-edge slat, and two large-diameter propellers have been investigated. The characteristics of this model at zero forward speed are reported in reference 4.

SYMBOLS

When a wing is located in the slipstream of a propeller, large forces and moments can be produced even though the free-stream velocity decreases to zero. For this condition, coefficients based on the free-stream dynamic pressure approach infinity and become meaningless. It appears appropriate, therefore, to base the coefficients on the dynamic pressure in the slipstream. The coefficients based on this dynamic pressure are indicated in the present paper by the use of a double prime. The relations between the thrust and the dynamic pressure and velocity in the slipstream have been derived in reference 1. The positive sense of forces, moments, and angles is indicated in figure 1. The pitching moments are presented with reference to the center of gravity shown in figure 2.

B	number of propeller blades
b	twice span of semispan wing, ft
$b_{.75R}$	propeller blade width at 75-percent-radius station, ft
C_L	lift coefficient, $\frac{\text{Lift}}{qS/2}$
C_L''	lift coefficient, $\frac{\text{Lift}}{q''S/2}$
C_m	pitching-moment coefficient, $\frac{M_Y}{q\bar{c}S/2}$
C_m''	pitching-moment coefficient, $\frac{M_Y}{q''\bar{c}S/2}$
$C_{m,p}''$	pitching-moment coefficient of propeller, $\frac{M_{Y,p}}{q''\bar{c}S/2}$
$C_{N,p}''$	normal-force coefficient of propeller, $\frac{N_p}{q''S/2}$

C_p power coefficient, $\frac{2\pi nQ}{\rho n^3 D^5}$

C_T thrust coefficient, $\frac{T}{\rho n^2 D^4}$

C_X longitudinal-force coefficient, $\frac{F_X}{qS/2}$

C_X'' longitudinal-force coefficient, $\frac{F_X}{q''S/2}$

T_c'' thrust coefficient, $\frac{T}{q''\frac{\pi}{4}D^2}$

$T_{c,nom}''$ nominal value of thrust coefficient (taken as the average value at low angles of attack)

c wing chord, ft

$\bar{c}$ mean aerodynamic chord, $\frac{2}{S}\int_0^{b/2} c^2 dy$, ft

c_s slat chord, ft

D propeller diameter, ft

L lift, lb

M_Y pitching moment, ft-lb

$M_{Y,p}$ propeller pitching moment, ft-lb

N_p propeller normal force, lb

n propeller rotational speed, rps

Q torque, ft-lb

q free-stream dynamic pressure, $\frac{1}{2}\rho V^2$, lb/sq ft

q''	slipstream dynamic pressure, $q + \frac{T}{\frac{\pi}{4}D^2}$, lb/sq ft
S	twice area of semispan wing, sq ft
T	thrust per propeller, lb
V	free-stream velocity, ft/sec
F_X	longitudinal force, lb
α	angle of attack, deg
$\beta_{.75R}$	propeller blade angle at 75-percent-radius station, deg
δ	surface deflection, deg
ρ	mass density of air, slugs/cu ft
σ	propeller solidity, $\frac{Bb_{.75R}}{0.75D\pi}$

Subscripts:

50	50-percent-chord sliding flap
30	30-percent-chord slotted flap
i	inboard propeller
o	outboard propeller
s	slat
h	horizontal tail
f	flap

MODEL AND APPARATUS

A semispan-wing model of a hypothetical four-propeller airplane was used in the present investigation. A drawing of the model with pertinent dimensions is presented as figure 2, and a photograph of the model mounted for testing is shown in figure 3. The principal geometric characteristics of the model are given in the following table:

Wing:	
Area (semispan), sq ft	5.50
Semispan, ft	3.67
Mean aerodynamic chord, ft	1.51
Aspect ratio	4.89
Taper ratio	0.80
Airfoil section	NACA 4415
Horizontal tail:	
Area (semispan), sq ft	1.65
Semispan, ft	2.0
Mean aerodynamic chord, ft	0.83
Aspect ratio	4.85
Taper ratio	0.66
Airfoil section	NACA 0012
Tail length (from $\bar{c}/4$ of wing to $\bar{c}/4$ of tail), ft	3.76
Propellers:	
Diameter, ft	2.0
Airfoil section	Clark Y
Solidity (per propeller), σ	0.07
Number of blades	3

The ordinates of the slotted flap were derived from the slotted flap 2-h of reference 5 and are presented in table I along with a sketch of the profile of the sliding flap. The cross section of the leading-edge slat is also shown in table I. For these tests the upper surface of the wing was not modified as it would have to be in a practical application in order to retract the slat; however, it is believed that this difference would have only a small effect on the results. The end plate, which was installed for all these tests, was made of 1/16-inch aluminum and is shown in figure 4. It was located 10.3 inches outboard of the center line of the outboard propeller.

The propellers were driven by variable-frequency electric motors from a common power supply. The speed of each propeller was determined by observing stroboscopic-type indicators to which were fed the output frequencies of small alternators connected to each motor shaft. Because the propeller blade angles were adjusted to give the same thrust from both propellers at zero angle of attack, their rotational speeds were usually matched within 10 rpm. The outboard propeller rotated against the tip vortex (right-hand rotation on right wing as tested) and the inboard propeller rotated in the opposite direction.

The motors were mounted inside nacelles through strain-gage beams (as shown in ref. 1) so that the thrust and torque of each propeller could be measured. The inboard nacelle was equipped with additional

instrumentation so that the propeller normal force and pitching moment could also be measured. The total model lift, longitudinal force, and pitching moment were measured on a balance at the root of the wing.

TESTS

The investigation was conducted in the Langley 300 MPH 7- by 10-foot tunnel. The tests were made at various free-stream dynamic pressures and propeller thrusts so selected as to maintain a dynamic pressure of about 4.8 pounds per square foot in the slipstream. The tests with the propellers off were also run at a dynamic pressure of 4.8. The desired thrust was obtained on both propellers at zero angle of attack by appropriate adjustment in the propeller blade angles and the thrust of the inboard propeller was held constant throughout the angle-of-attack range. Because of different inflow conditions, the thrust of the outboard propeller varied slightly from the desired value at angles of attack other than zero.

The Reynolds number in the slipstream, based on the mean aerodynamic chord of 1.505 feet, was 0.62×10^6.

In order to minimize the time required for the tests, the operating conditions were chosen so that only two propeller blade-angle settings were required. A blade angle of about 7° was used for tests at the higher thrust coefficients, and a blade angle of about 20° was used for the lower thrust coefficients.

TUNNEL-WALL EFFECTS AND CORRECTIONS

Large effects of the tunnel walls on the data were encountered during the tests. These effects are shown in figure 5 where the data obtained at zero forward speed in the tunnel are compared with the results obtained from tests in a large room (ref. 4). The tests in the tunnel were made with a curtain suspended in the diffuser of the tunnel so as to prevent the propellers of the model from setting up a recirculation of air in the tunnel. In addition, the doors into the tunnel (immediately downstream of the test section) were open to prevent a circulation from being set up within the test section.

The effects of the tunnel-wall restrictions have been determined only for the case of zero forward speed ($T_c'' = 1.0$) and for the flap deflections shown in figure 5, but they are probably also present to an unknown extent at other thrust coefficients and at lower flap deflections (particularly at high angles of attack). Procedures for correcting for these effects are not known.

The power-off data and the data for low angles of attack and low flap deflections (power-on) are probably not appreciably influenced by these effects. Normal potential-flow corrections for the effect of the constraint of the tunnel walls and the blockage of the model have been applied by the methods of references 1, 6, and 7. In determining these corrections only the aerodynamic forces were used. (Direct propeller thrust was subtracted from the data.)

PRESENTATION OF RESULTS

The results of the investigation are presented in the following figures:

	Figures
Tunnel-wall effects at $T_c'' = 1.0$	5
Data with propellers and nacelles off:	
Effect of flap deflection (slat off)	6 to 8
Effect of slat	9
Effect of slipstream:	
Flaps neutral	10
Flaps deflected	11 and 12
Effect of slat	12 and 13
Effect of stabilizer	14 to 16
Propeller characteristics	17 and 18

DISCUSSION

Because of the current interest in flight at very low speeds and the general scarcity of data of the type obtained in this investigation, the test results are presented herein, although it is known that the data include large tunnel-wall effects. No detailed discussion is presented; however, two results of the investigation should be noted.

Although the wing is almost completely immersed in the slipstreams, the data indicate that, with the slat off, stalling would be encountered in steady level flight or in conditions approaching steady level flight. This result is indicated for the wing with the flaps neutral in figure 10(e). On this plot $C_X'' = 0$ indicates steady level flight, negative values of C_X'' indicate decelerating or gliding flight, and positive values of C_X'' indicate accelerating or climbing flight. For the

three highest thrust-coefficient conditions tested, maximum lift was encountered at positive values of C_X''. At $C_X'' = 0$ (steady level flight), the drop in lift indicates that the wing is stalled.

With the rear flap deflected (fig. 11(e)) the stall is delayed somewhat but is more severe. With both flaps deflected (fig. 12(e)) the data indicate that level flight could be achieved without the wing stalling; however, in order to make a landing approach, C_X'' must be negative and under these conditions the wing would stall violently.

Adding the leading-edge slat (fig. 13(e)) effectively delays the stall. No attempt was made to determine an optimum slat configuration for stall control. The slat arrangement used was chosen for good pitching-moment and ground-effect characteristics in hovering flight.

An examination of the pitching-moment data at low forward speeds (figs. 12, 13, 15, and 16) indicates that, with the incidence settings used herein, the flow on the horizontal tail is stalled on the lower surface. The pitching-moment data with the horizontal tail on, therefore, are not representative of what could probably be obtained with a complete configuration, but are included because they are believed to be of general interest and because the slat-effectiveness data are also shown in these figures.

CONCLUDING REMARKS

Stalling was observed to occur on a wing equipped with a 50-percent-chord sliding flap and a 30-percent-chord slotted flap operating in the slipstream of two large-diameter propellers in conditions approaching steady level flight at high-power conditions; however, this stall was effectively delayed by the addition of a leading-edge slat.

Large tunnel-wall effects for which there are no known corrections were encountered.

Langley Aeronautical Laboratory,
National Advisory Committee for Aeronautics,
Langley Field, Va., October 23, 1956.

REFERENCES

1. Kuhn, Richard E., and Draper, John W.: Investigation of the Aerodynamic Characteristics of a Model Wing-Propeller Combination and of the Wing and Propeller Separately at Angles of Attack Up to 90°. NACA Rep. 1263, 1956. (Supersedes NACA TN 3304 by Draper and Kuhn.)

2. Kuhn, Richard E., and Draper, John W.: An Investigation of a Wing-Propeller Configuration Employing Large-Chord Plain Flaps and Large-Diameter Propellers for Low-Speed Flight and Vertical Take-Off. NACA TN 3307, 1954.

3. Kuhn, Richard E., and Draper, John W.: Investigation of Effectiveness of Large-Chord Slotted Flaps in Deflecting Propeller Slipstreams Downward for Vertical Take-Off and Low-Speed Flight. NACA TN 3364, 1955.

4. Kuhn, Richard E.: Investigation of Effectiveness of a Wing Equipped With a 50-Percent-Chord Sliding Flap, a 30-Percent-Chord Slotted Flap, and a 30-Percent-Chord Slat in Deflecting Propeller Slipstreams Downward for Vertical Take-Off. NACA TN 3919, 1957.

5. Wenzinger, Carl J., and Harris, Thomas A.: Wind-Tunnel Investigation of an N.A.C.A. 23012 Airfoil With Various Arrangements of Slotted Flaps. NACA Rep. 664, 1939.

6. Gillis, Clarence L., Polhamus, Edward C., and Gray, Joseph L., Jr.: Charts for Determining Jet-Boundary Corrections for Complete Models in 7- by 10-Foot Closed Rectangular Wind Tunnels. NACA WR L-123, 1945. (Formerly NACA ARR L5G31.)

7. Herriot, John G.: Blockage Corrections for Three-Dimensional-Flow Closed-Throat Wind Tunnels, With Consideration of the Effect of Compressibility. NACA Rep. 995, 1950. (Supersedes NACA RM A7B28.)

TABLE I

WING, FLAP, AND SLAT ORDINATES

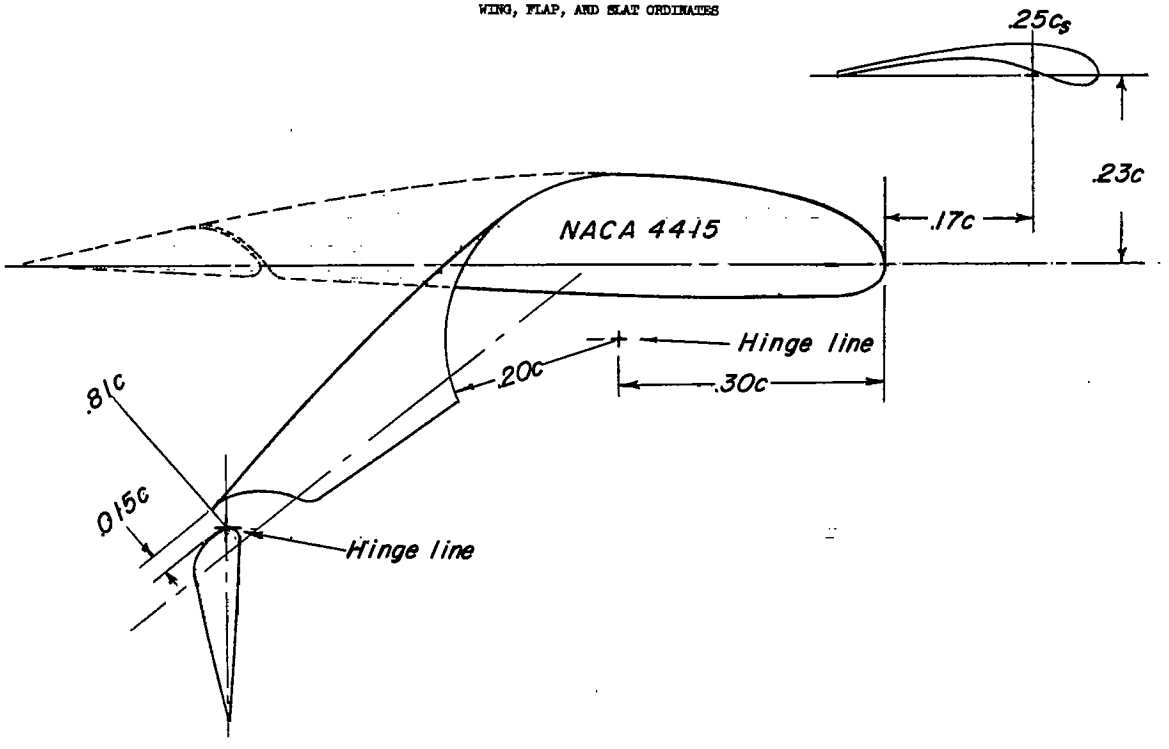

Slotted-flap ordinates

Station, fraction of wing chord	Ordinate, fraction of wing chord		
	Slot	Flap nose	
		Upper	Lower
0.65	-0.0180	------	------
.66	-.0175	------	------
.67	-.0169	------	------
.68	-.0145	------	------
.69	-.0080	------	------
.70	.0160	0.0075	0.0075
.705	-------	.0210	-.0020
.71	.0280	.0260	-.0050
.72	.0375	.0350	-.0080
.73	.0430	.0415	-.0115
.74	.0470	.0465	-.0125
.75	.0500	.0490	-.0125
.76	.0520	.0510	------
.77	.0530	.0520	------
.78	.0535	.0525	------
.79	.0535	.0525	------
.80	.0530	.0520	------
.81	.0531	.0515	------
.82	-------	.0505	------
.83	-------	.0485	------

Slat ordinates

Station, fraction of slat chord	Ordinates, fraction of slat chord	
	Upper	Lower
0	0	0
.025	.060	-.023
.050	.083	-.027
.075	.097	-.025
.100	.105	-.023
.150	.115	-.007
.200	.120	.012
.250	.122	.030
.300	.122	.046
.400	.116	.070
.500	.105	.080
.600	.090	.071
.700	.073	.056
.800	.055	.039
.900	.035	.020
1.000	.013	0

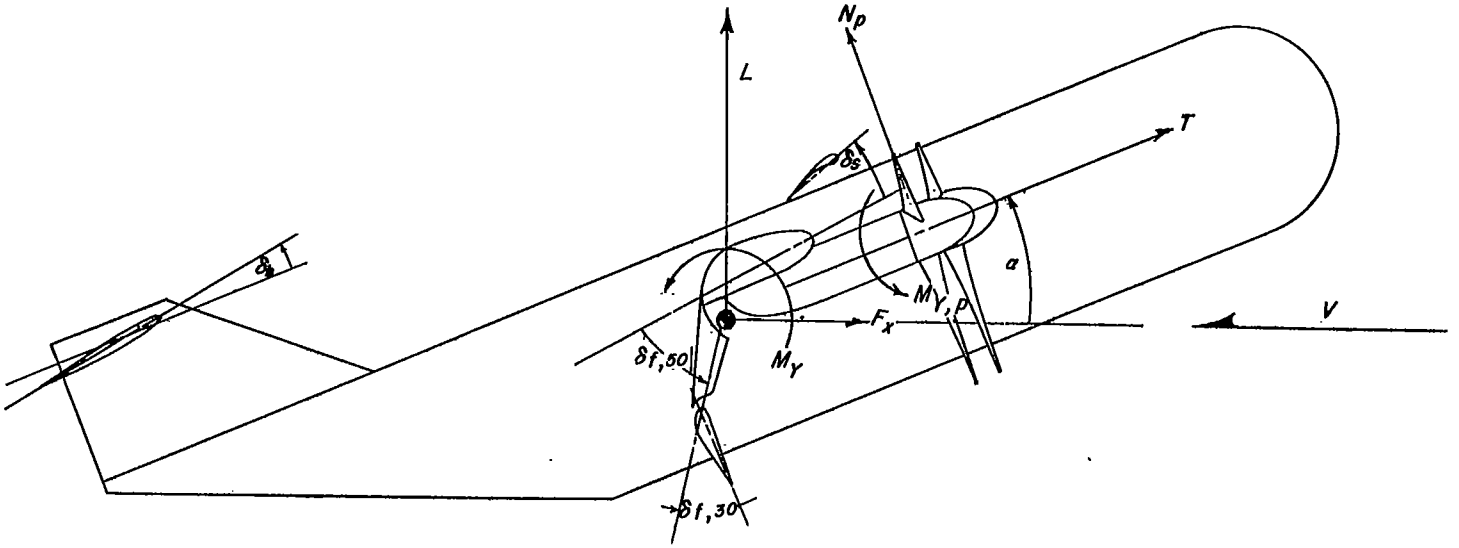

Figure 1.- Conventions used to define positive sense of forces, moments, and angles.

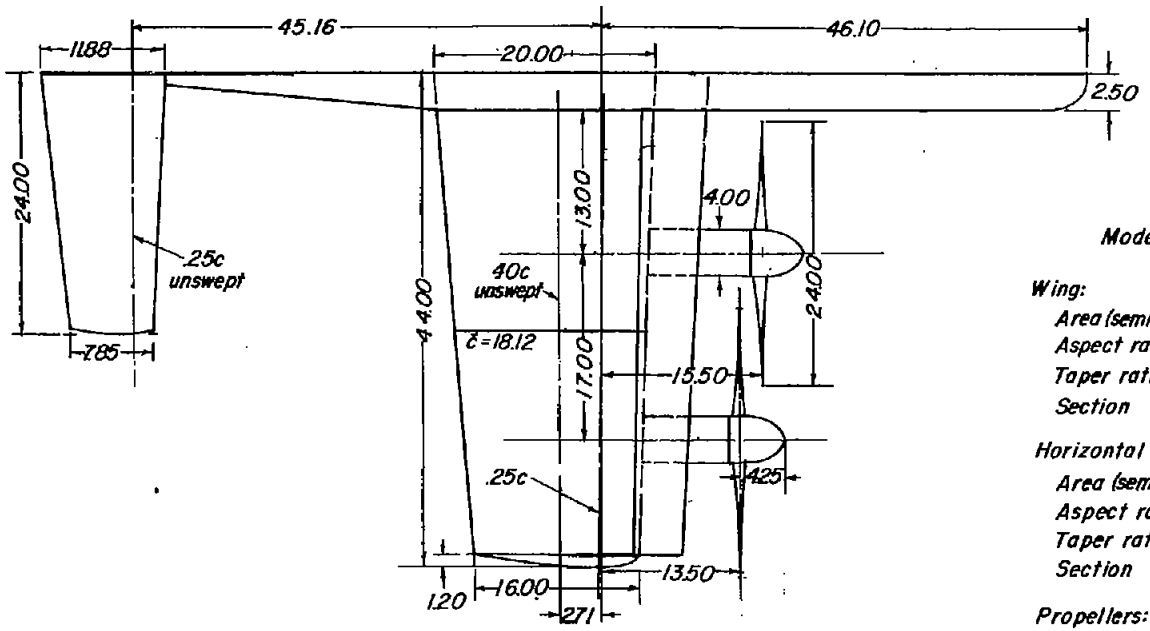

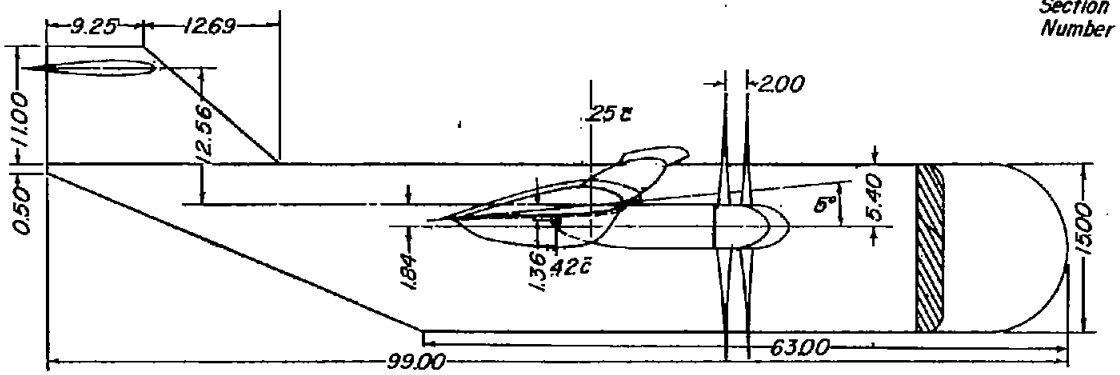

Model characteristics

Wing:		
Area (semispan), sq ft		5.50
Aspect ratio		4.89
Taper ratio		0.80
Section	NACA	4415
Horizontal tail:		
Area (semispan), sq ft		1.65
Aspect ratio		4.85
Taper ratio		0.661
Section	NACA	0012
Propellers:		
Disk area (each) sq ft		3.14
Solidity (each)		0.07
Section		Clark y
Number of blades		3

Figure 2.- Drawing of model. All dimensions are in inches.

L-91043

Figure 3.- Photograph of the model installed on the ceiling of the Langley 300 MPH 7- by 10-foot tunnel. $\alpha = 40^{\circ}$.

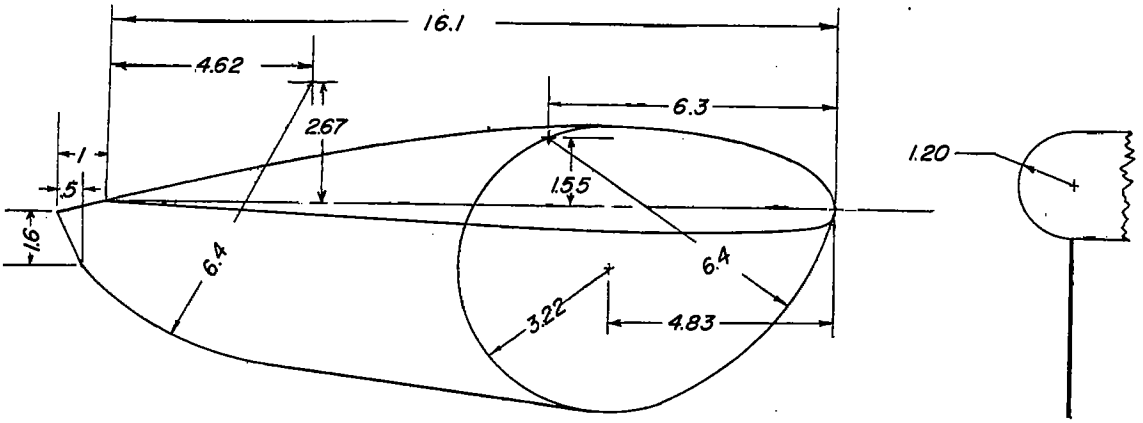

Flaps neutral

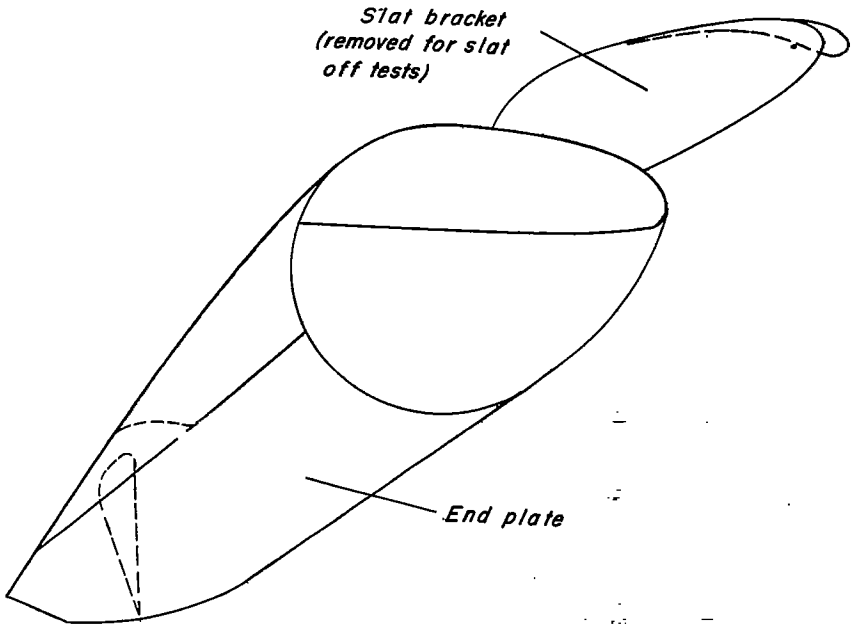

Flaps deflected

Figure 4.- Details of the end plate.

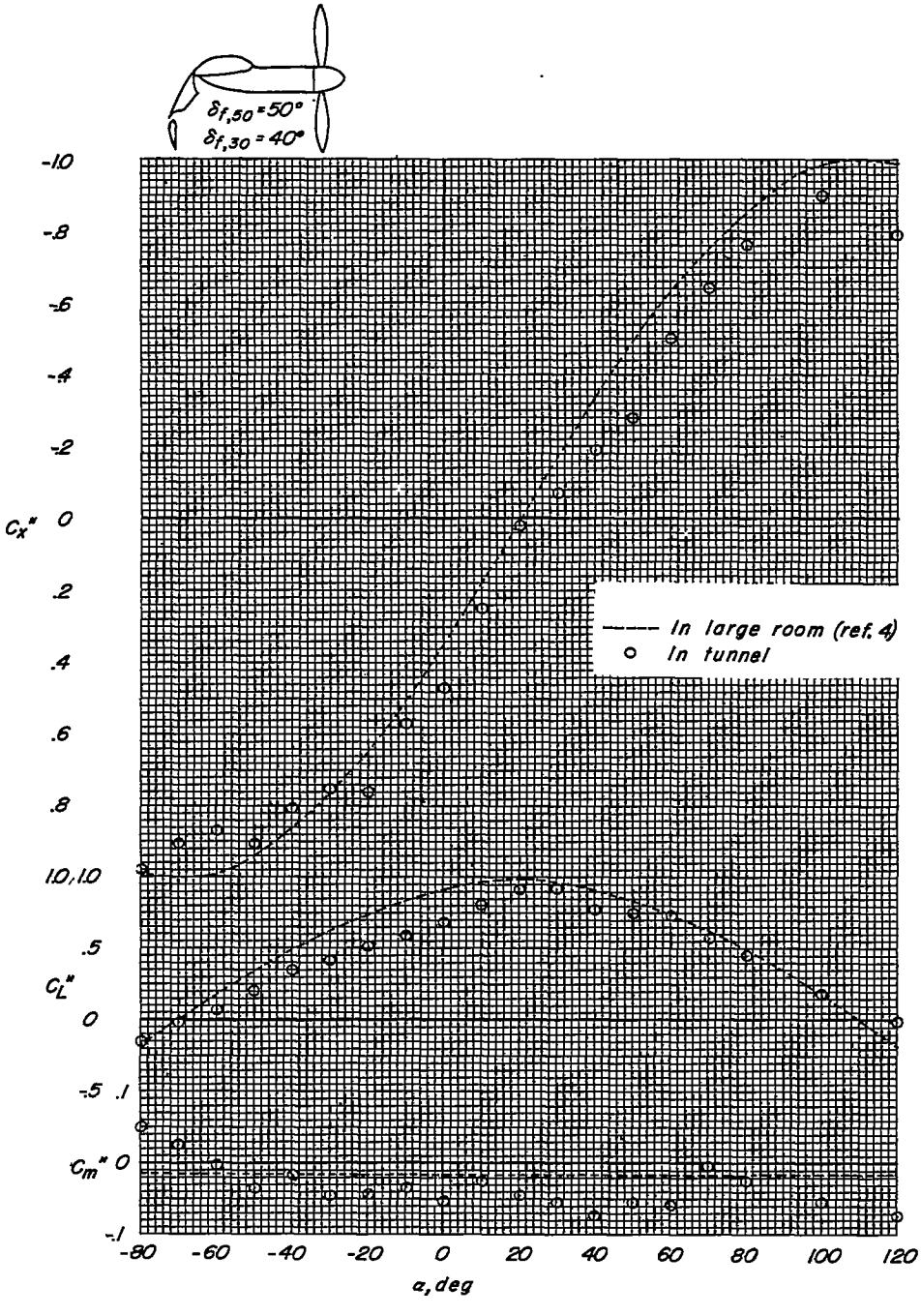

Figure 5.- Effect of tunnel-wall constraint on aerodynamic characteristics at zero forward speed.

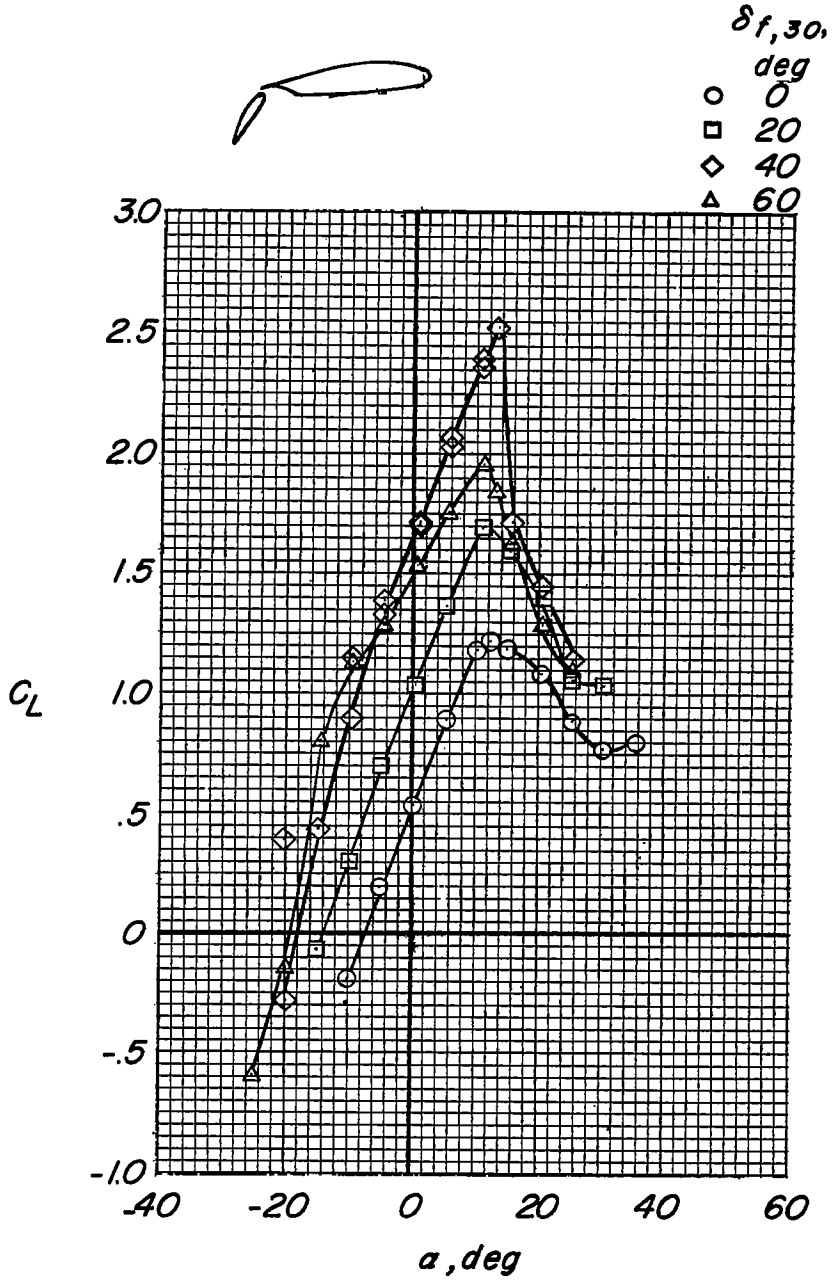

(a) Lift coefficient.

Figure 6.- Effect of flap deflection. $\delta_{f,50} = 0^{\circ}$; propellers and nacelles off; slat off; stabilizer off.

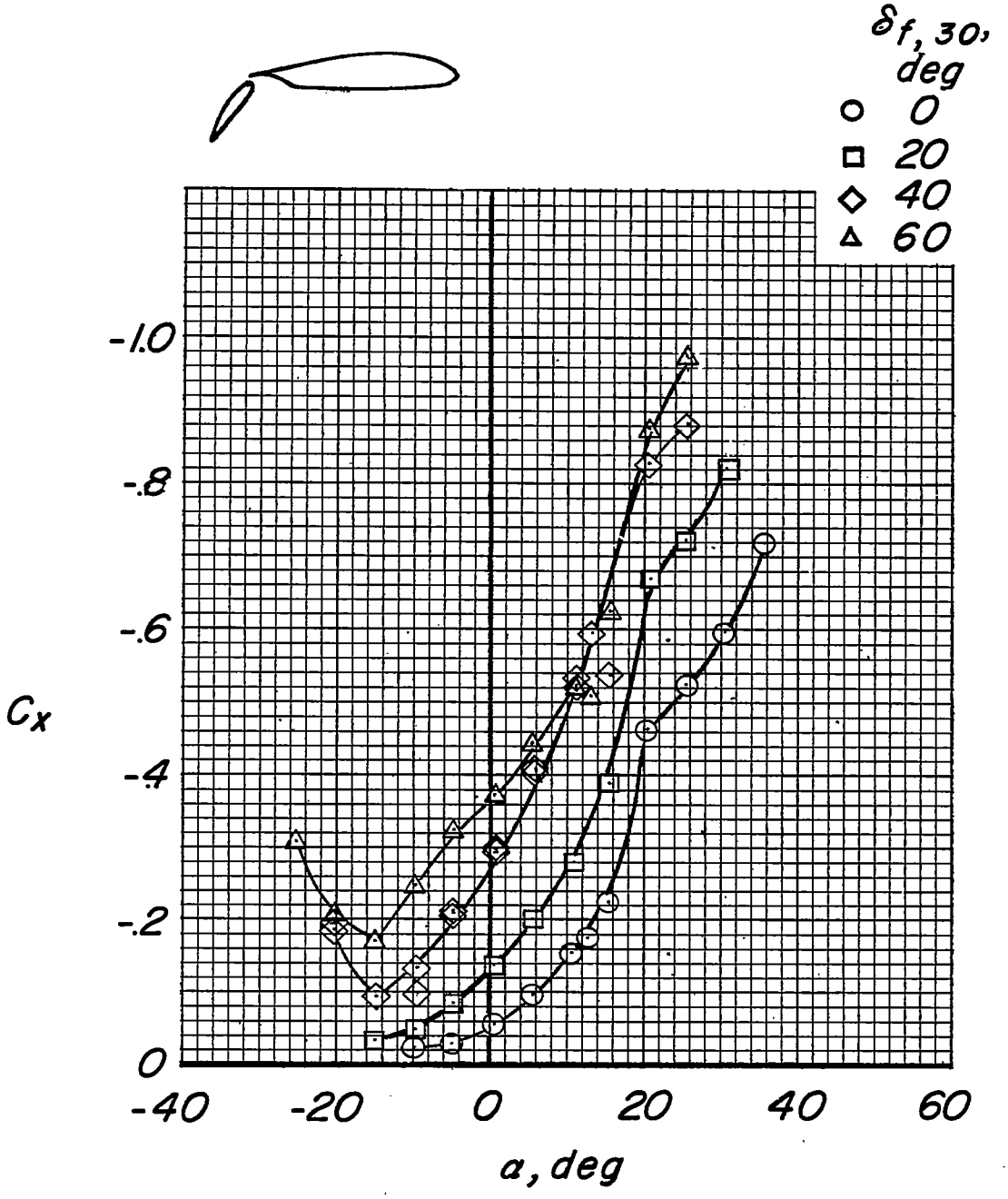

(b) Longitudinal-force coefficient.

Figure 6.- Continued.

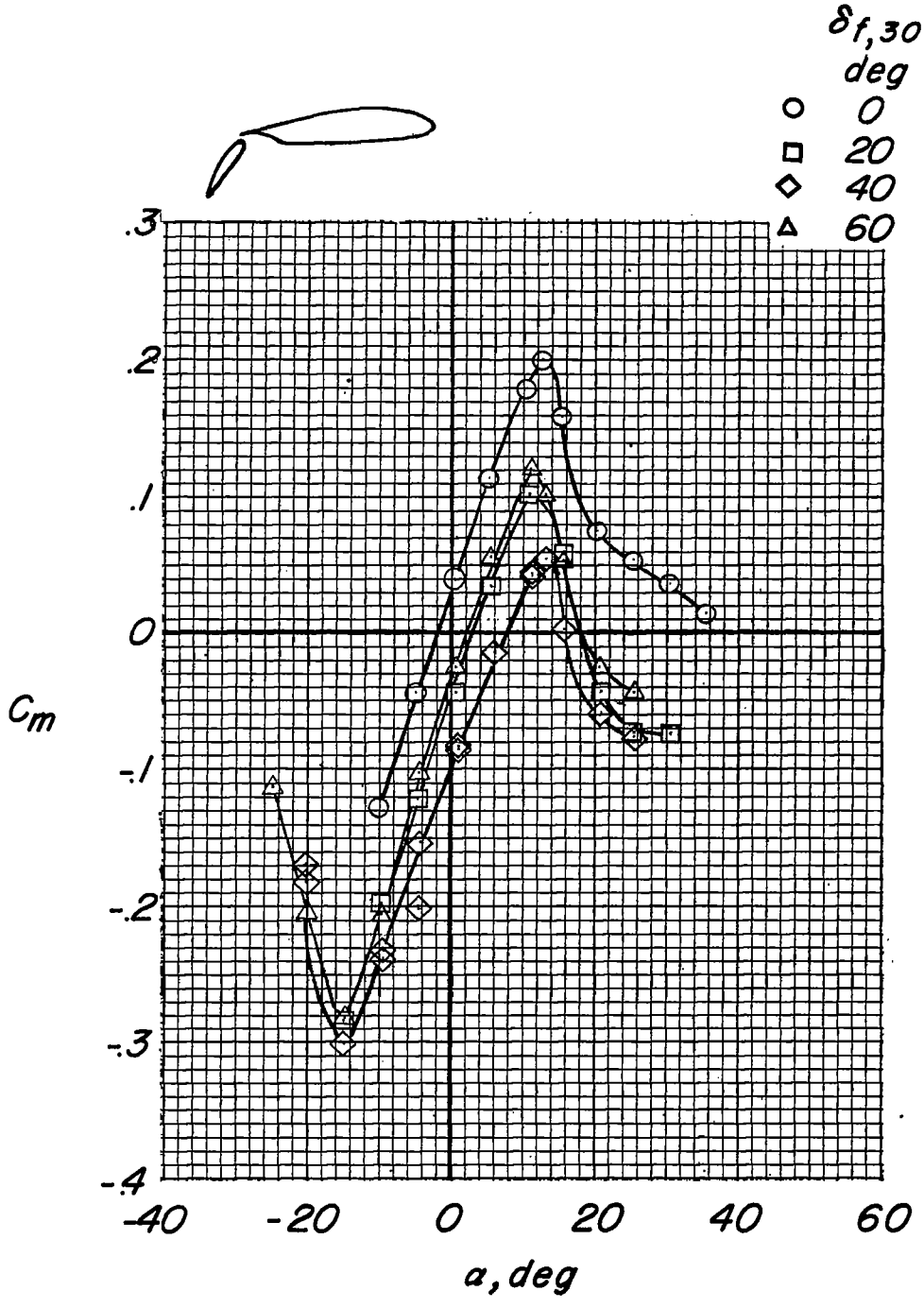

(c) Pitching-moment coefficient.

Figure 6.- Continued.

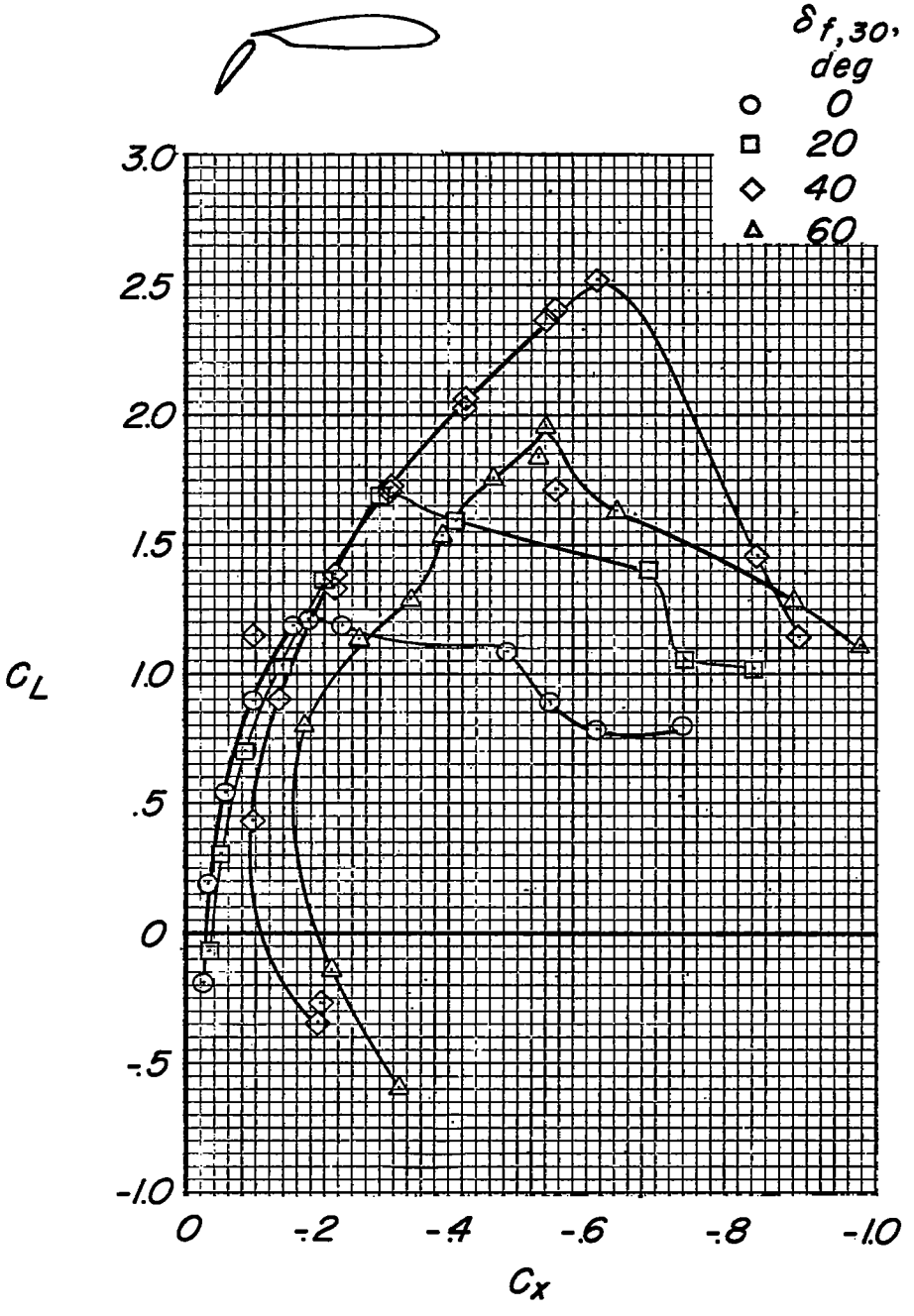

(d) Variation of C_L with C_X.

Figure 6.- Concluded.

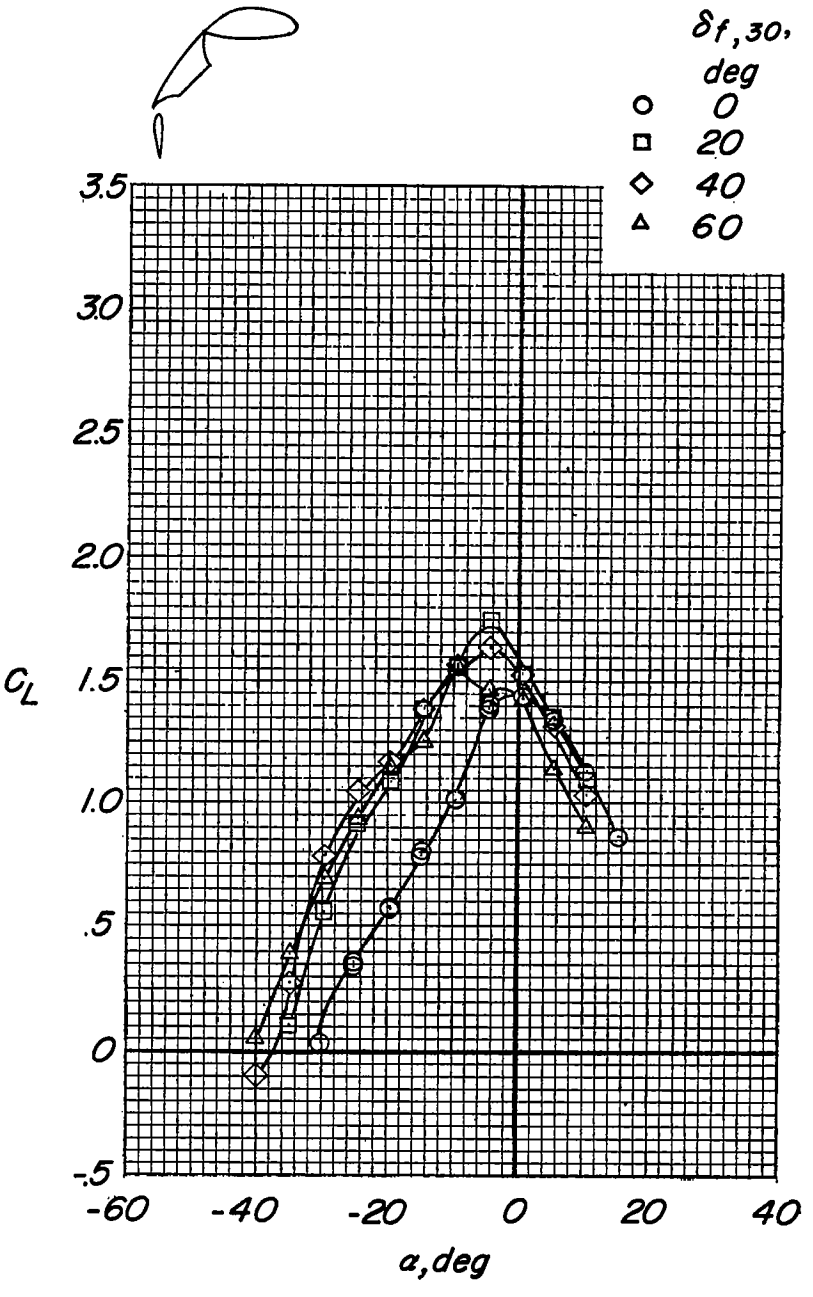

(a) Lift coefficient.

Figure 7.- Effect of flap deflection. $\delta_{f,50} = 50°$; slat off; stabilizer off; propellers and nacelles off.

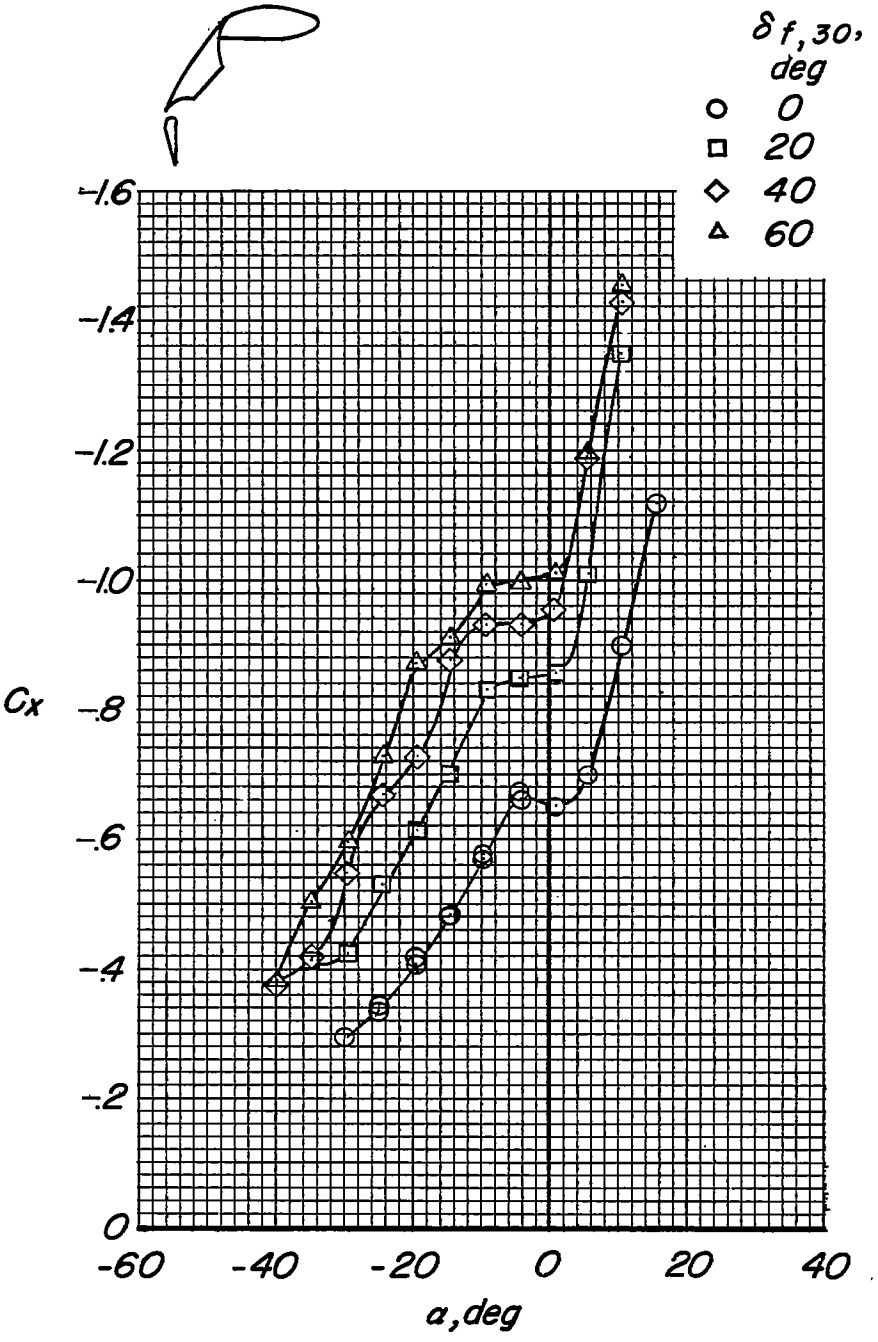

(b) Longitudinal-force coefficient.

Figure 7.- Continued.

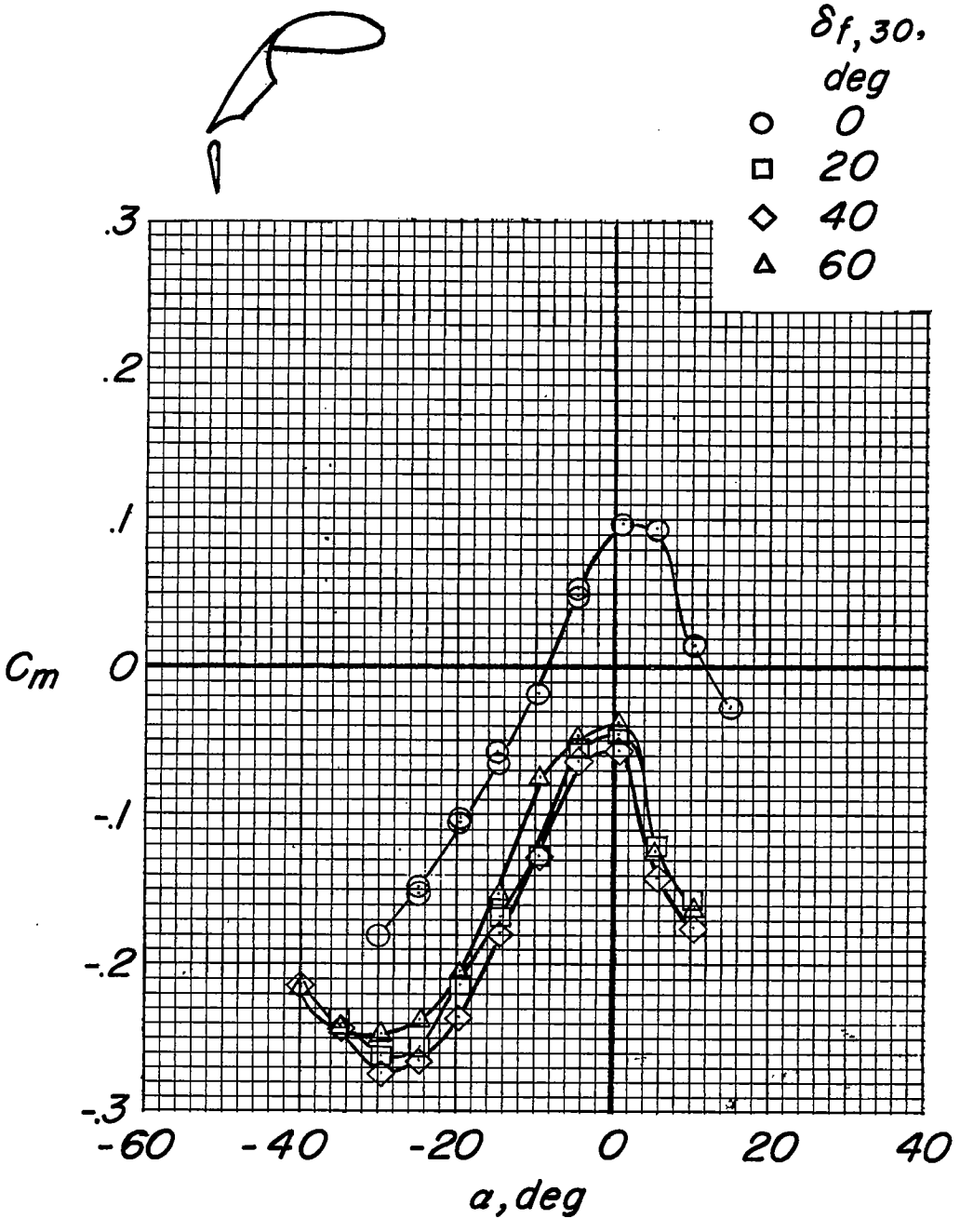

(c) Pitching-moment coefficient.

Figure 7.- Continued.

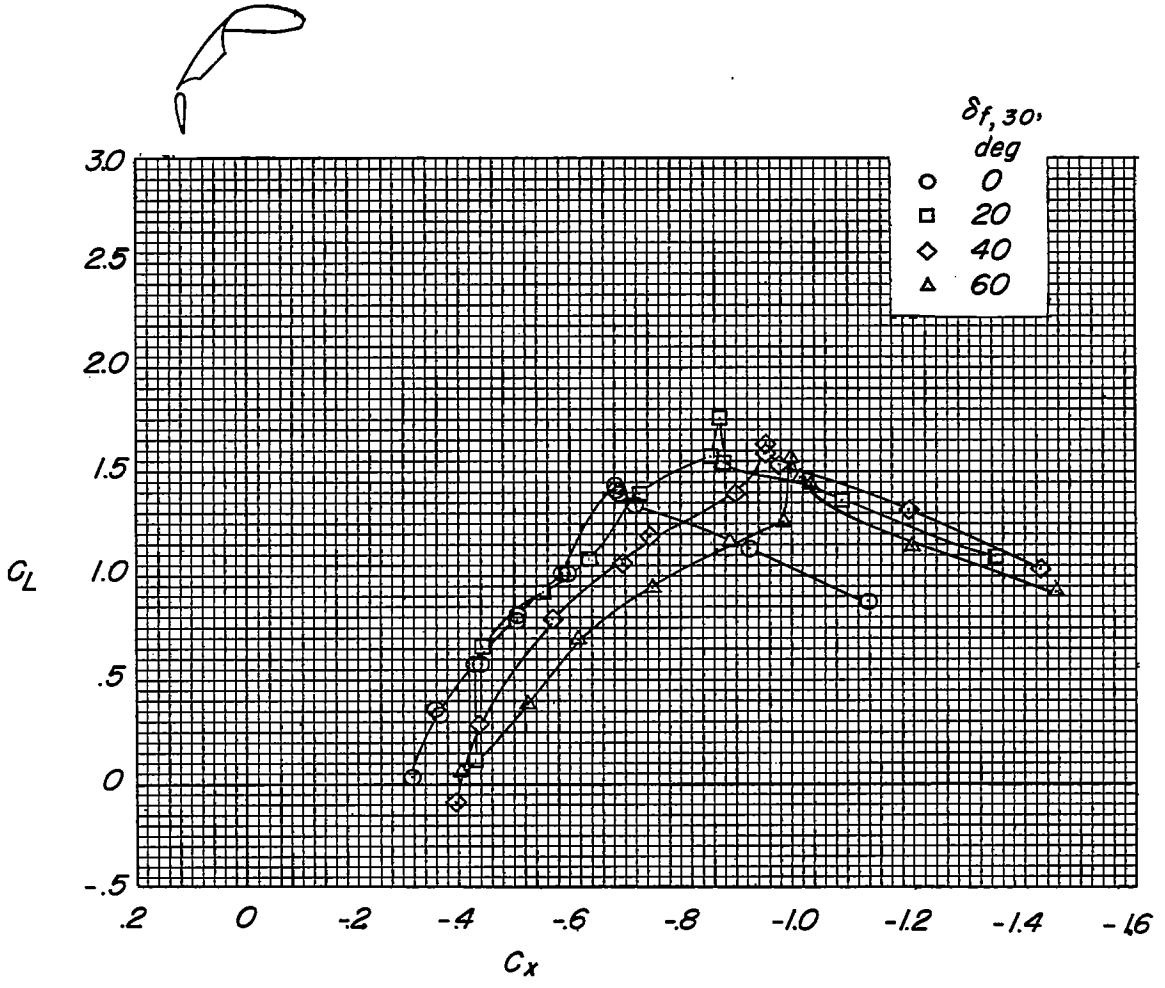

(d) Variation of C_L with C_X.

Figure 7.- Concluded.

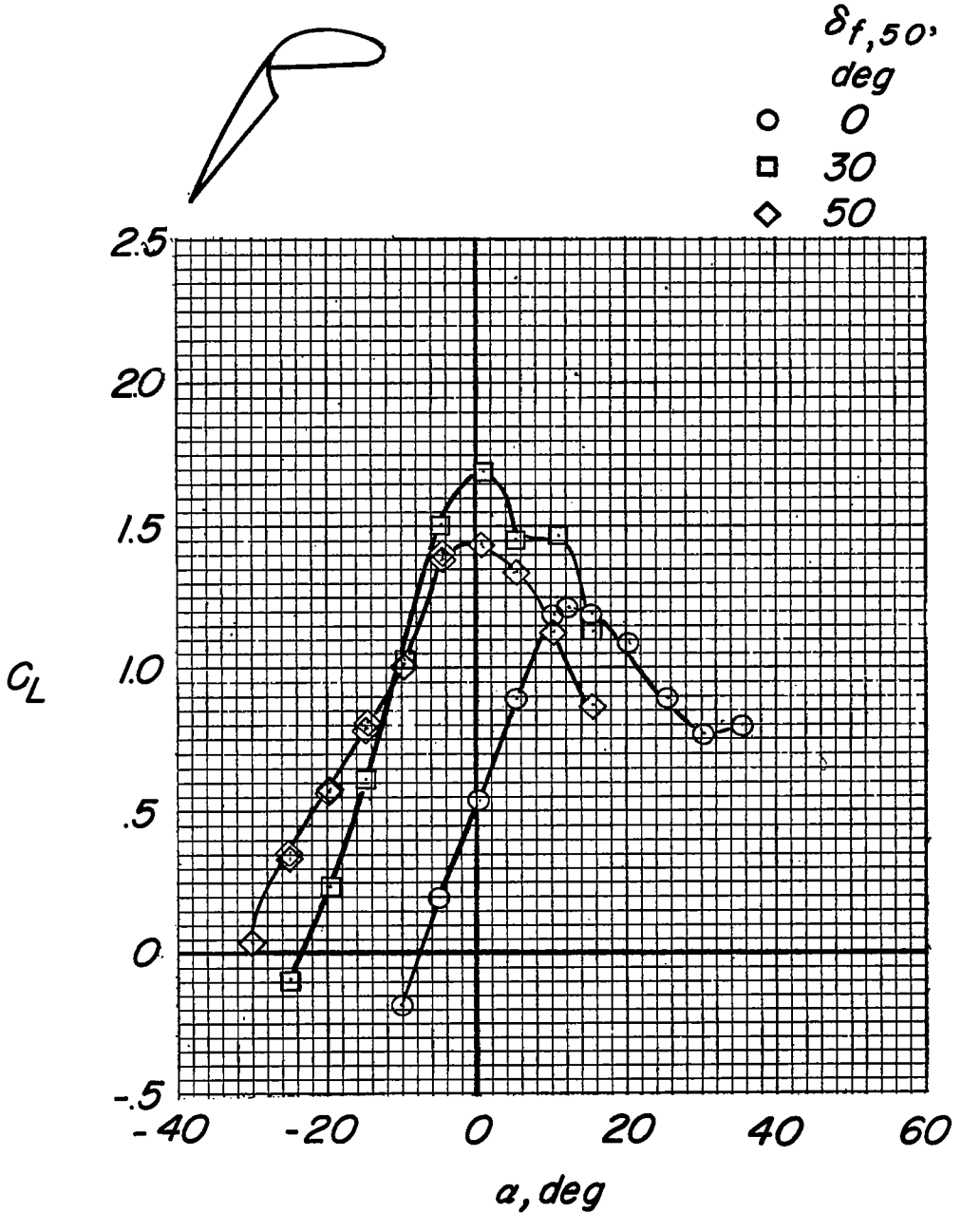

(a) Lift coefficient.

Figure 8.- Effect of flap deflection. $\delta_{f,30} = 0^\circ$; propellers and nacelles off; slat-off; stabilizer off.

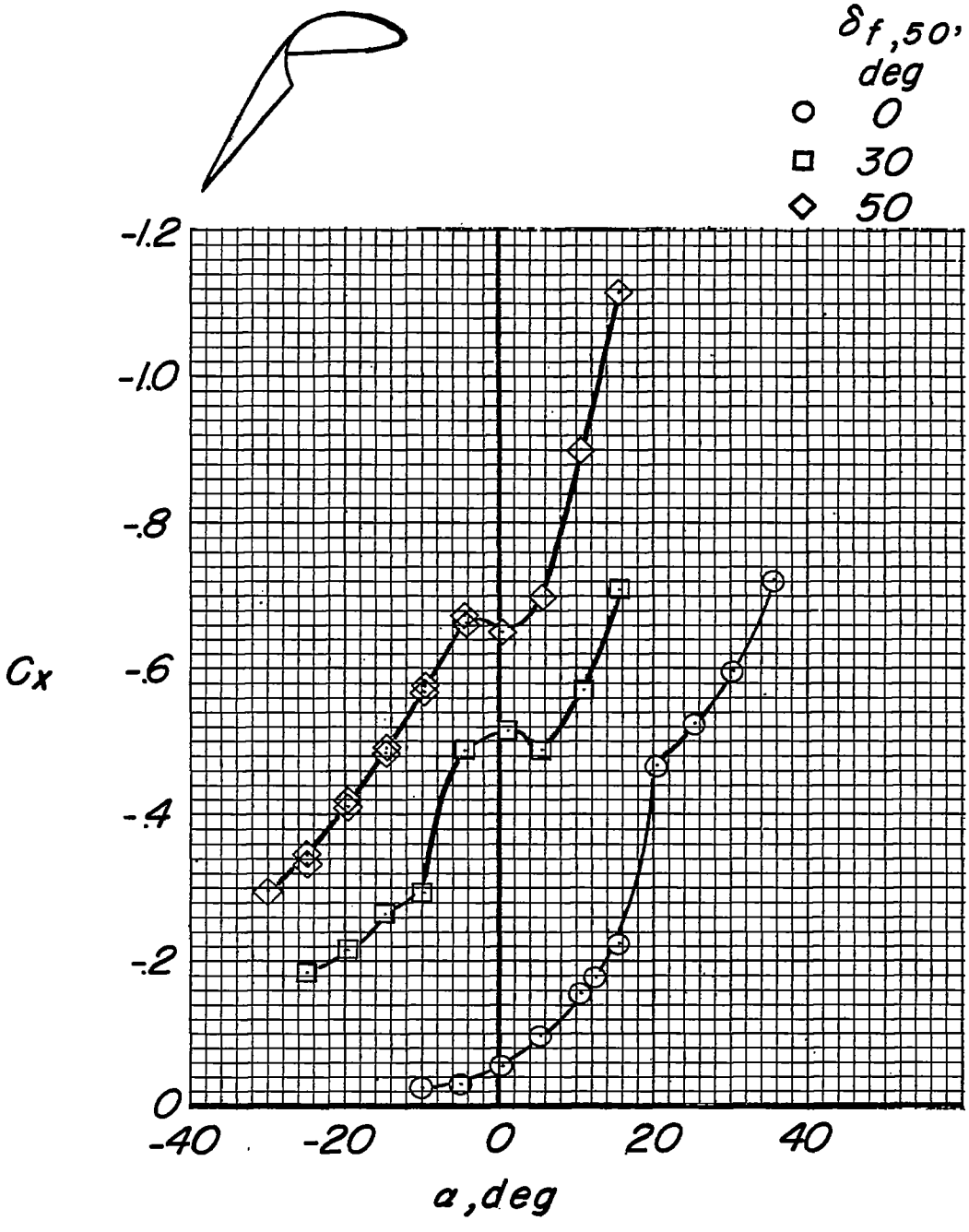

(b) Longitudinal-force coefficient.

Figure 8.- Continued.

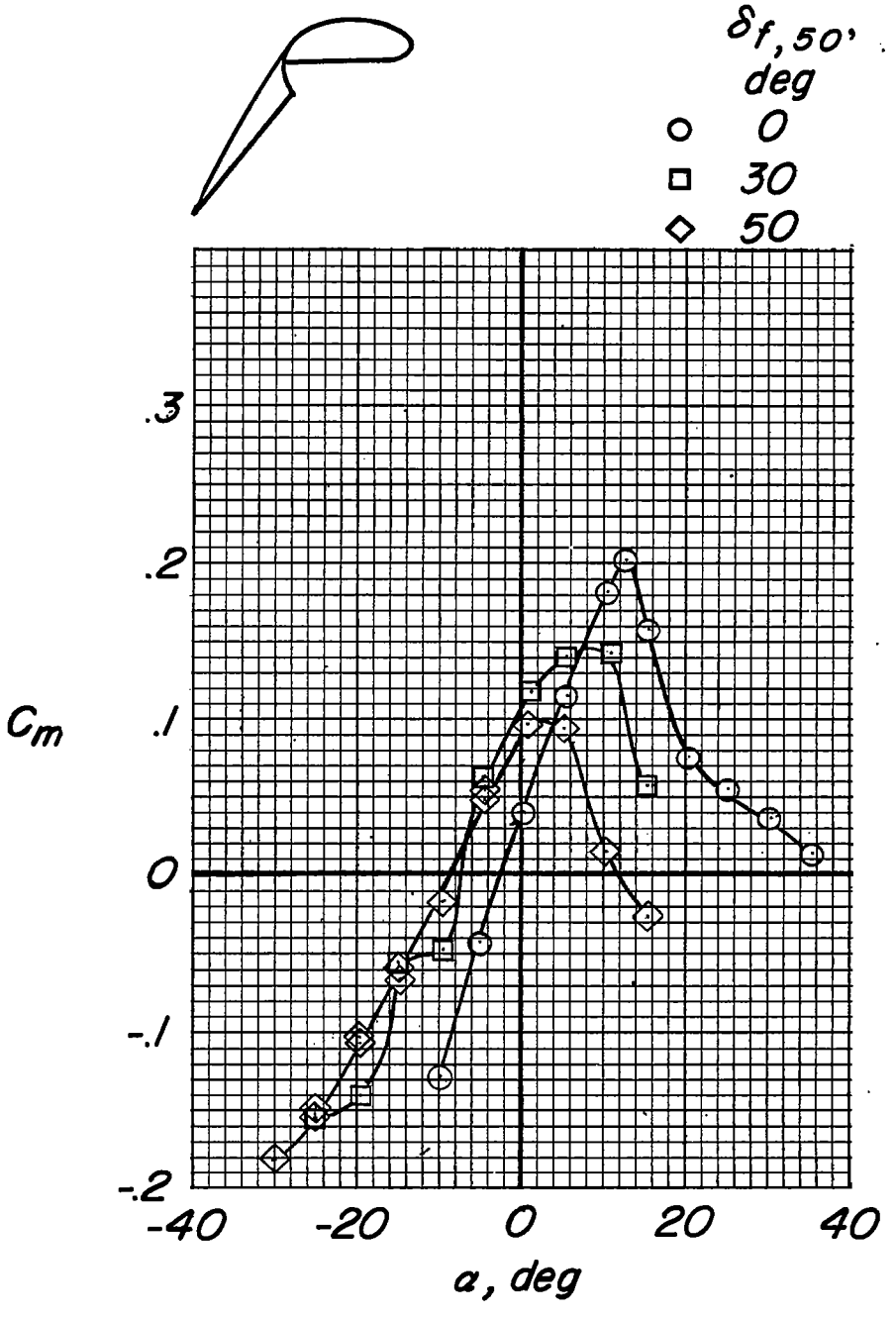

(c) Pitching-moment coefficient.

Figure 8.- Continued.

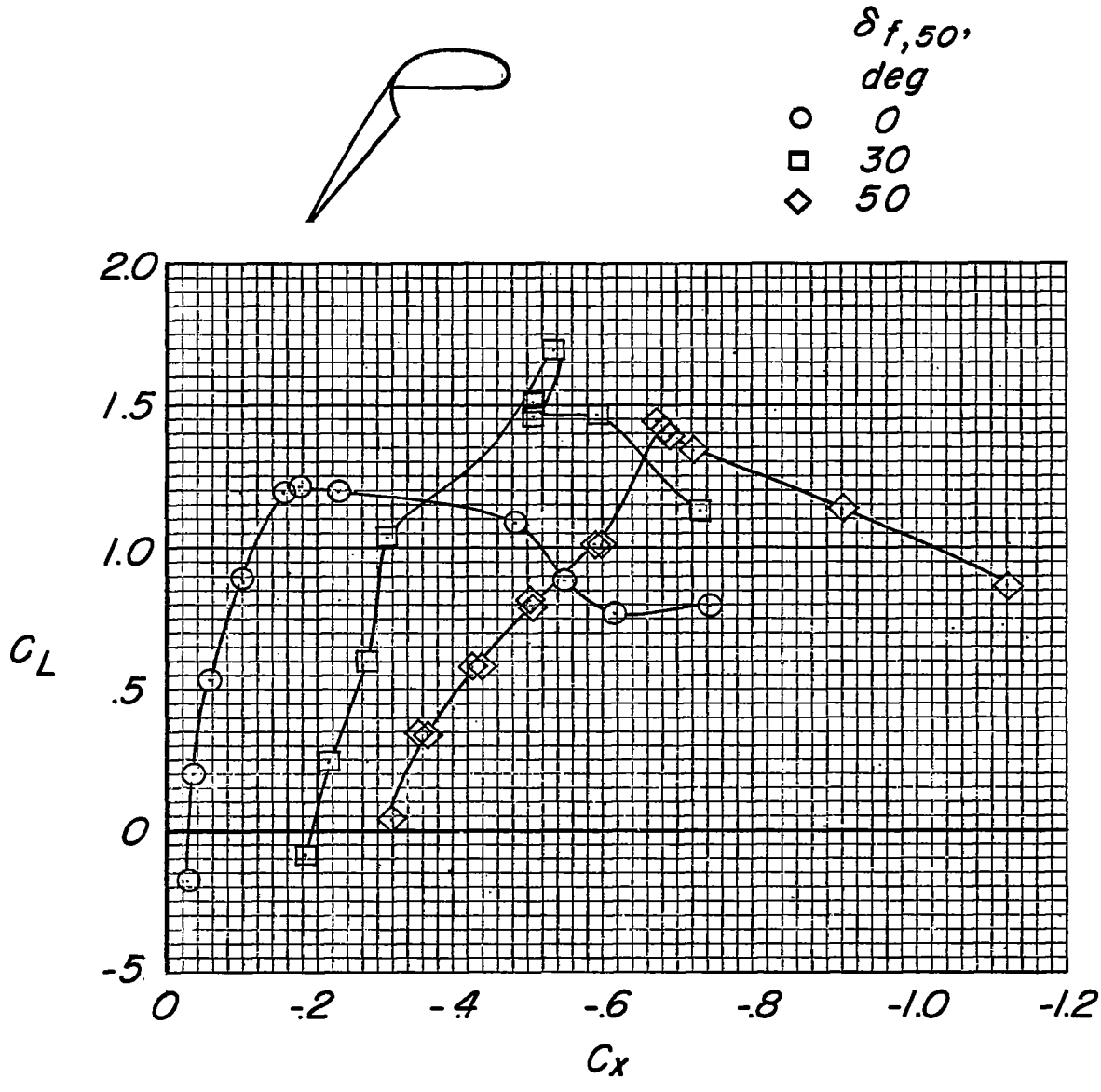

(d) Variation of C_L with C_X.

Figure 8.- Concluded.

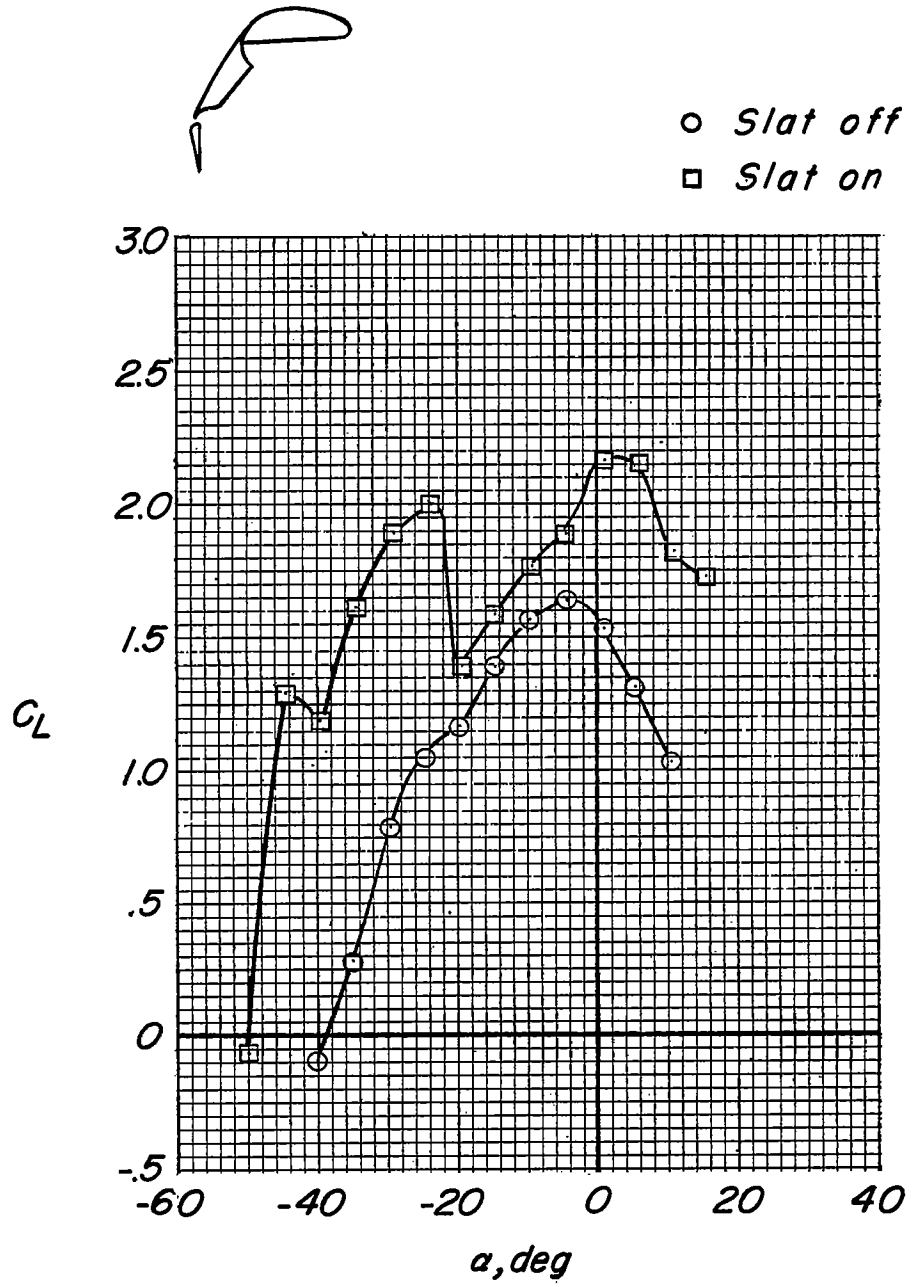

(a) Lift coefficient.

Figure 9.- Effect of slat. $\delta_{f,50} = 50^\circ$; $\delta_{f,30} = 40^\circ$; stabilizer off; propellers and nacelles off.

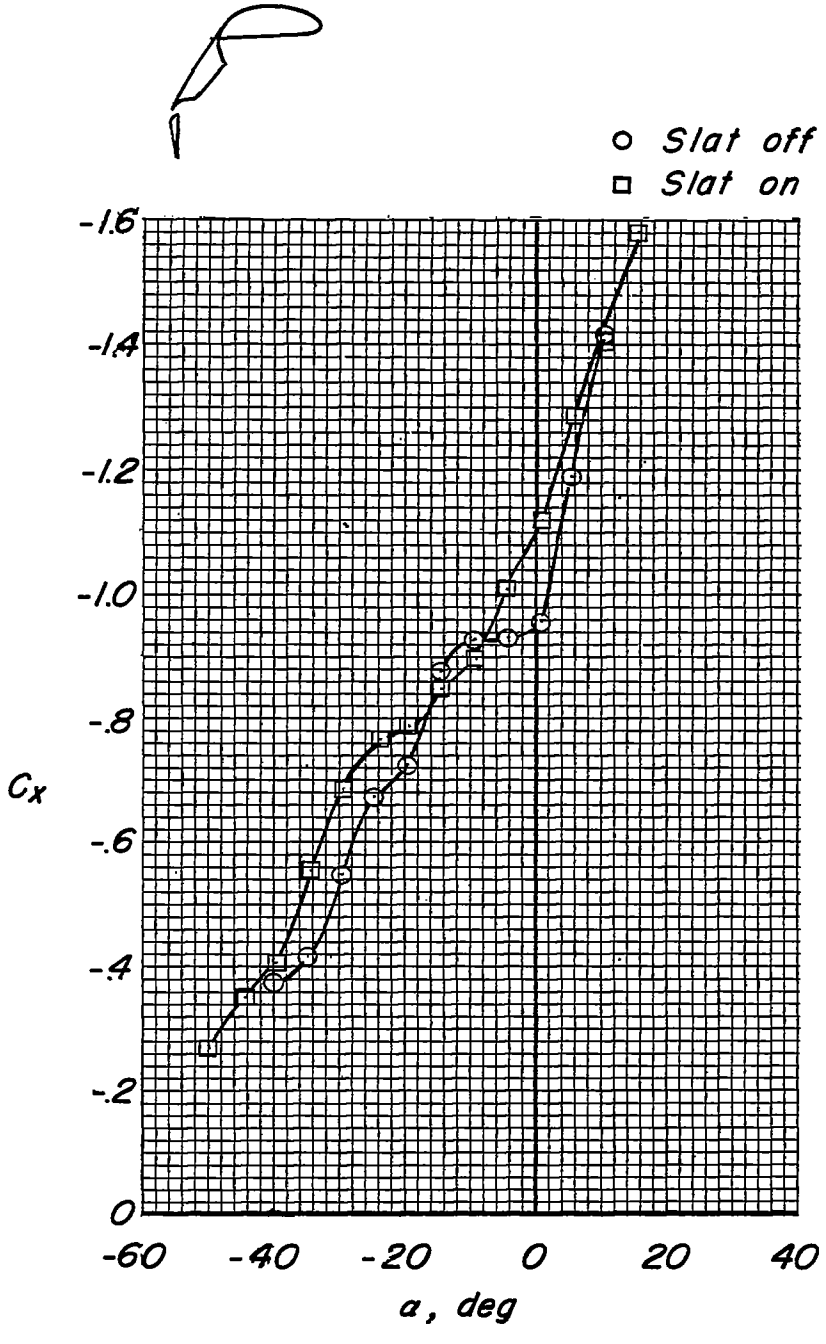

(b) Longitudinal-force coefficient.

Figure 9.- Continued.

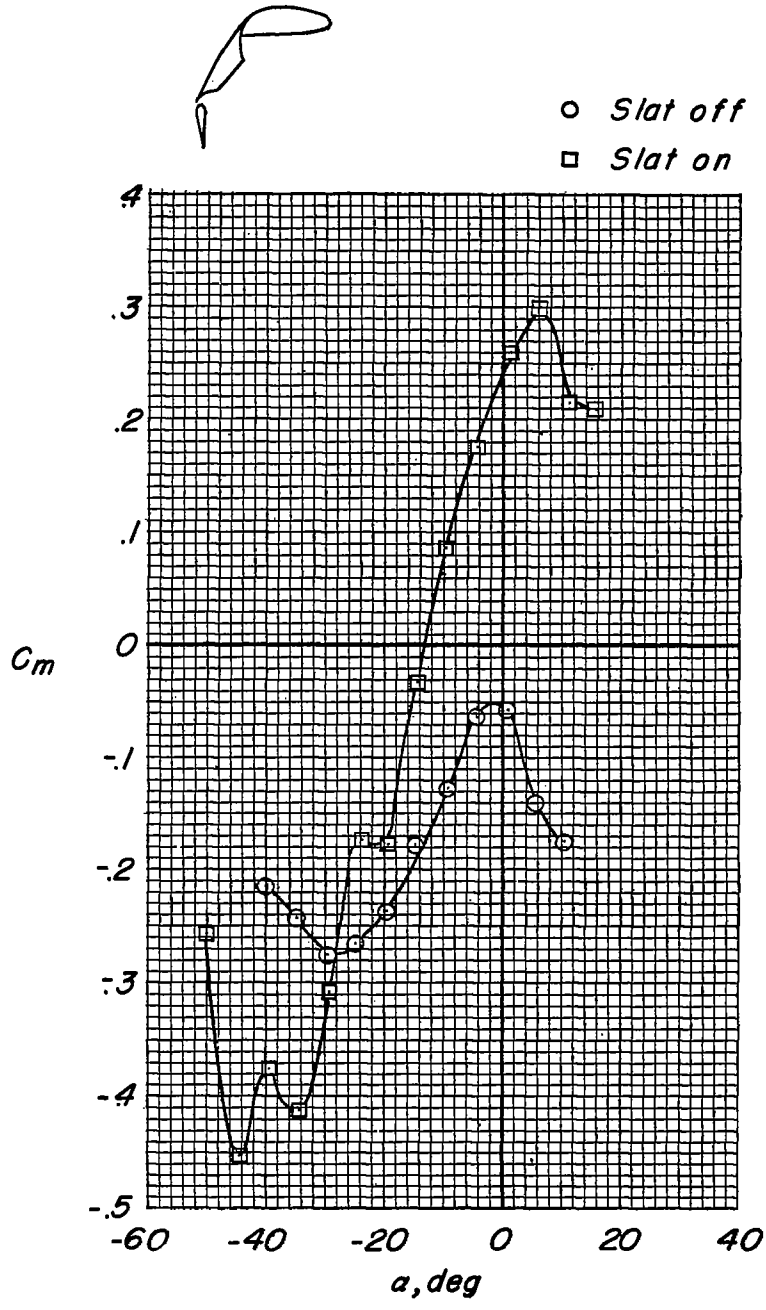

(c) Pitching-moment coefficient.

Figure 9.- Continued.

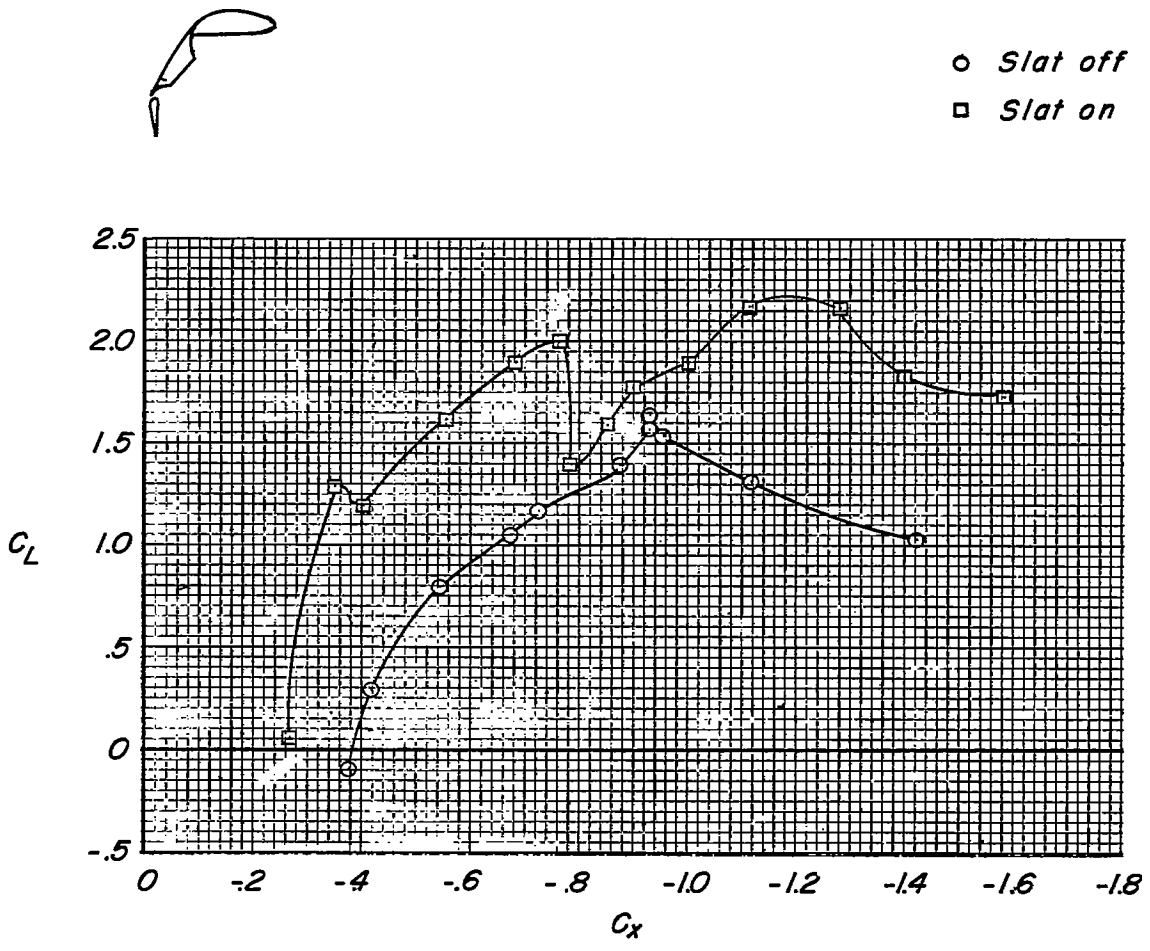

(d) Variation of C_L with C_X.

Figure 9.- Concluded.

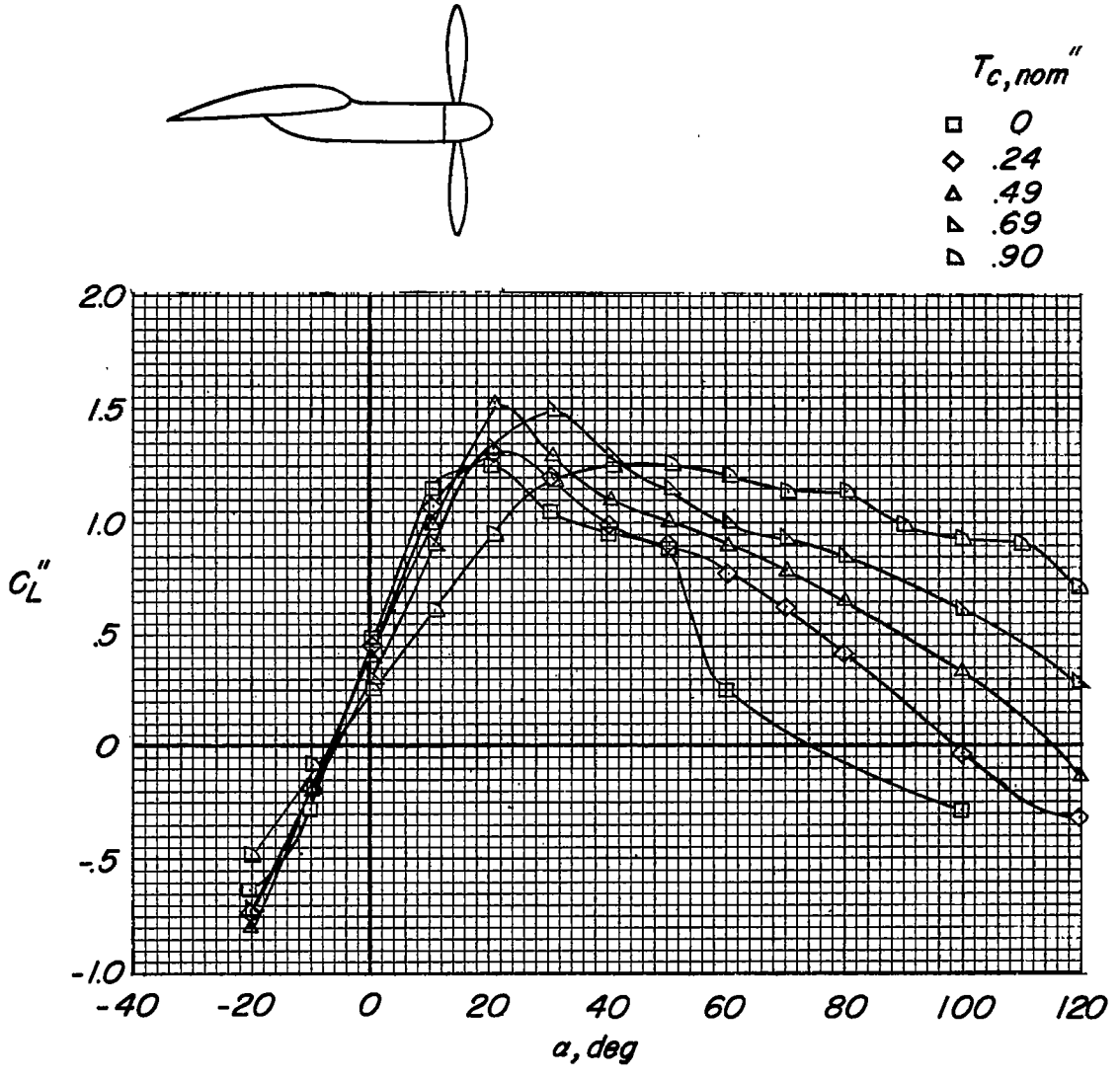

(a) Lift coefficient.

Figure 10.- Effect of slipstream. $\delta_{f,50} = 0^\circ$; $\delta_{f,30} = 0^\circ$; slat off; stabilizer off.

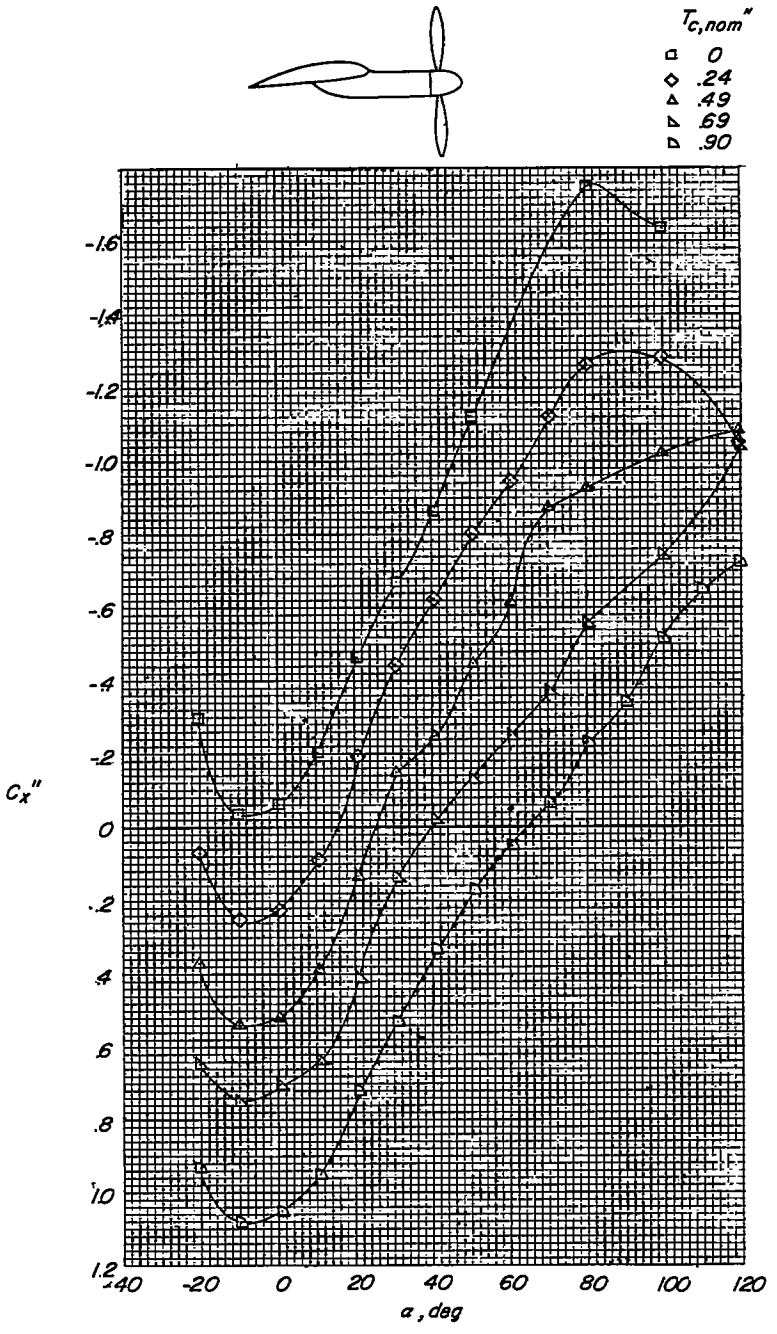

(b) Longitudinal-force coefficient.

Figure 10.- Continued.

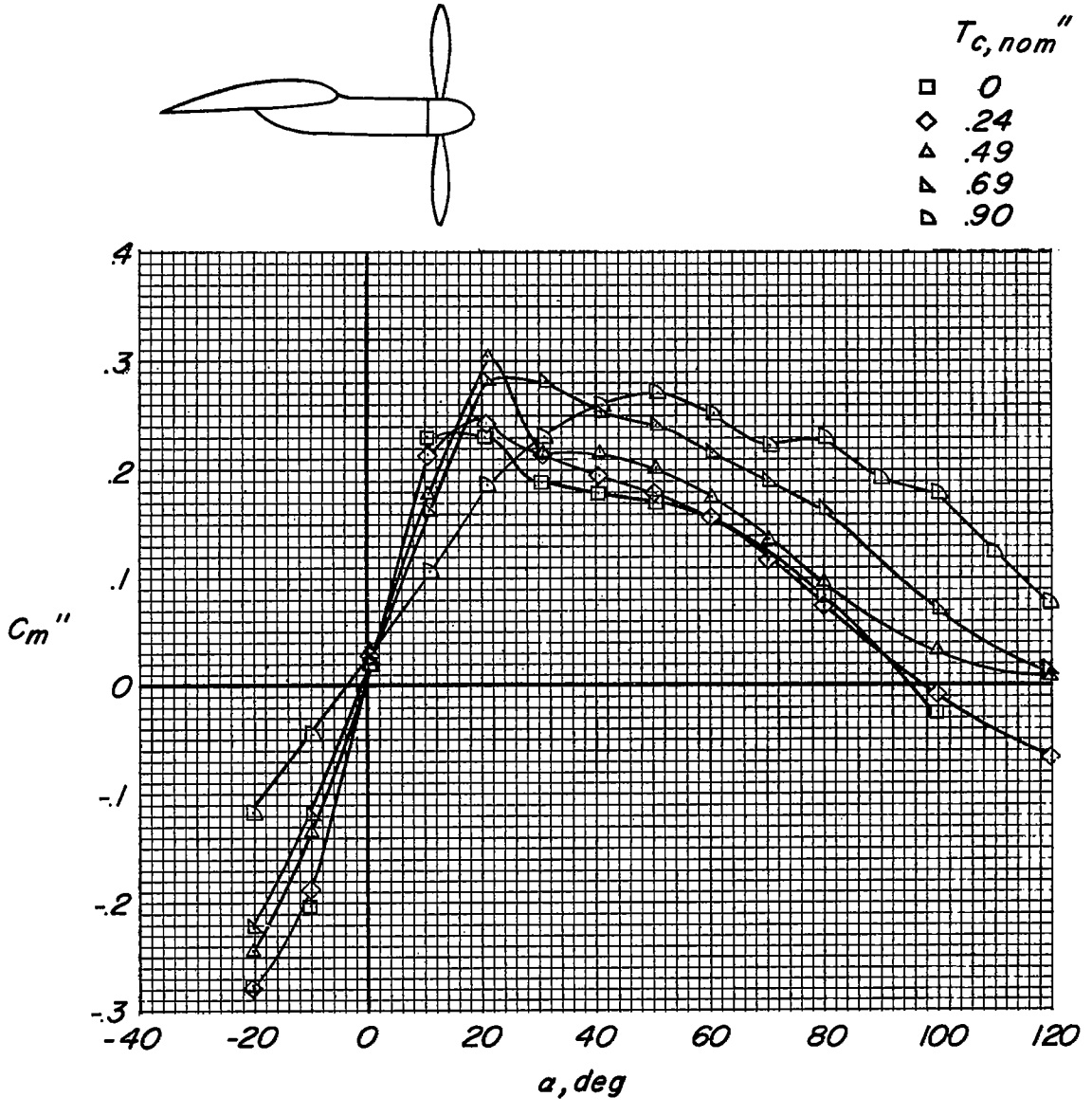

(c) Pitching-moment coefficient.

Figure 10.- Continued.

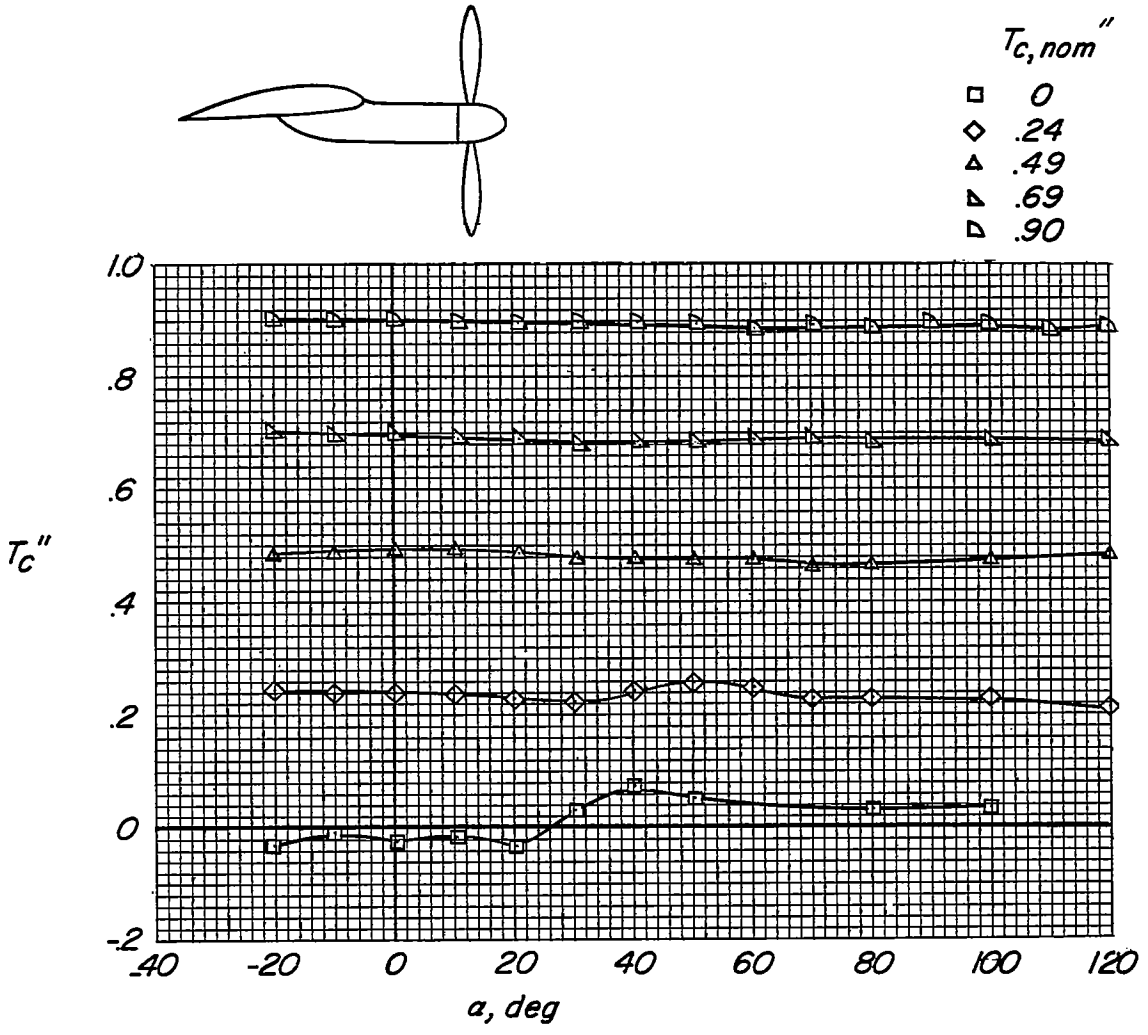

(d) Thrust coefficient.

Figure 10.- Continued.

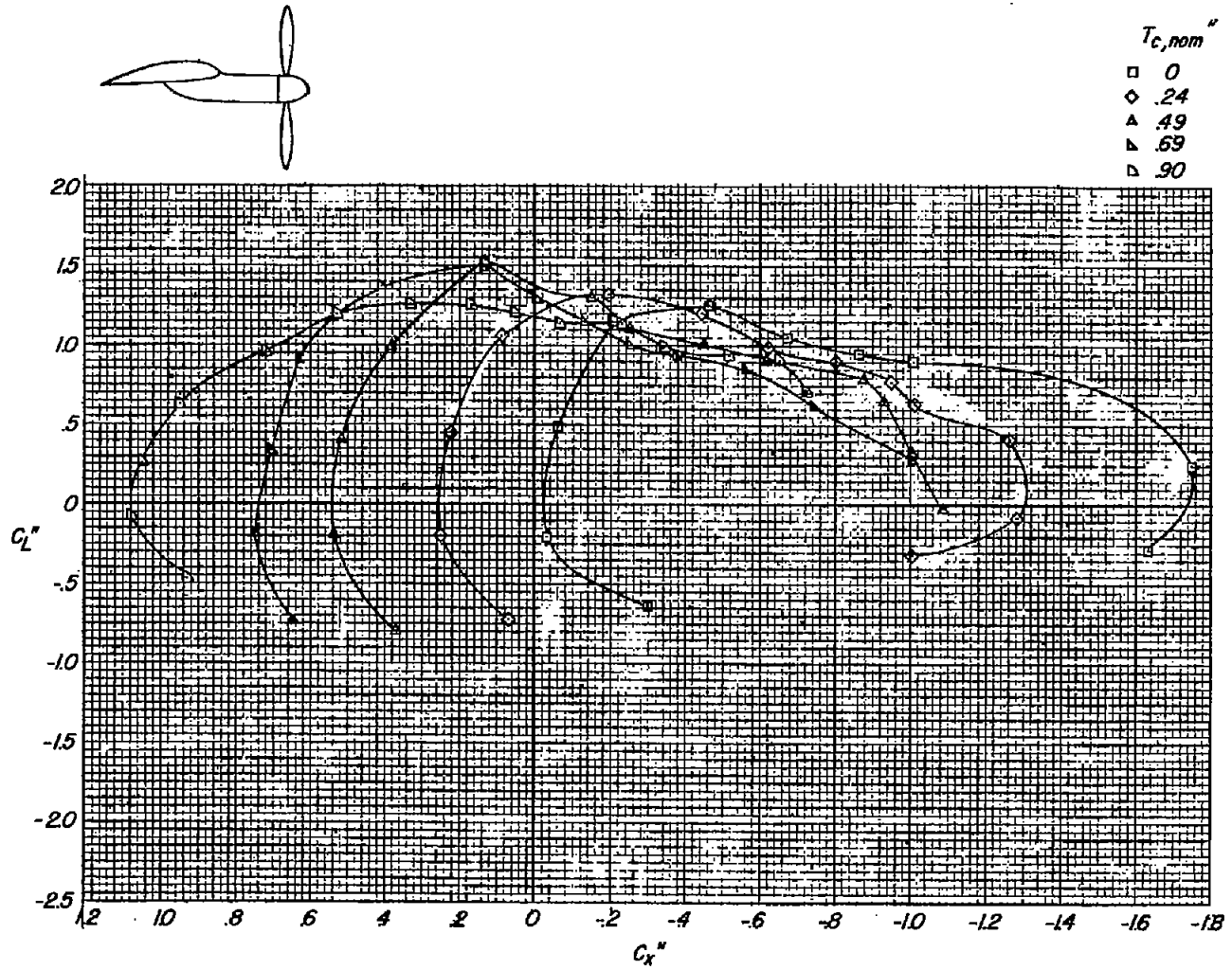

(e) Variation of C_L" with C_X".

Figure 10.- Concluded.

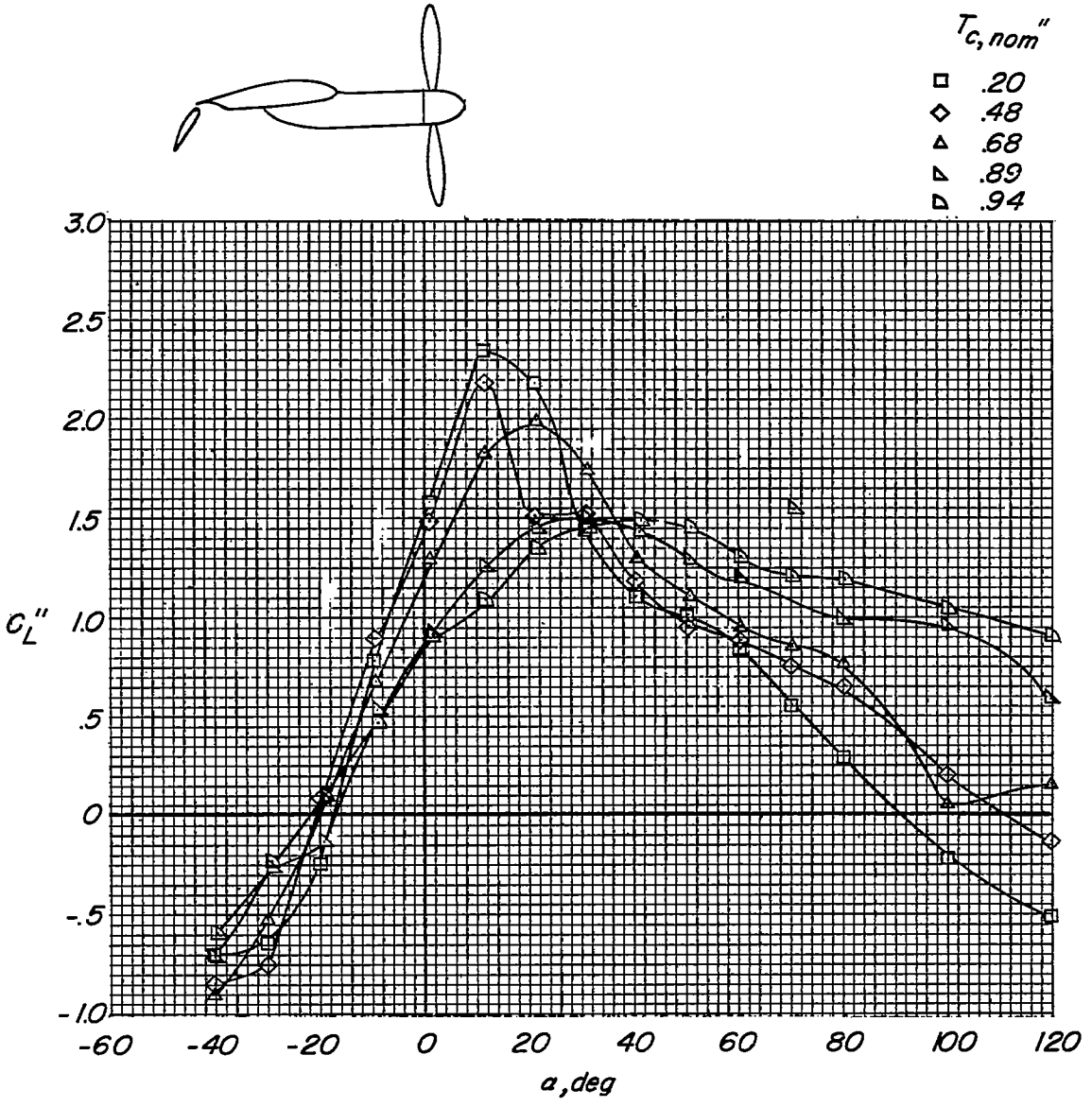

(a) Lift coefficient.

Figure 11.- Effect of slipstream. $\delta_{f,50} = 0°$; $\delta_{f,30} = 40°$; slat off; stabilizer off.

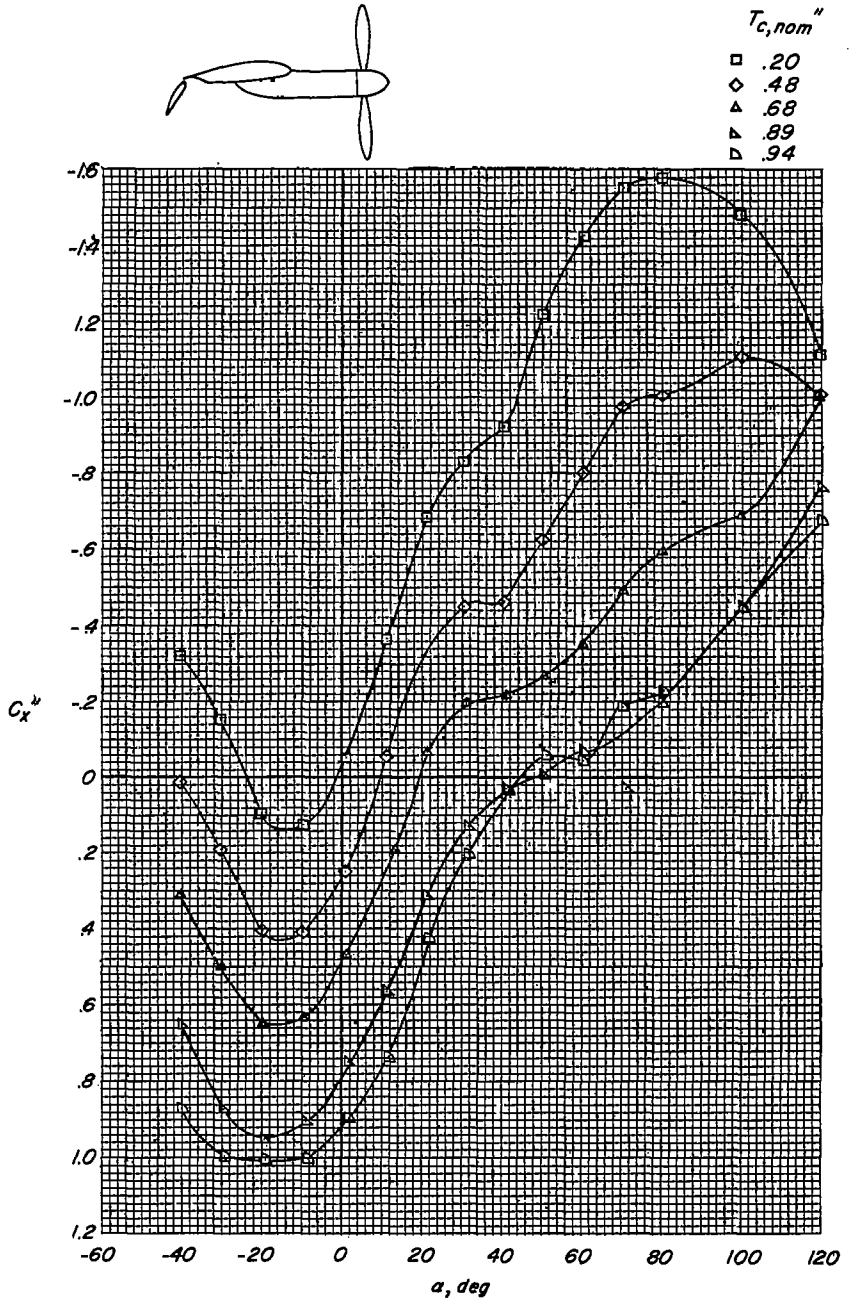

(b) Longitudinal-force coefficient.

Figure 11.- Continued.

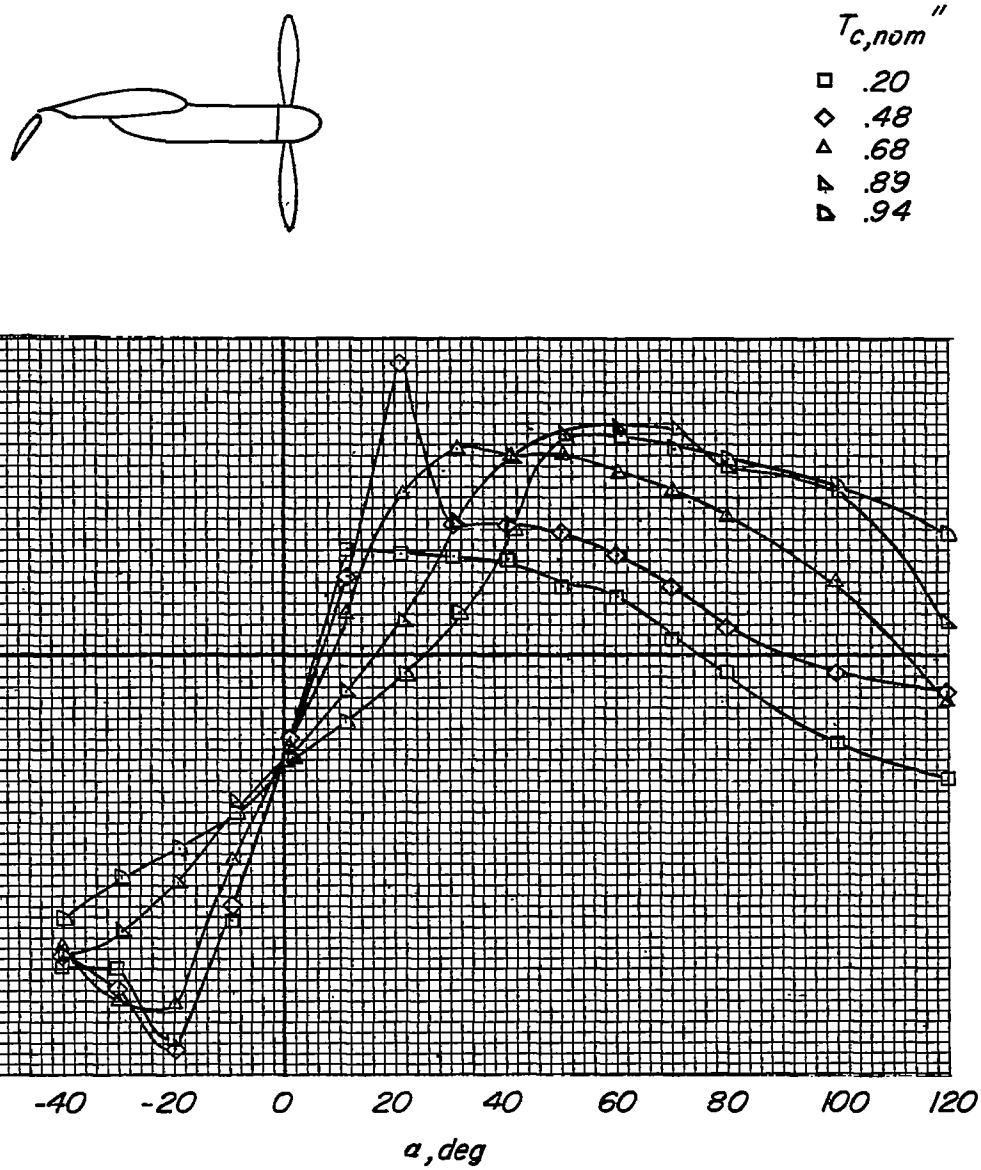

(c) Pitching-moment coefficient.

Figure 11.- Continued.

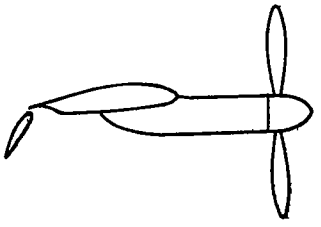

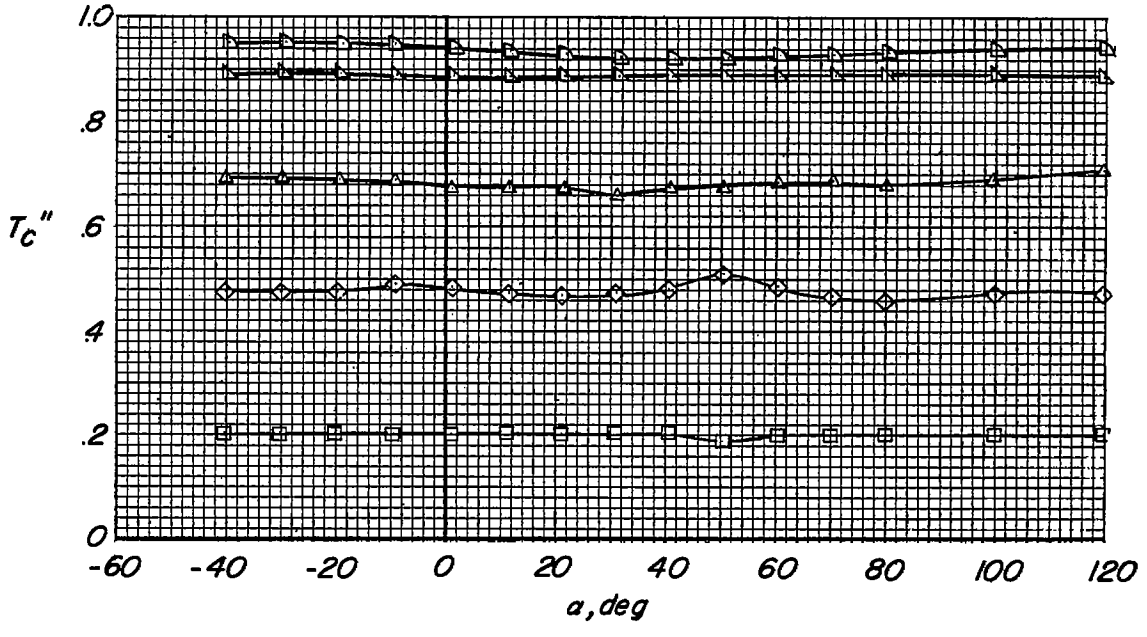

(d) Thrust coefficient.

Figure 11.- Continued.

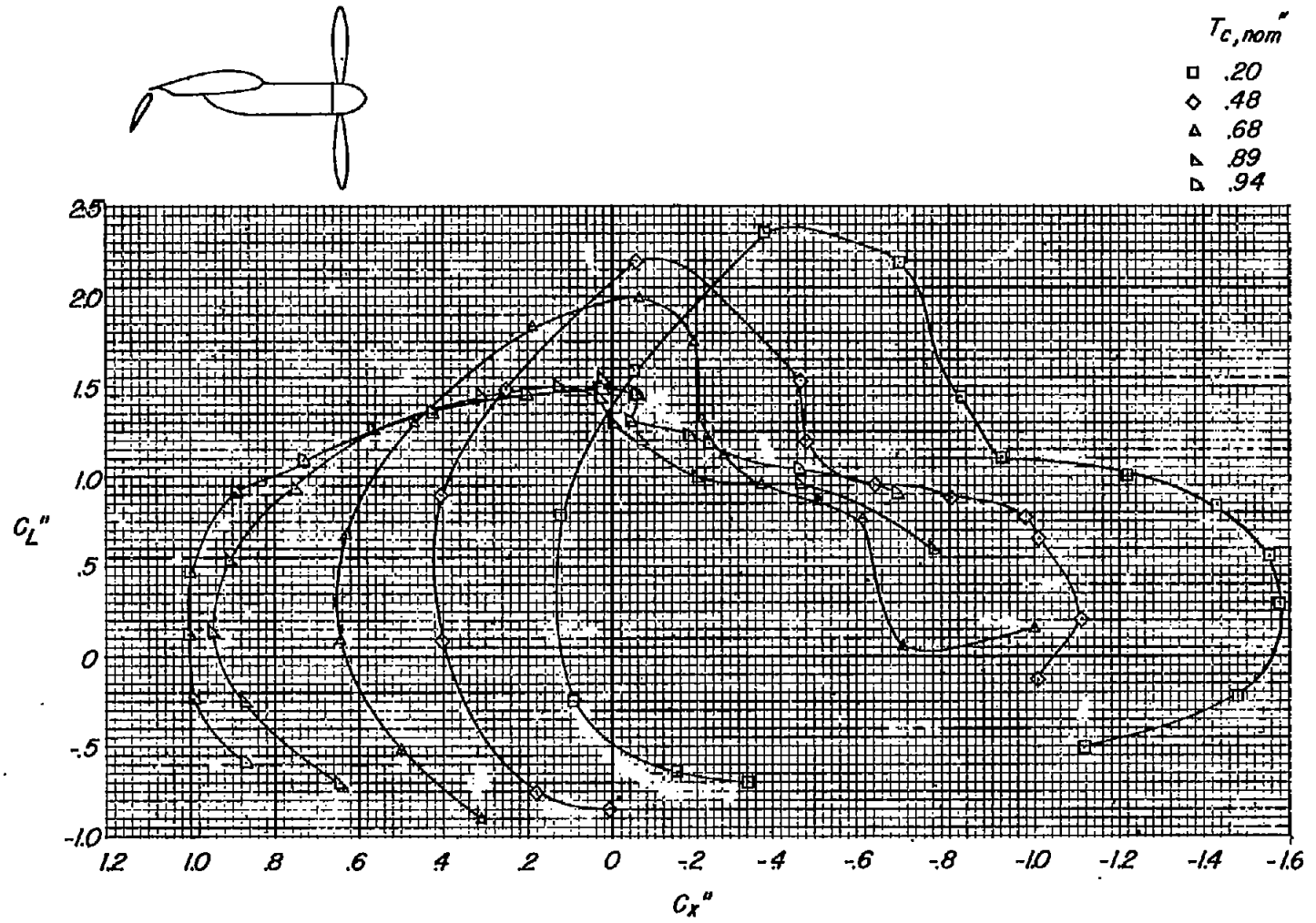

(e) Variation of C_L'' with C_X''.

Figure 11.- Concluded.

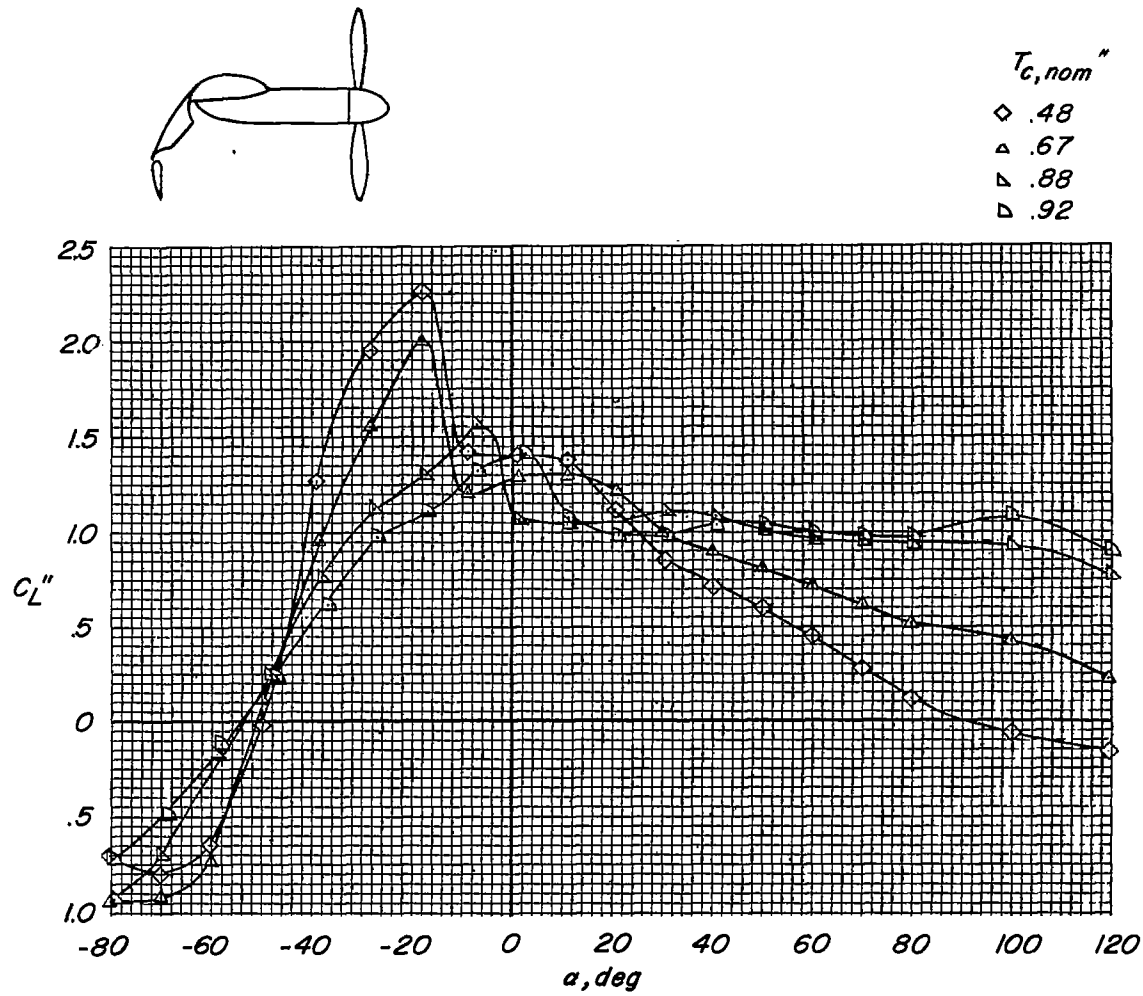

(a) Lift coefficient.

Figure 12.- Effect of slipstream. $\delta_{f,50} = 50^\circ$; $\delta_{f,30} = 40^\circ$; slat off; $\delta_h = 10^\circ$.

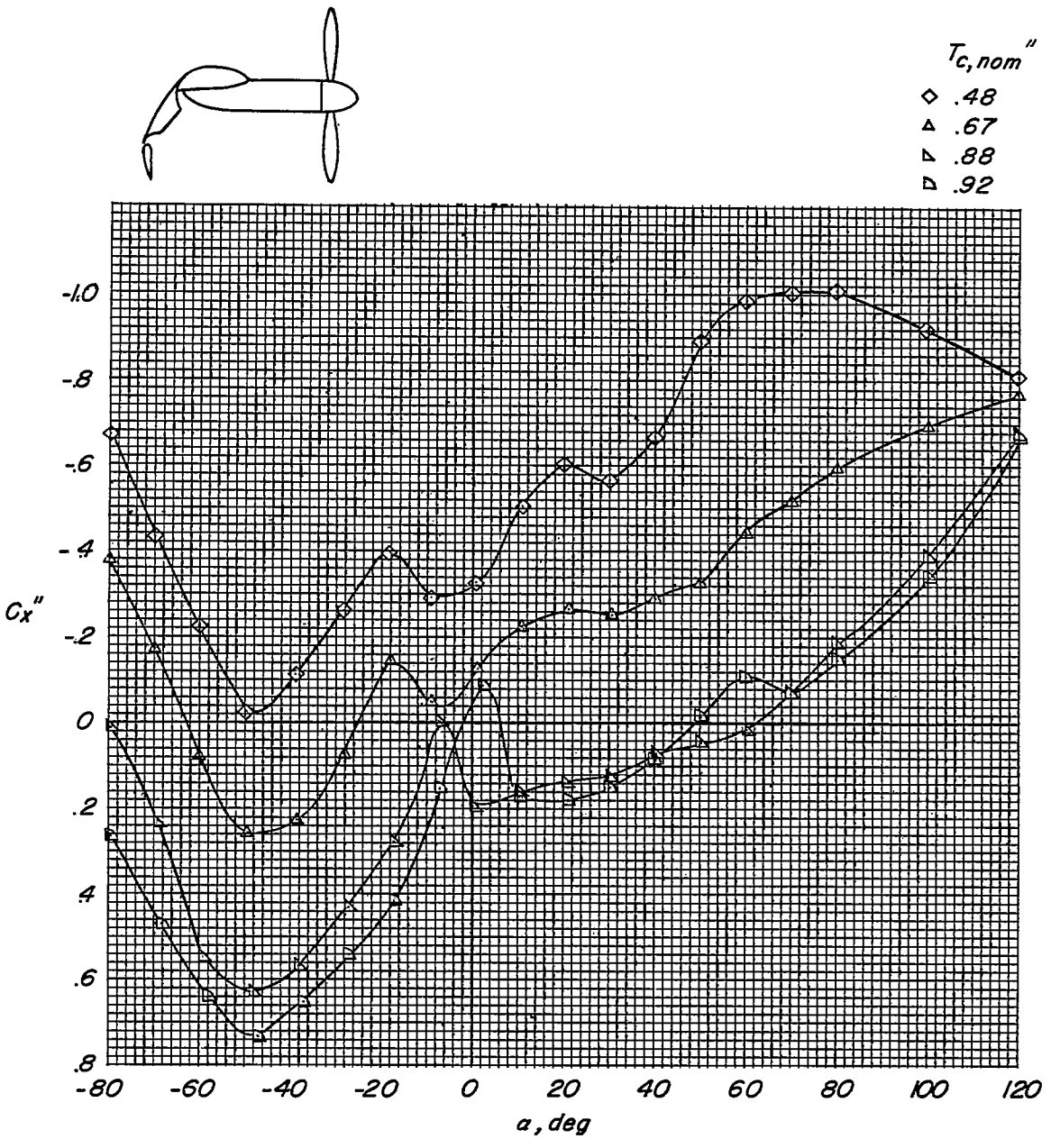

(b) Longitudinal-force coefficient.

Figure 12.- Continued.

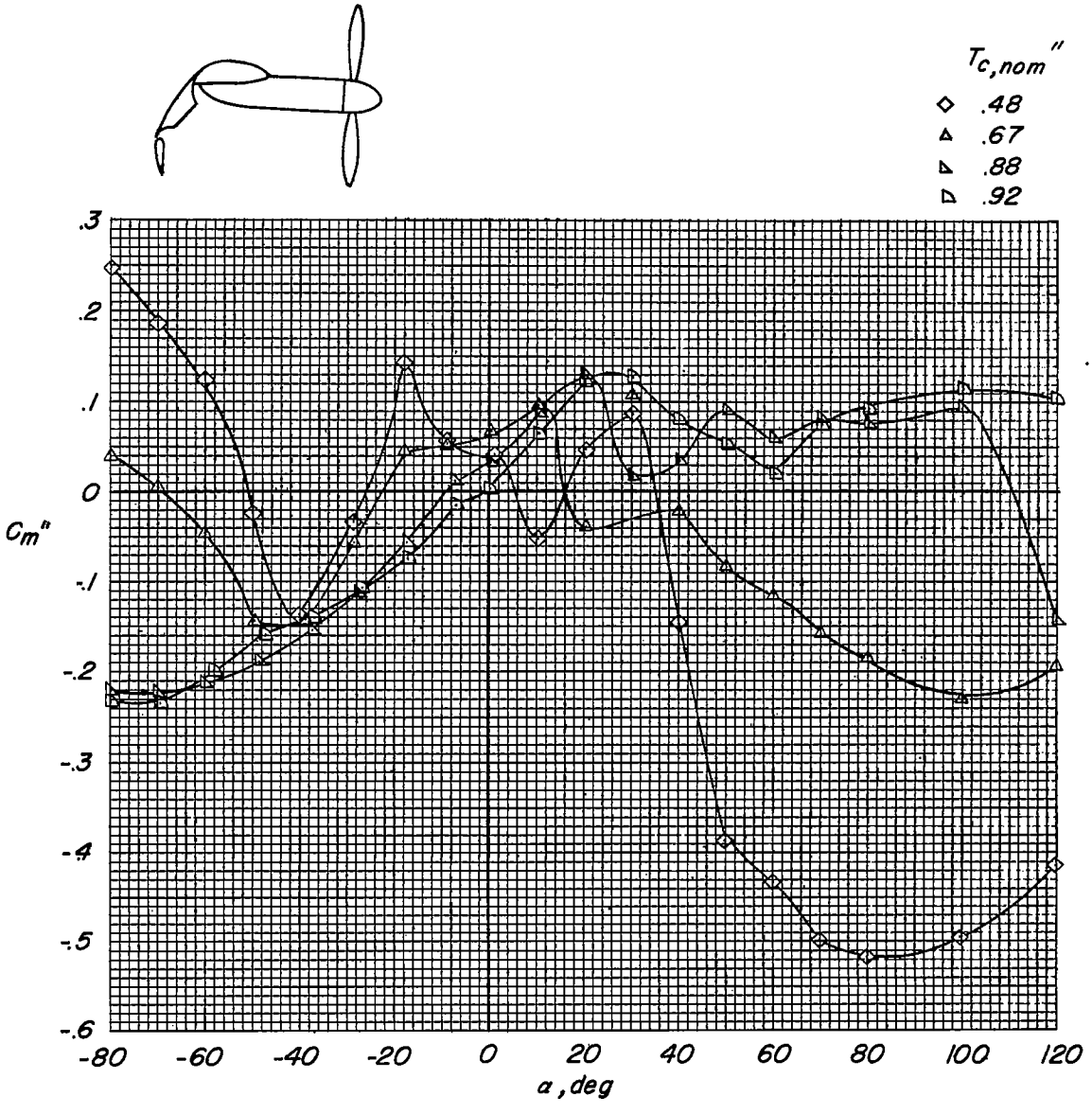

(c) Pitching-moment coefficient.

Figure 12.- Continued.

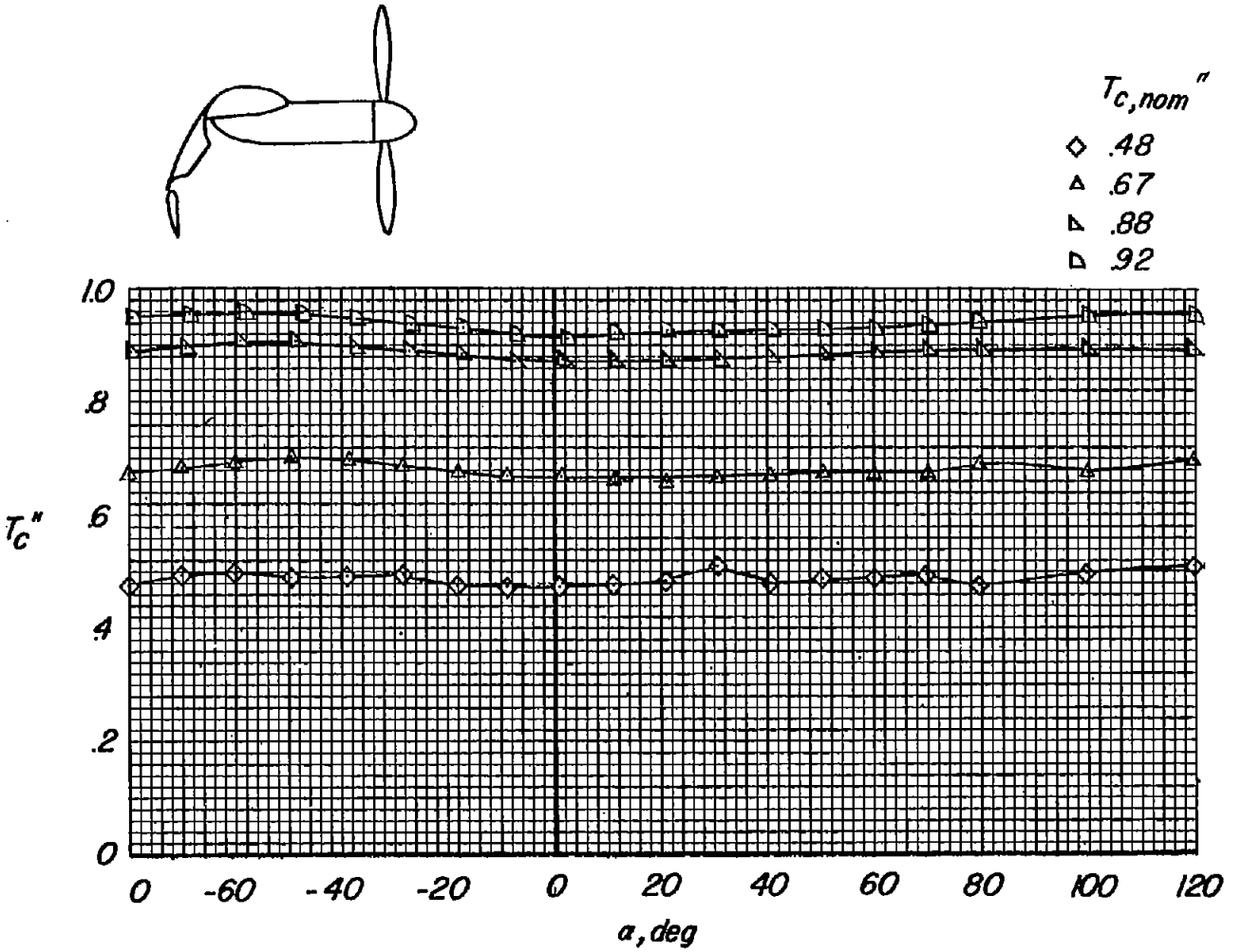

(d) Thrust coefficient.

Figure 12.- Continued.

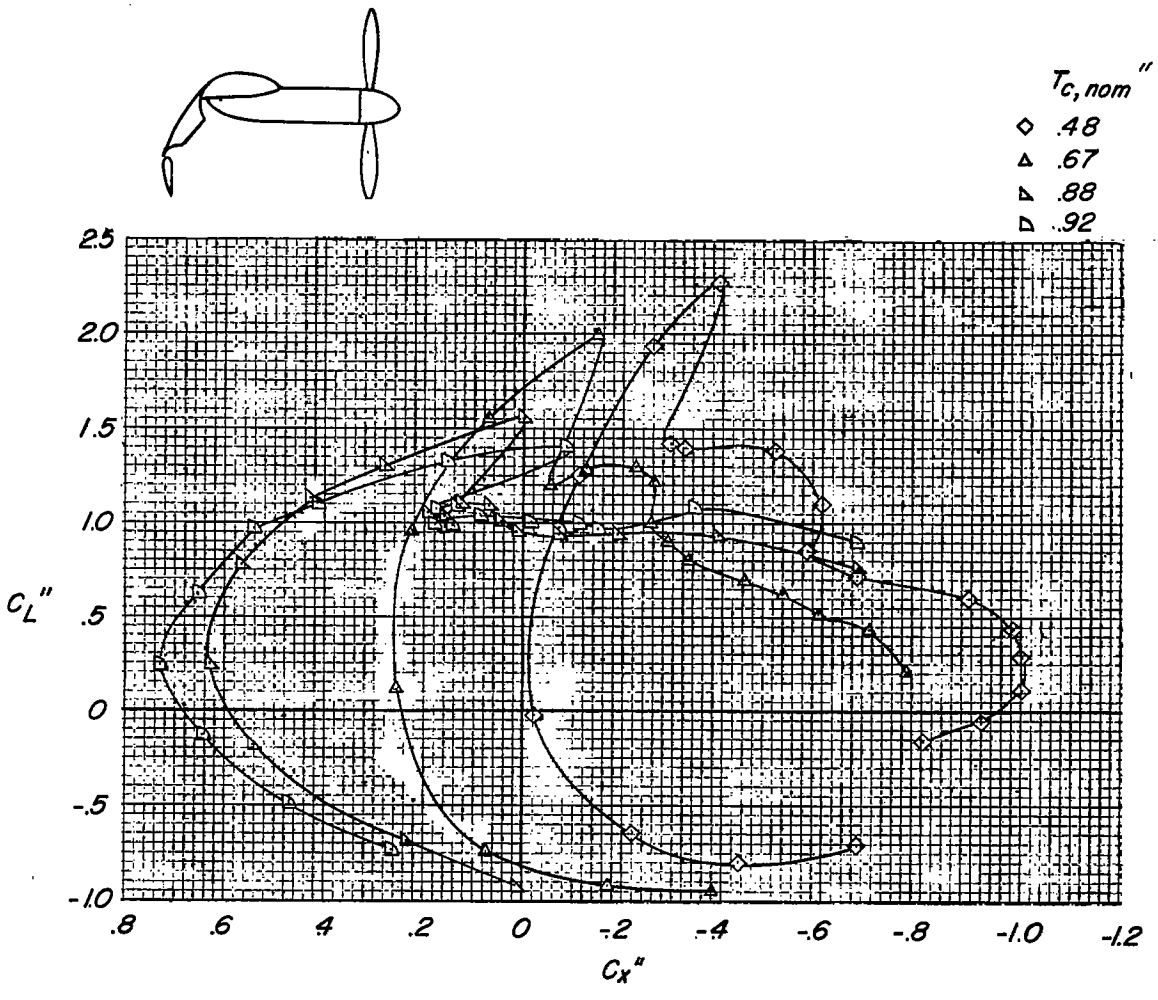

(e) Variation of C_L" with C_X".

Figure 12.- Concluded.

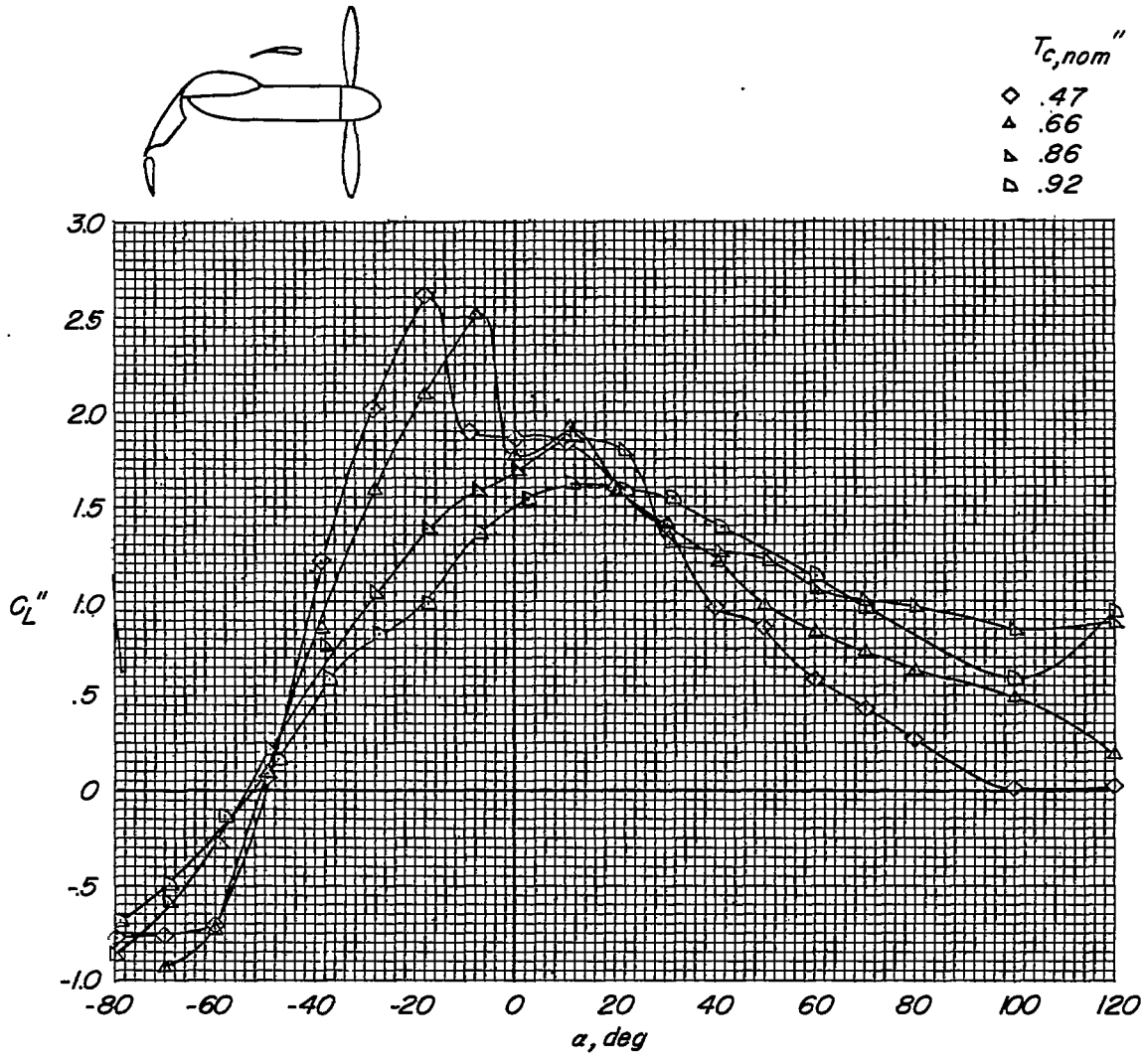

(a) Lift coefficient.

Figure 13.- Effect of slipstream. $\delta_{f,50} = 50°$; $\delta_{f,30} = 40°$; $\delta_s = 0°$; $\delta_h = 10°$.

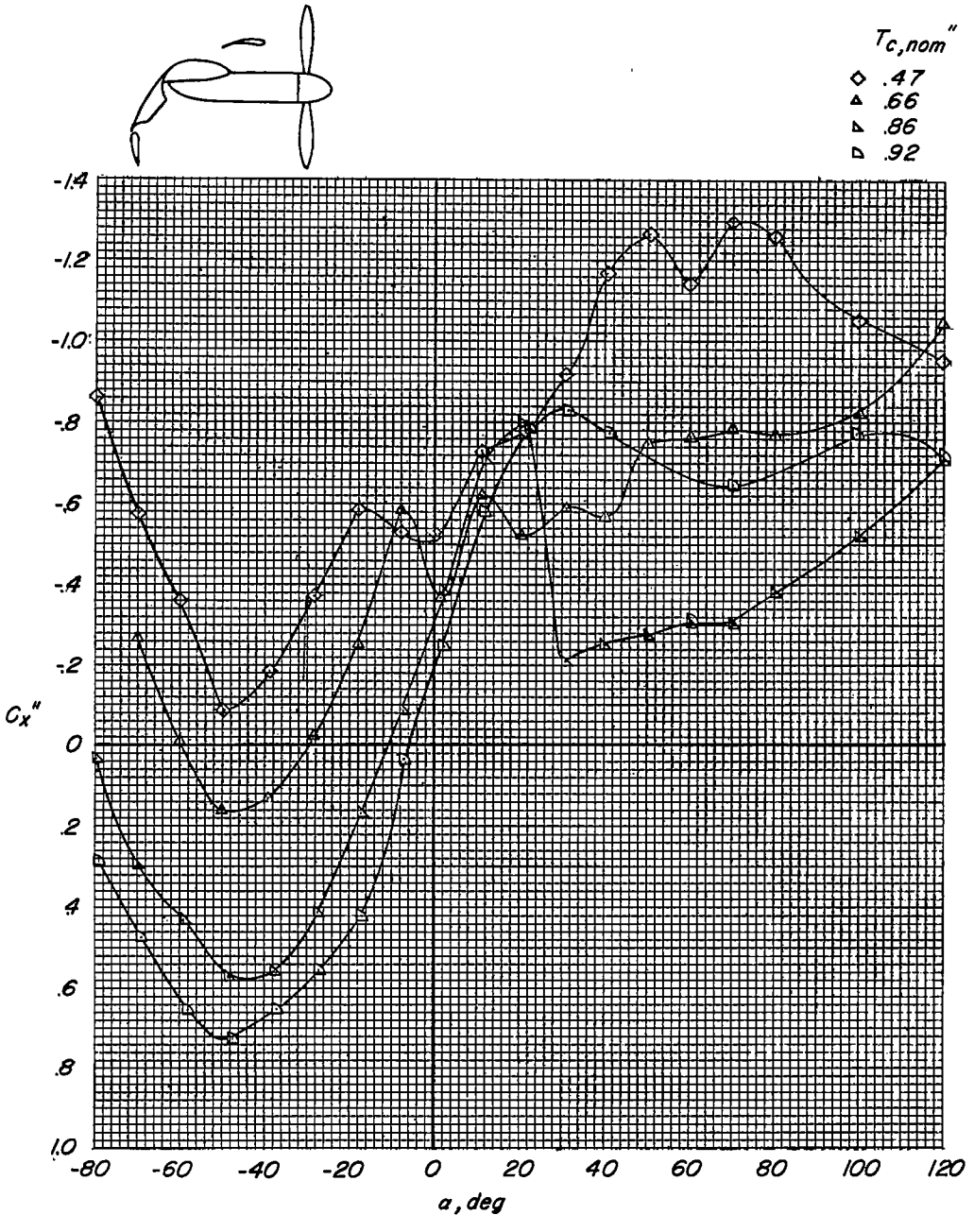

(b) Longitudinal-force coefficient.

Figure 13.- Continued.

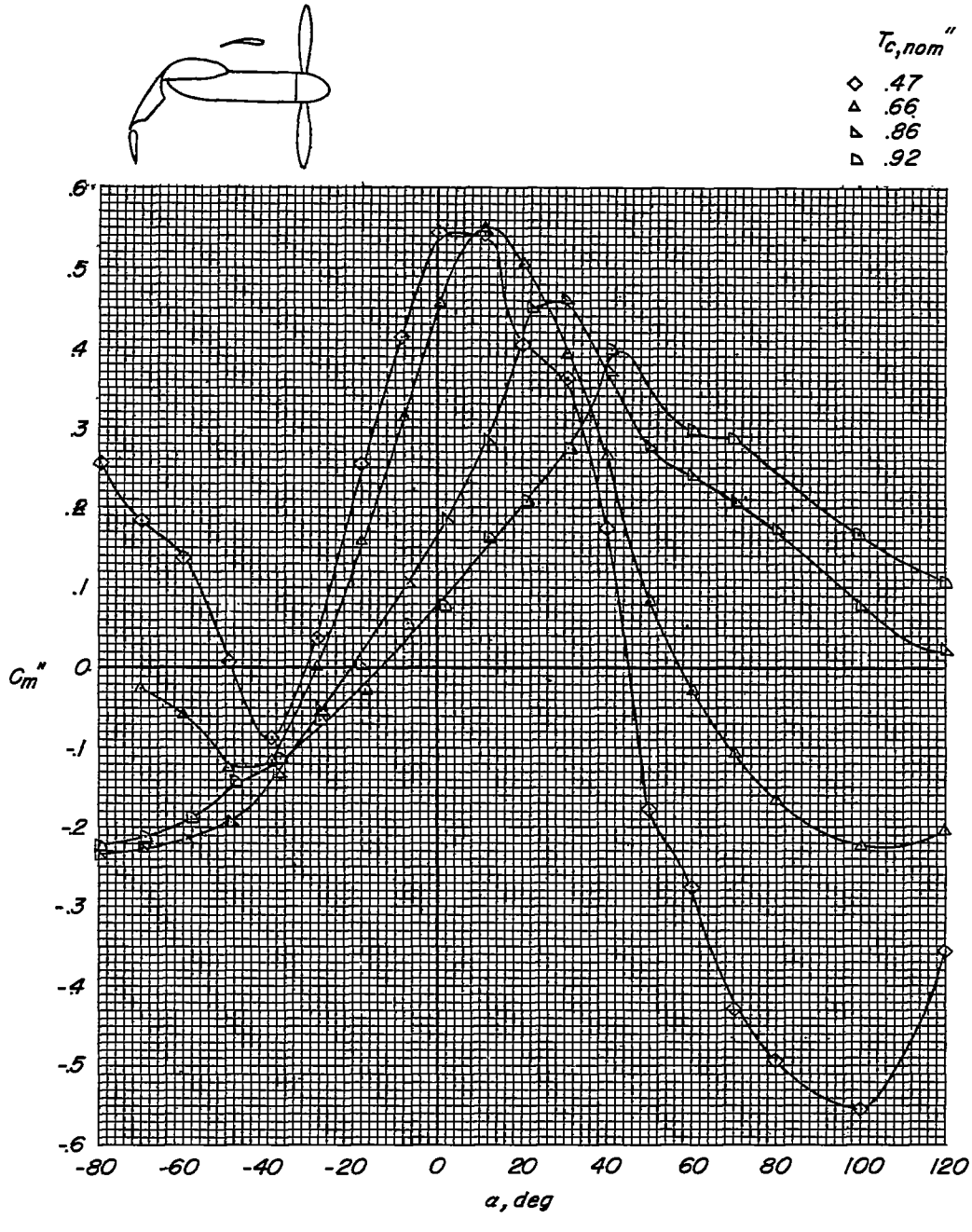

(c) Pitching-moment coefficient.

Figure 13.- Continued.

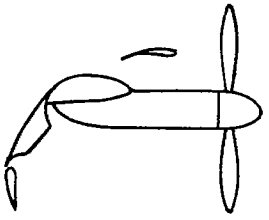

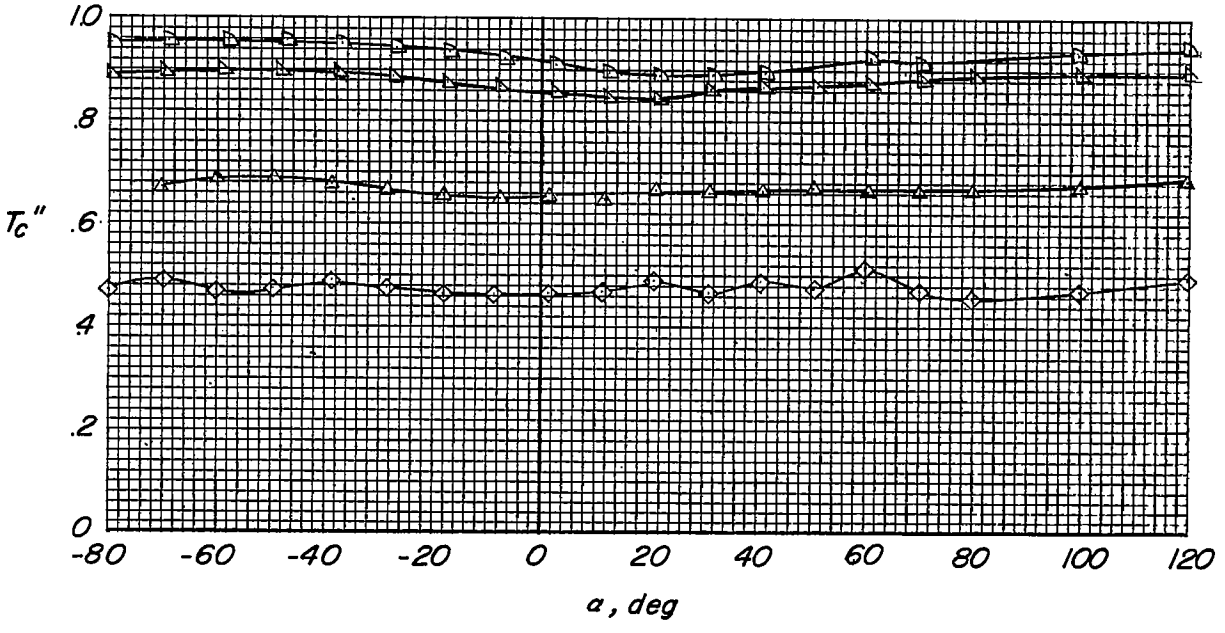

(d) Thrust coefficient.

Figure 13.- Continued.

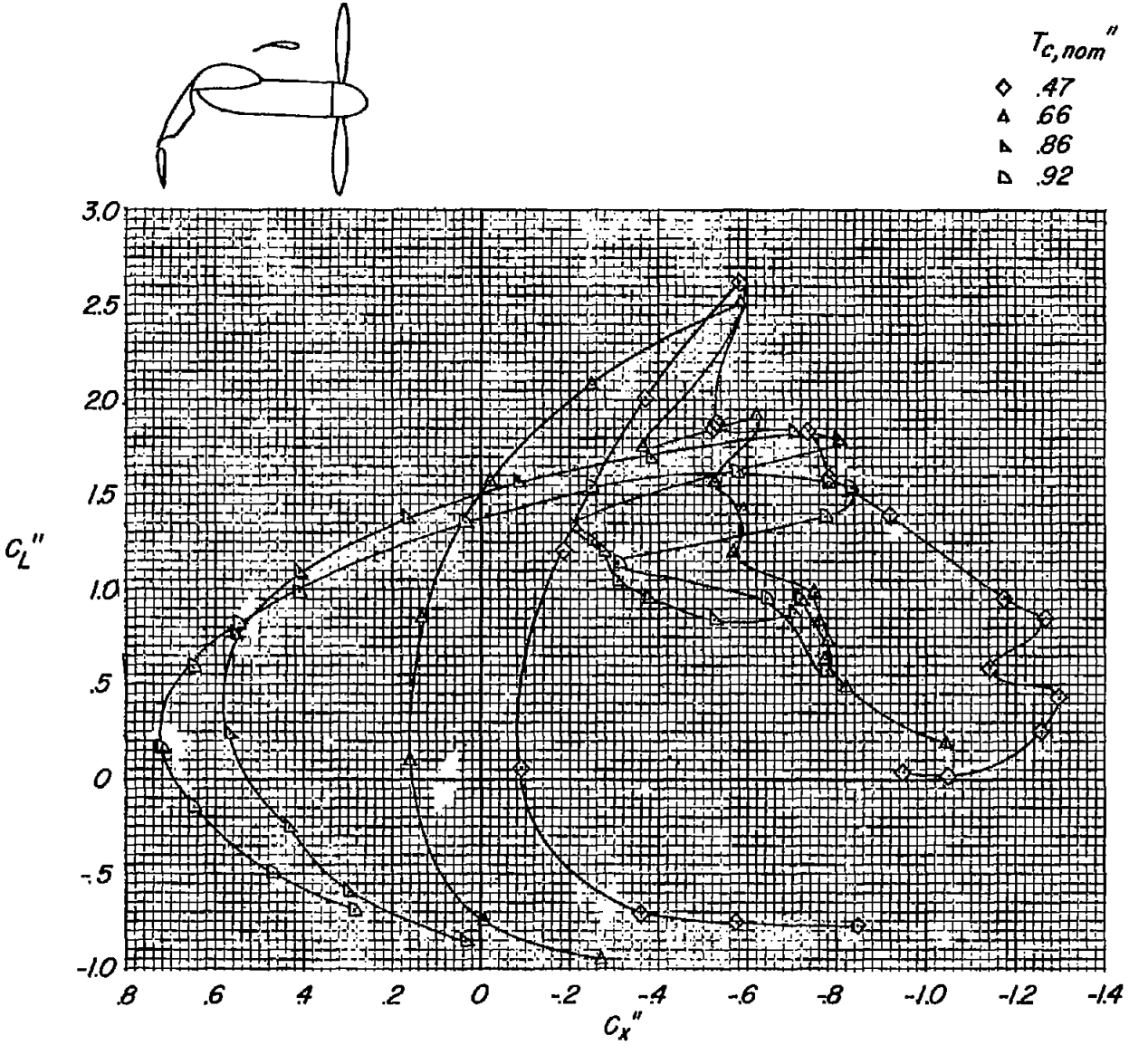

(e) Variation of C_L" with C_X".

Figure 13.- Concluded.

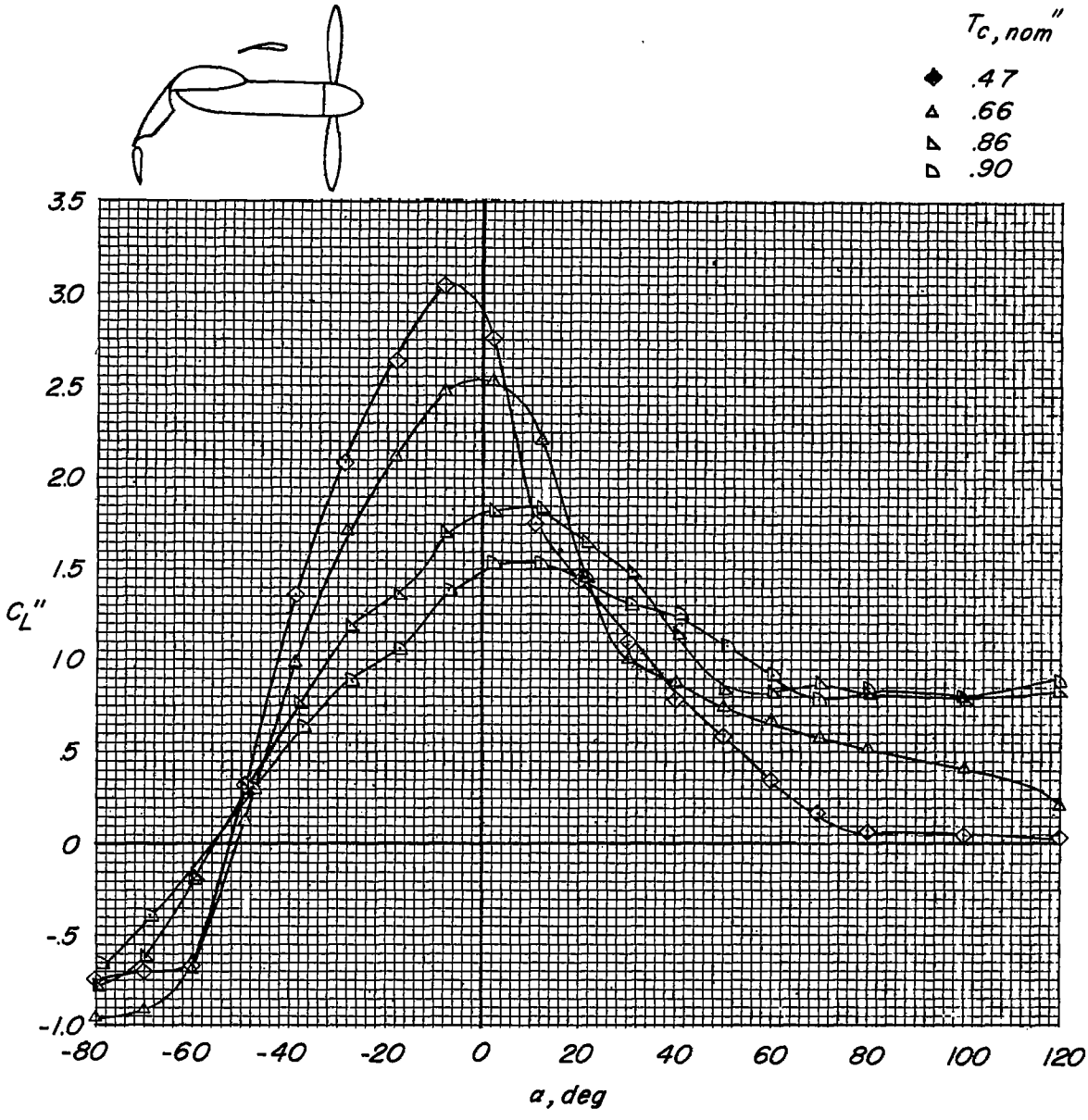

(a) Lift coefficient.

Figure 14.- Effect of slipstream. $\delta_{f,50} = 50°$; $\delta_{f,30} = 40°$; $\delta_s = 10°$; stabilizer off.

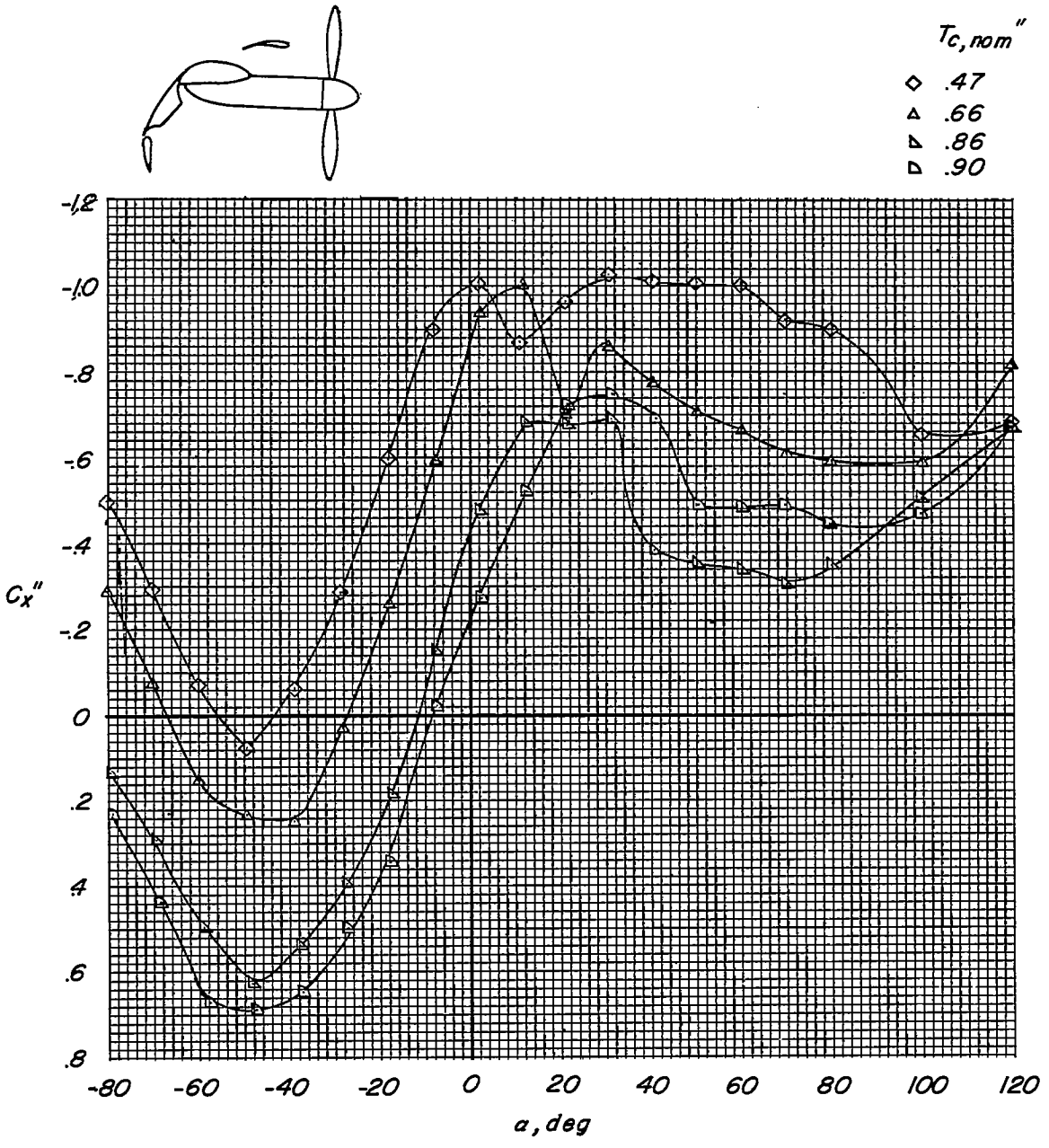

(b) Longitudinal-force coefficient.

Figure 14.- Continued.

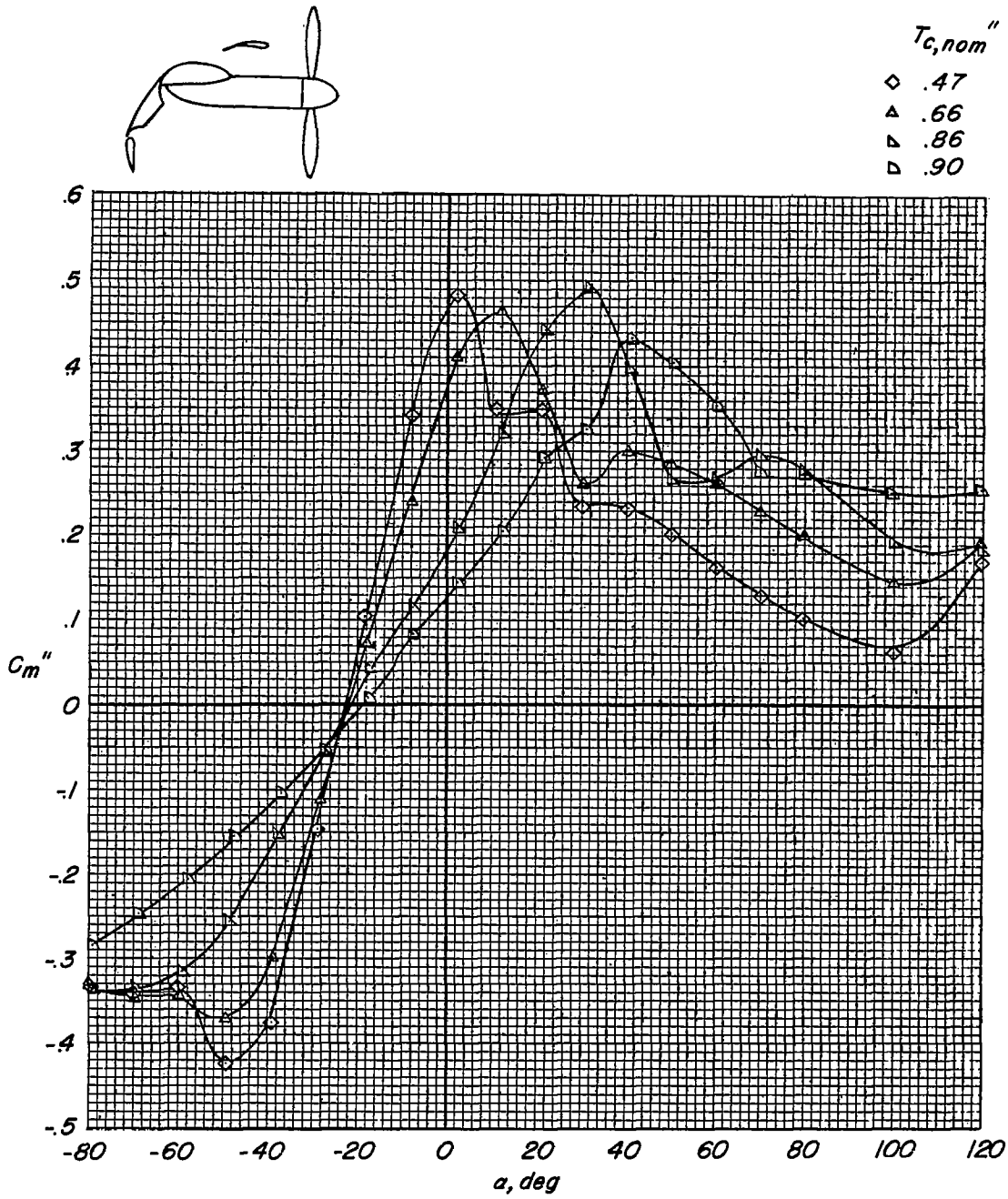

(c) Pitching-moment coefficient.

Figure 14.- Continued.

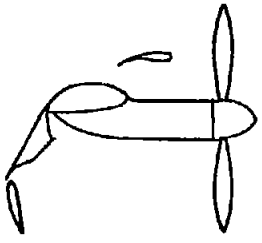

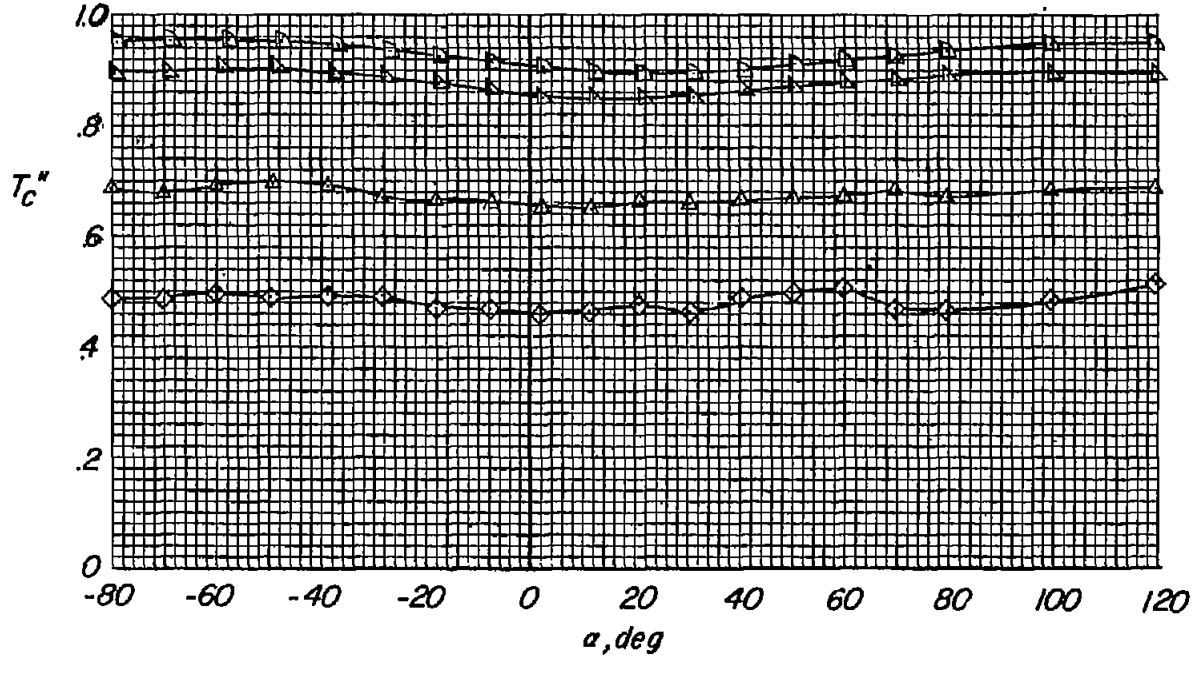

(d) Thrust coefficient.

Figure 14.- Continued.

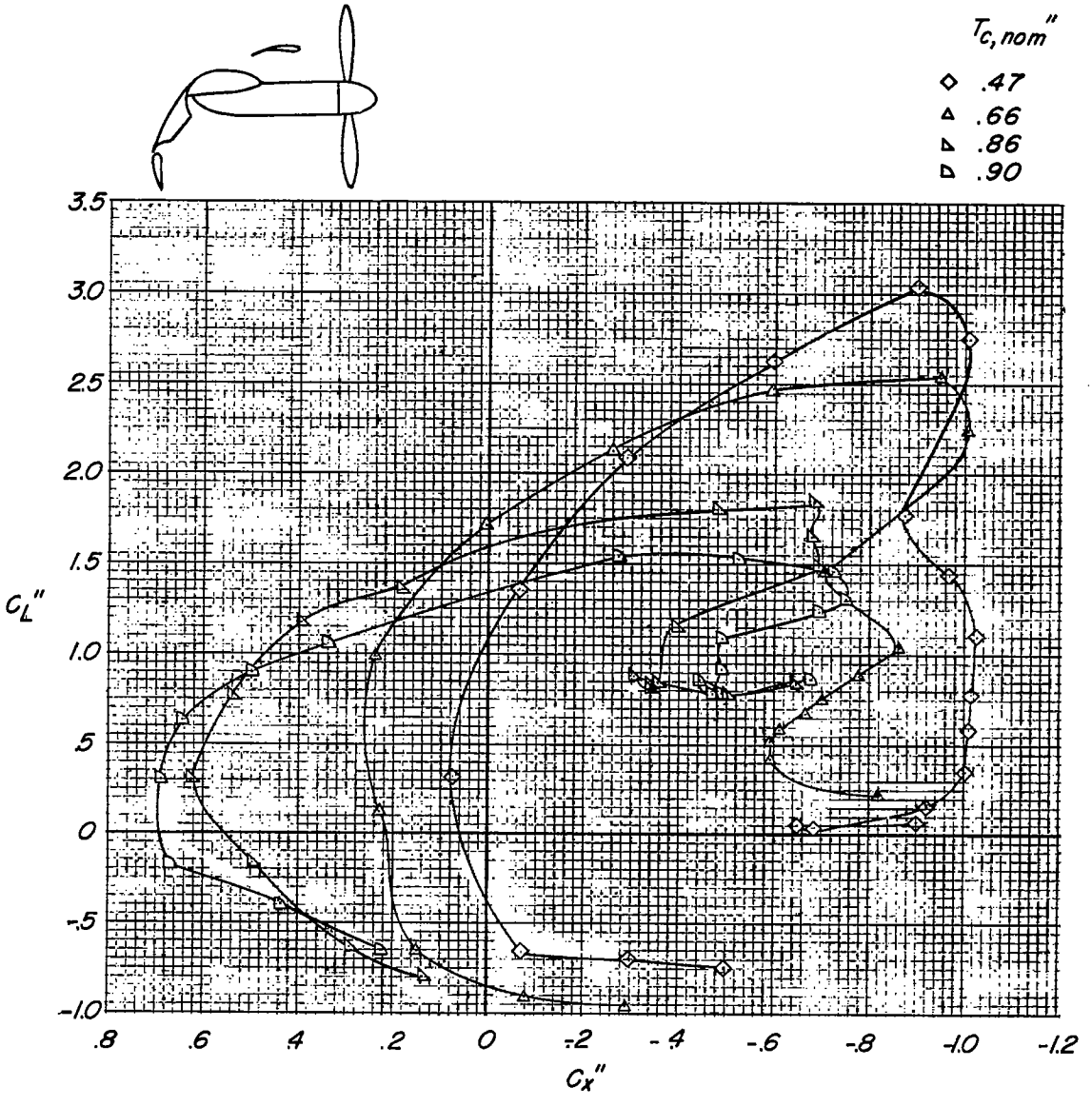

(e) Variation of C_L'' with C_X''.

Figure 14.- Concluded.

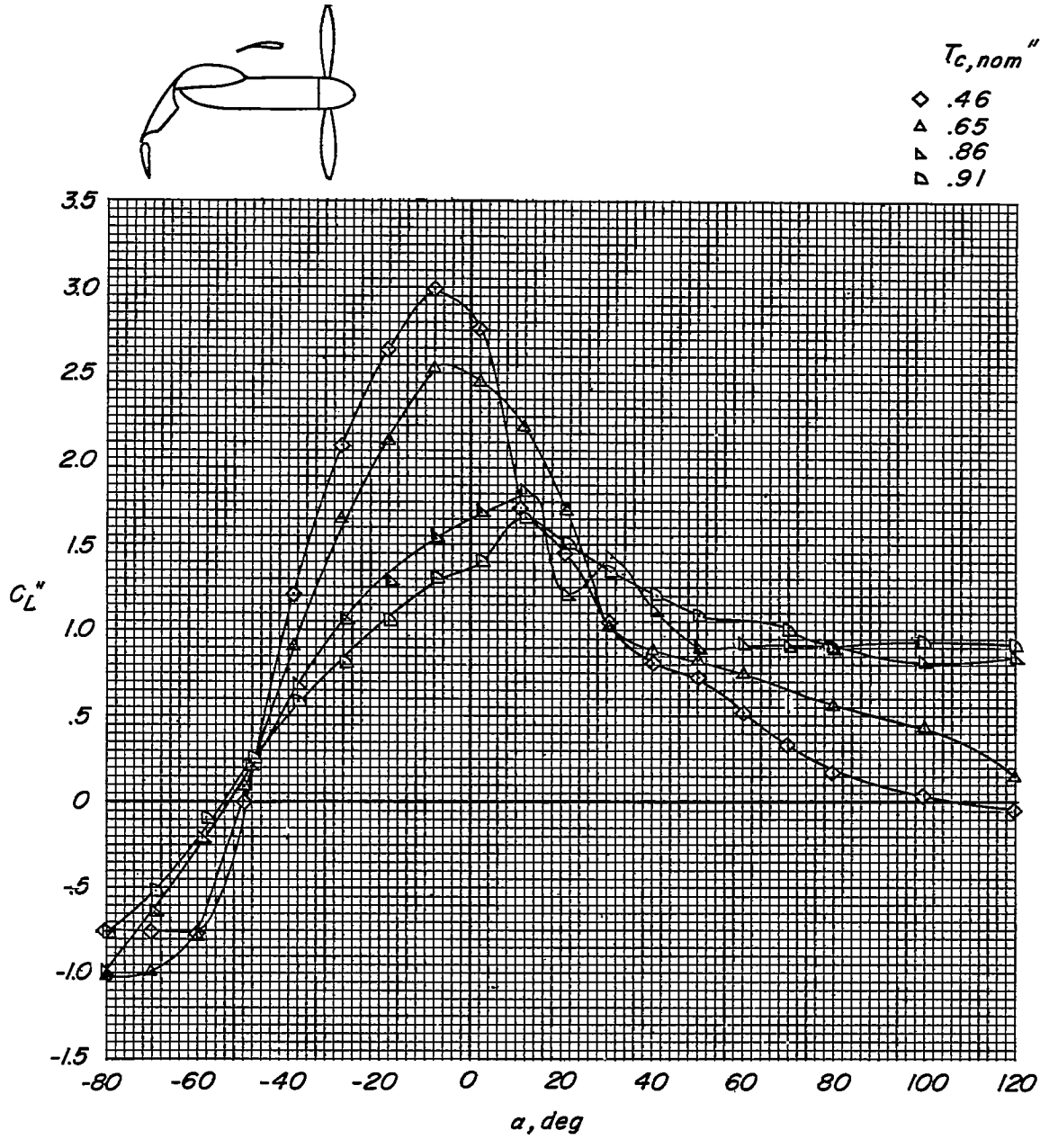

(a) Lift coefficient.

Figure 15.- Effect of slipstream. $\delta_{f,30} = 40^\circ$; $\delta_{f,50} = 50^\circ$; $\delta_s = 10^\circ$; $\delta_h = 0^\circ$.

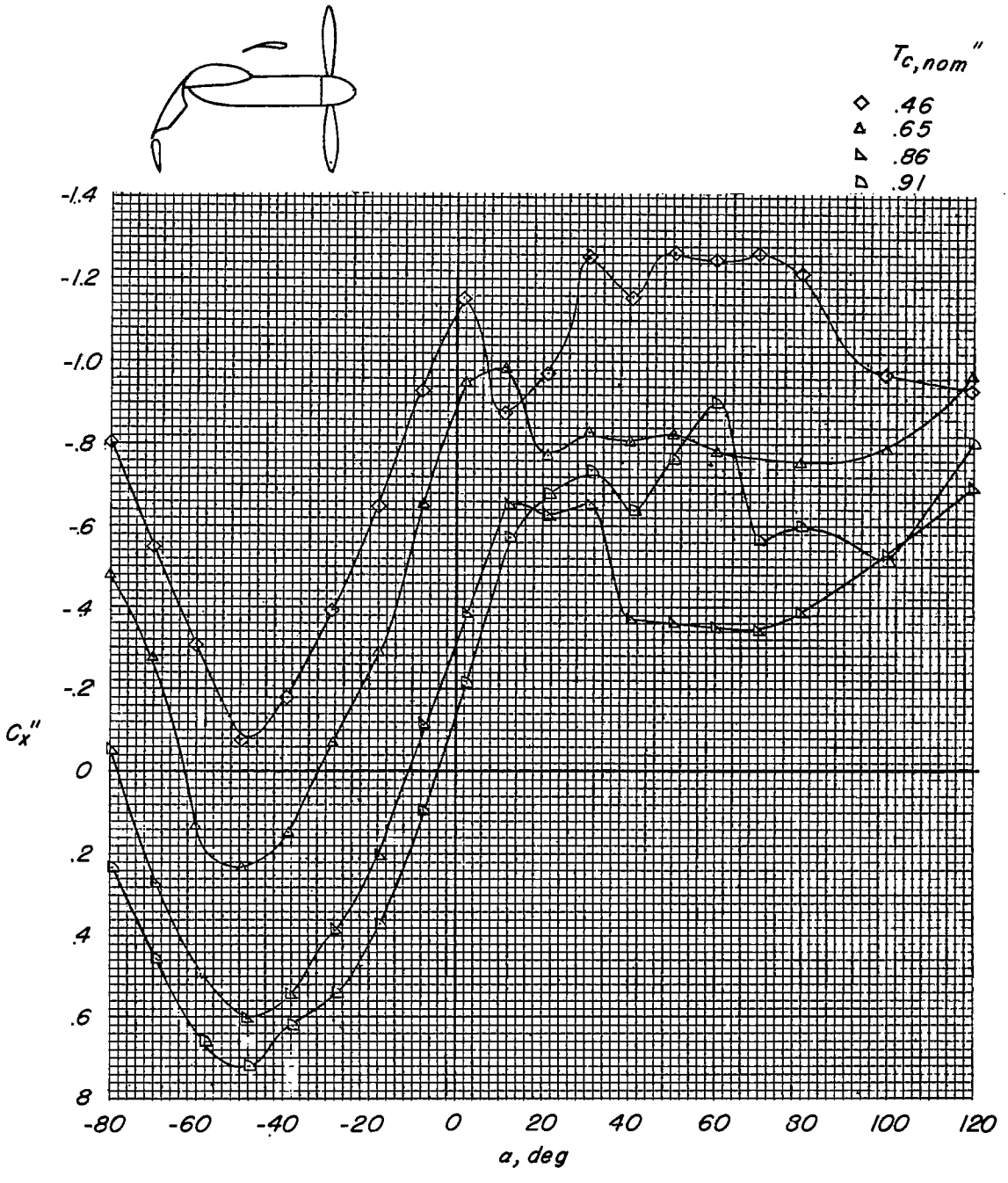

(b) Longitudinal-force coefficient.

Figure 15.- Continued.

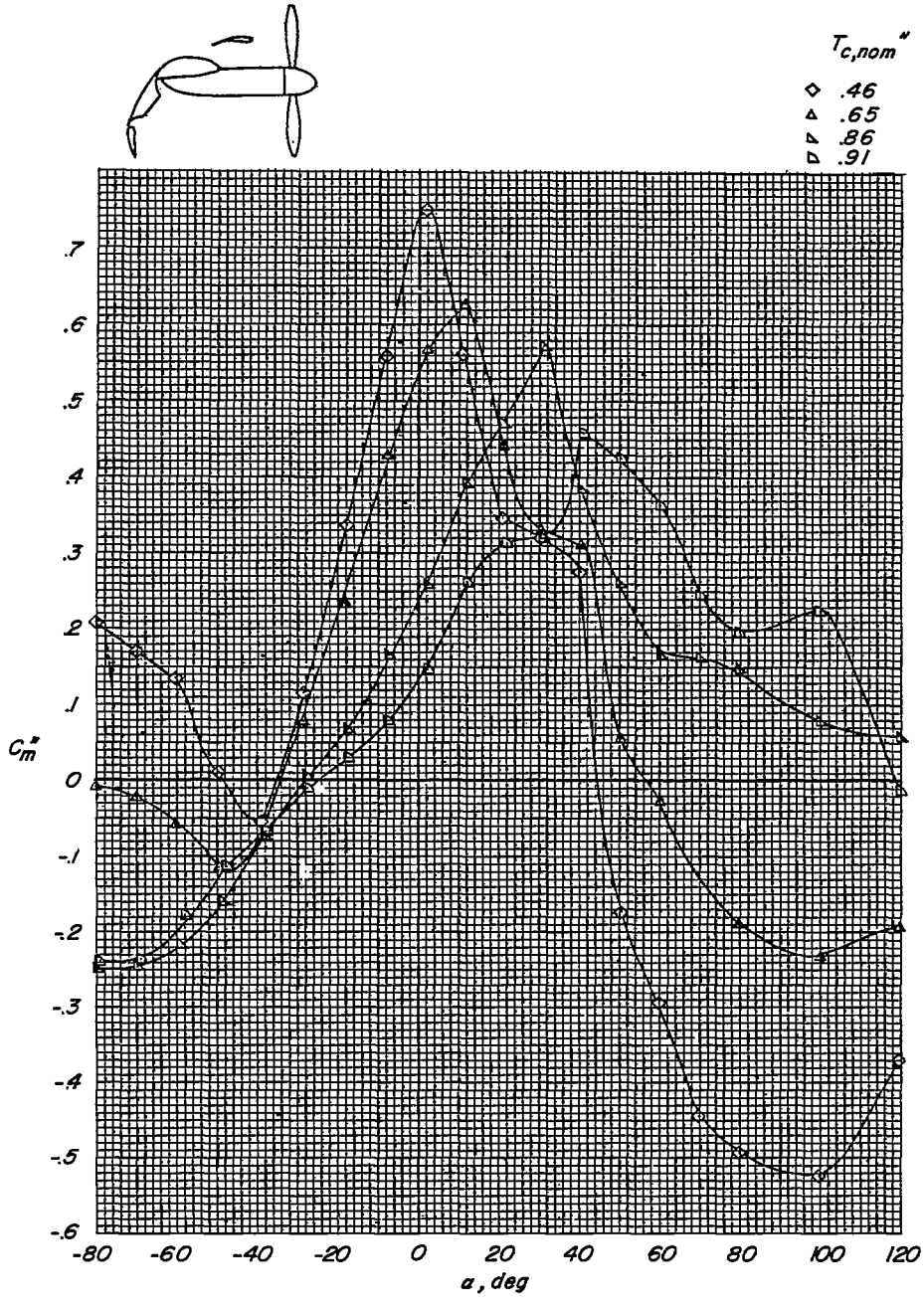

(c) Pitching-moment coefficient.

Figure 15.- Continued.

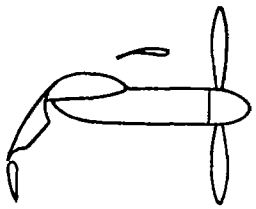

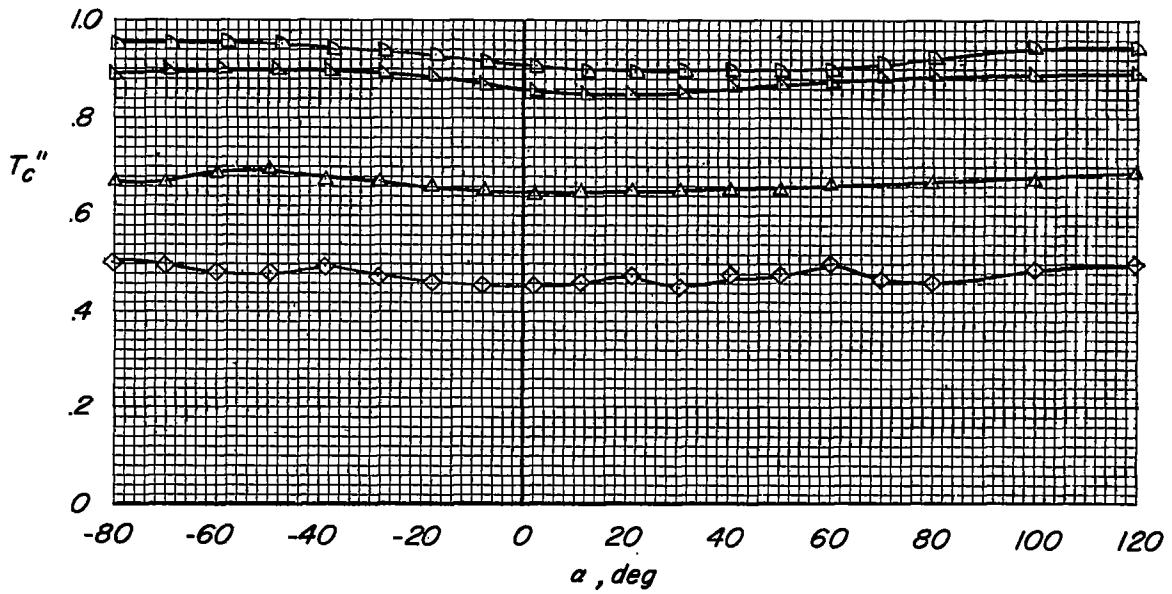

(d) Thrust coefficient.

Figure 15.- Continued.

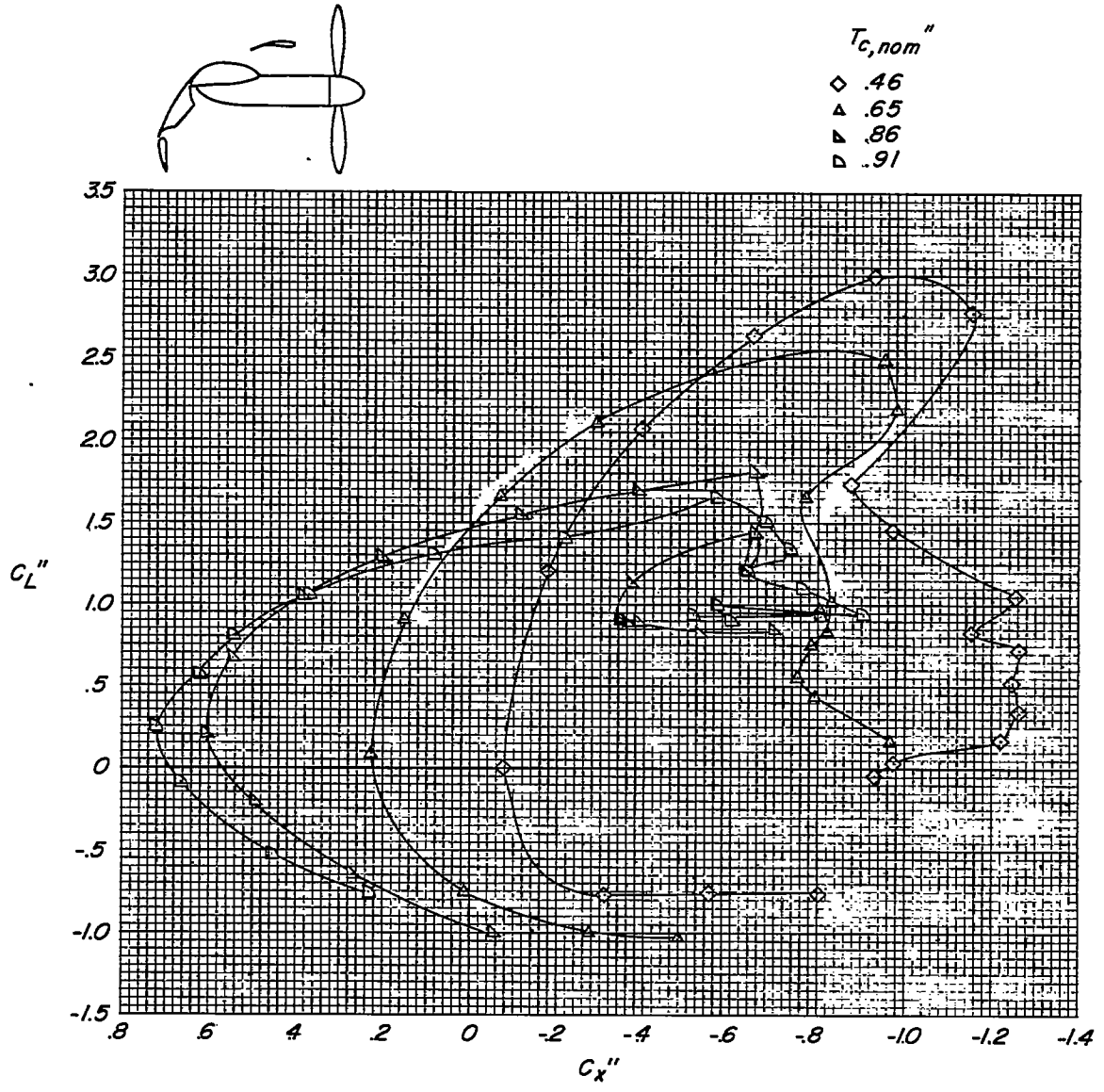

(e) Variation of C_L" with C_X".

Figure 15.- Concluded.

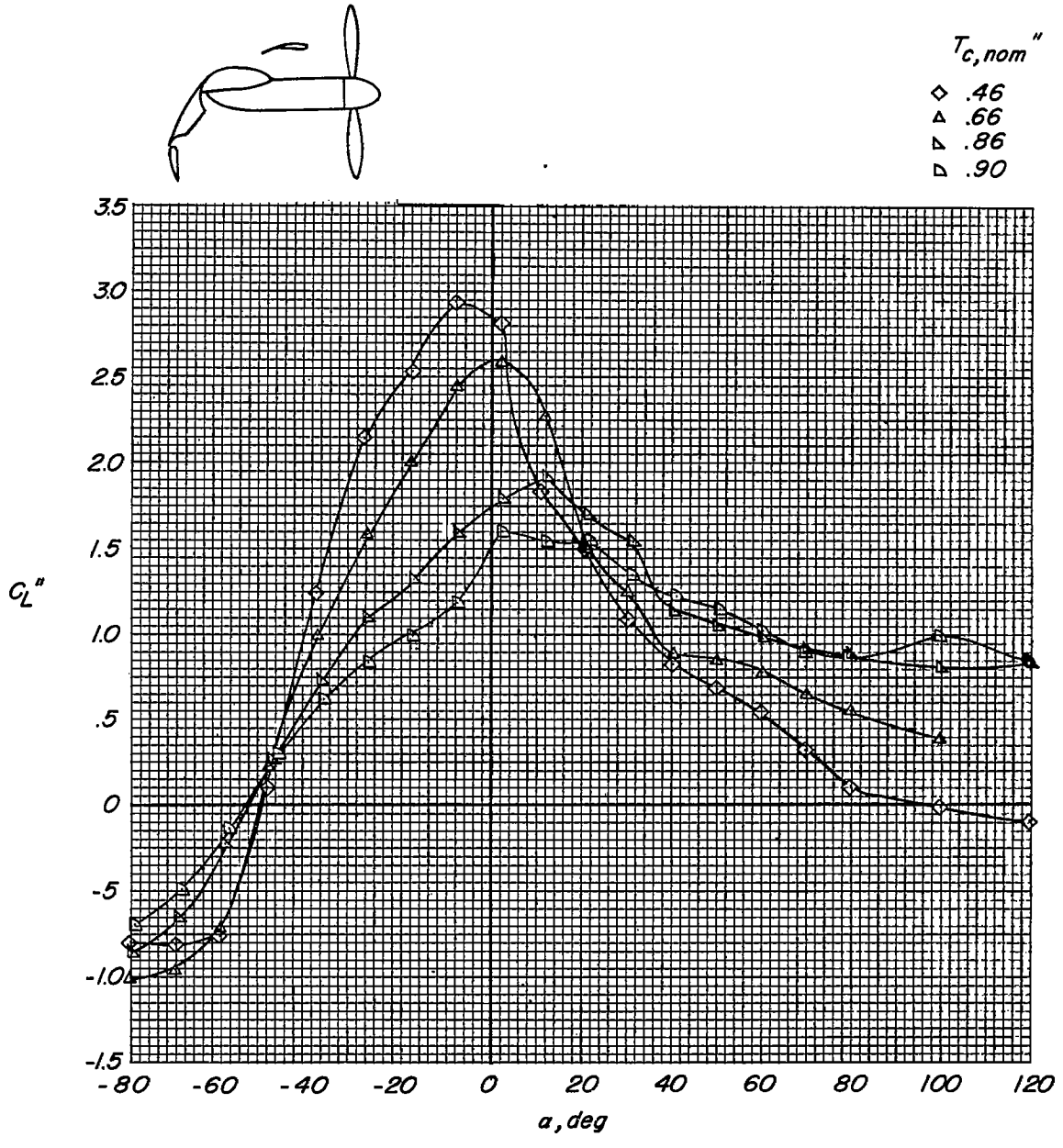

(a) Lift coefficient.

Figure 16.- Effect of slipstream. $\delta_{f,30} = 40°$; $\delta_{f,50} = 50°$; $\delta_s = 10°$; $\delta_h = 10°$.

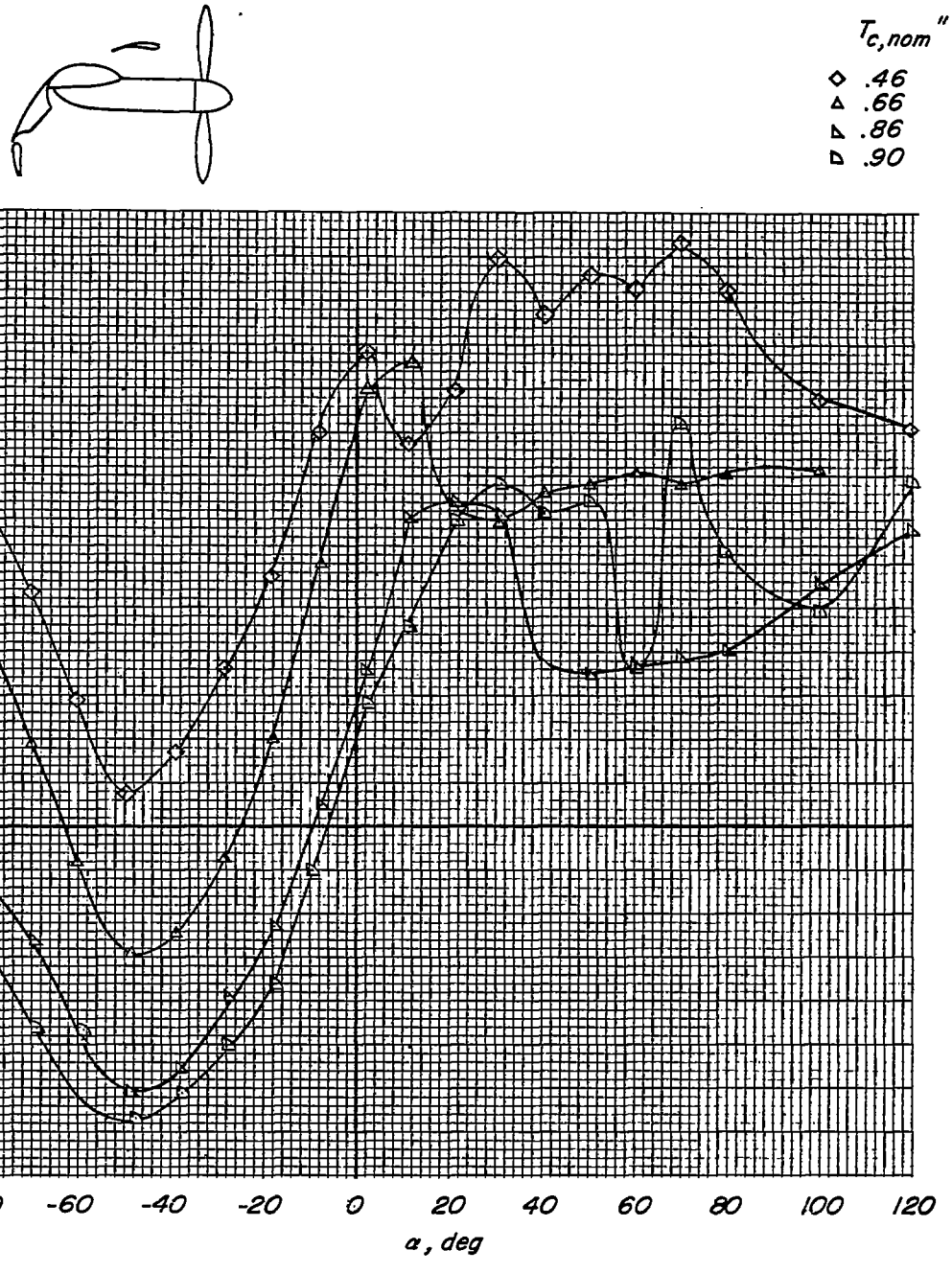

(b) Longitudinal-force coefficient.

Figure 16.- Continued.

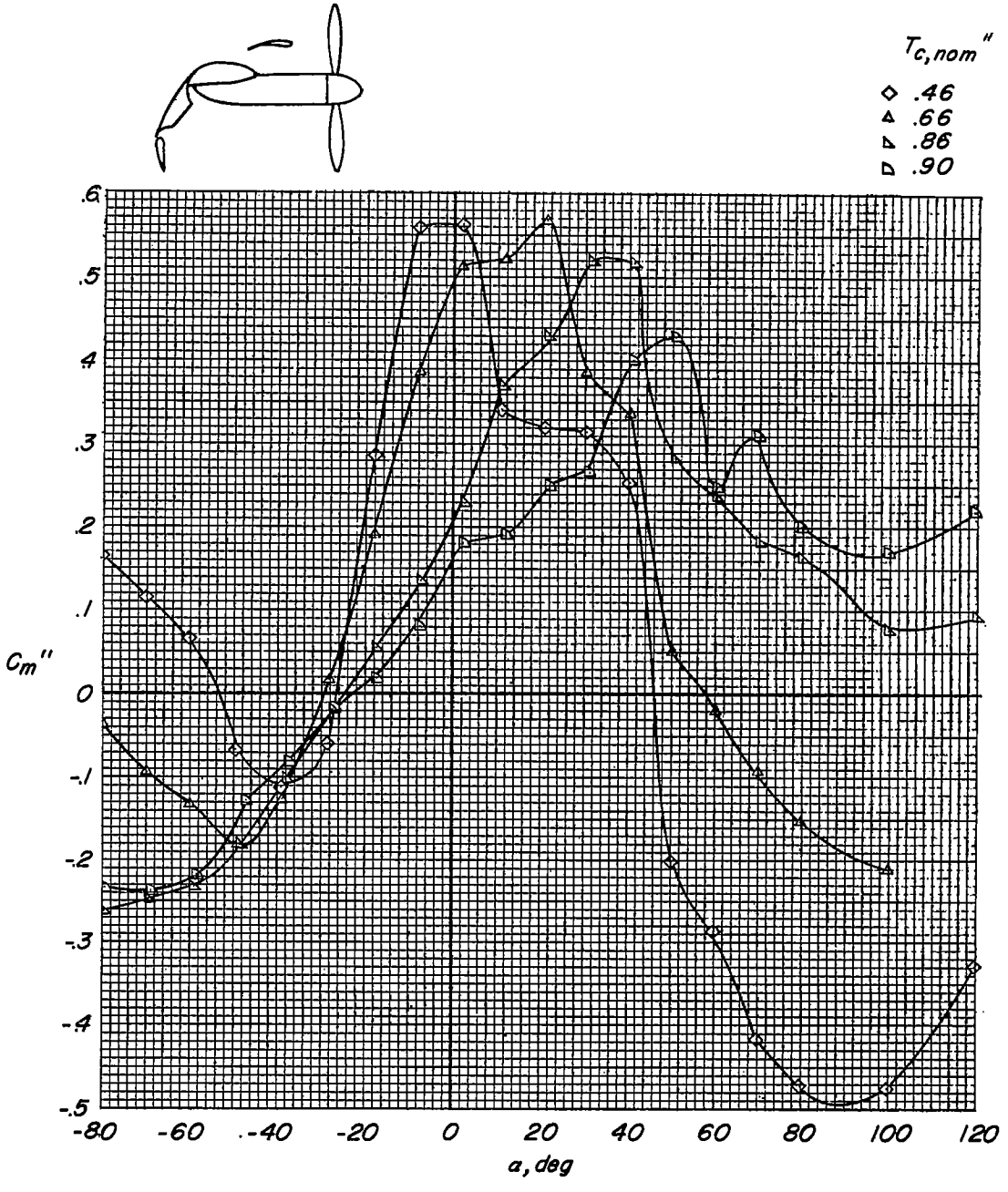

(c) Pitching-moment coefficient.

Figure 16.- Continued.

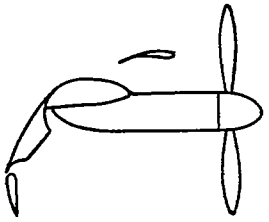

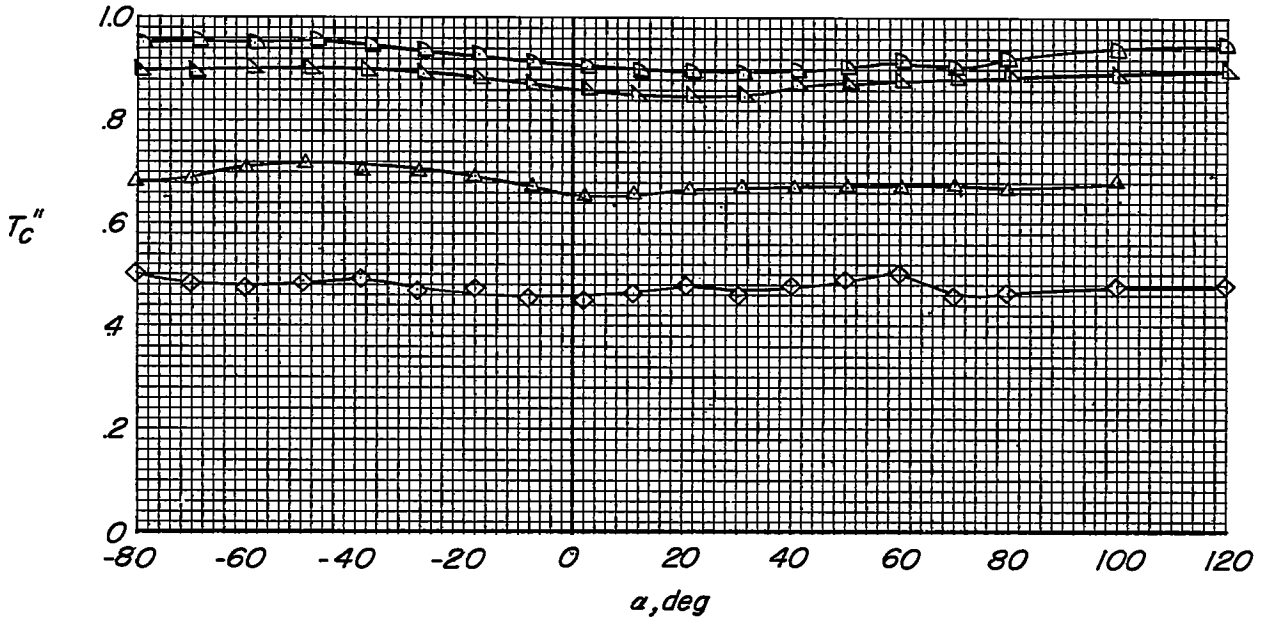

(d) Thrust coefficient.

Figure 16.- Continued.

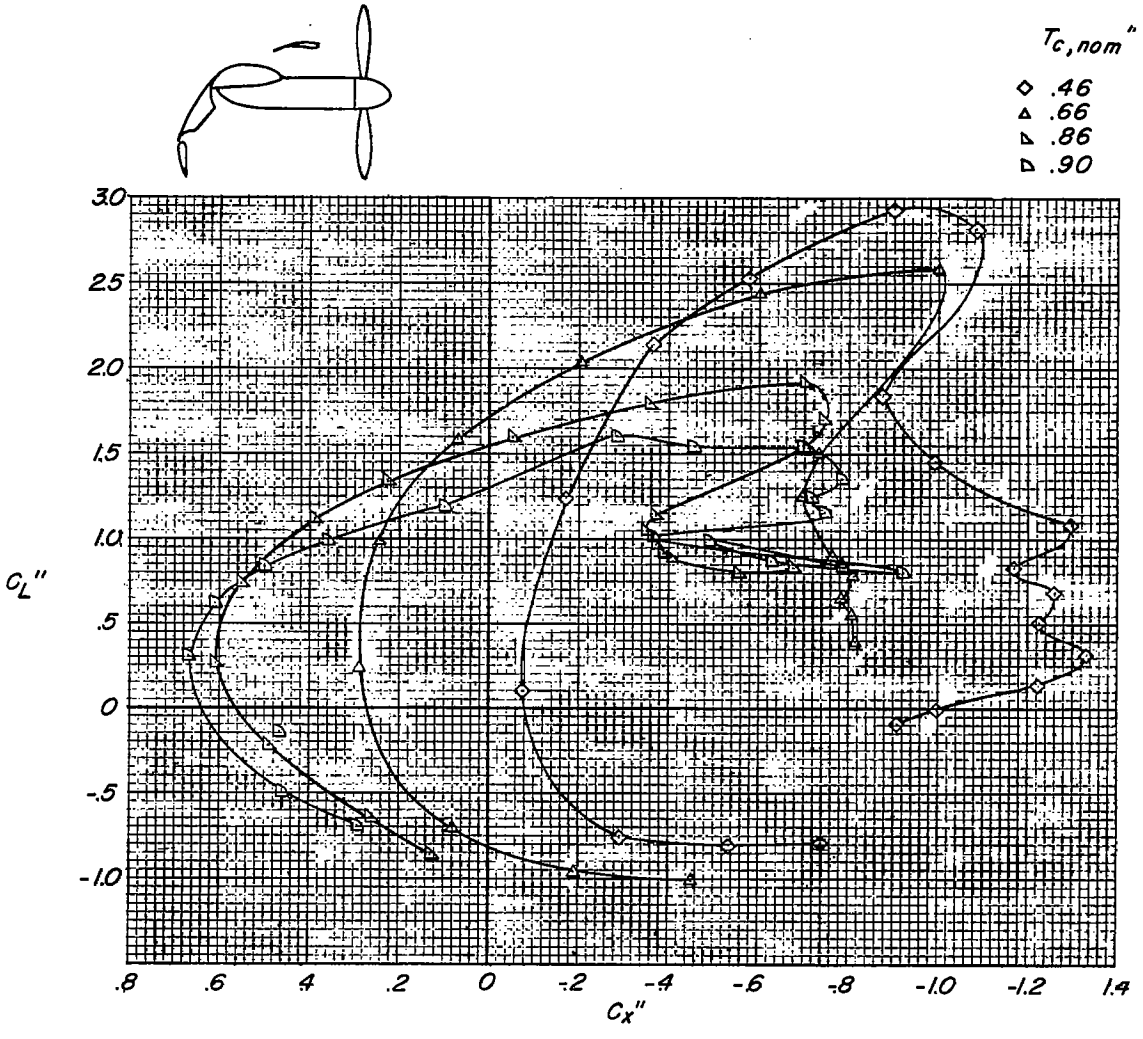

(e) Variation of C_L" with C_X".

Figure 16.- Concluded.

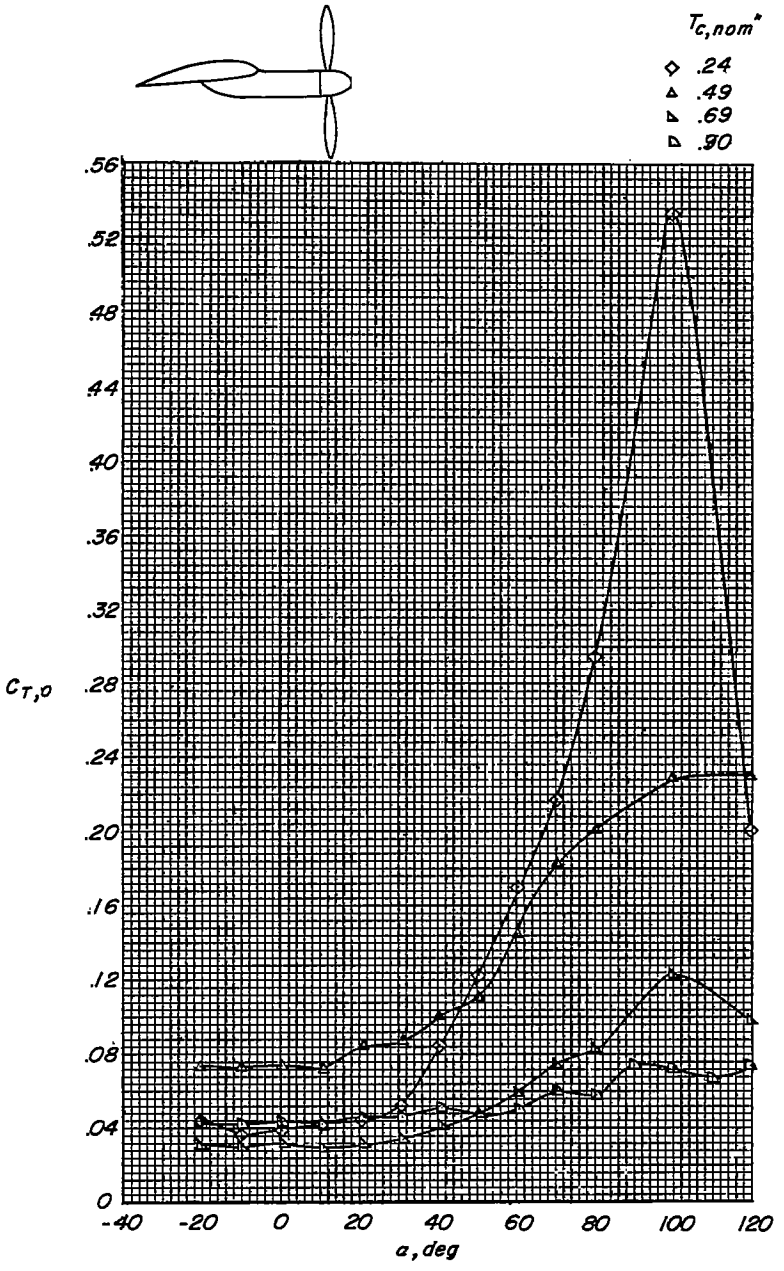

(a) Thrust coefficient. Outboard propeller.

Figure 17.- Propeller characteristics. $\delta_{f,50} = 0^{\circ}$; $\delta_{f,30} = 0^{\circ}$; slat off; stabilizer off.

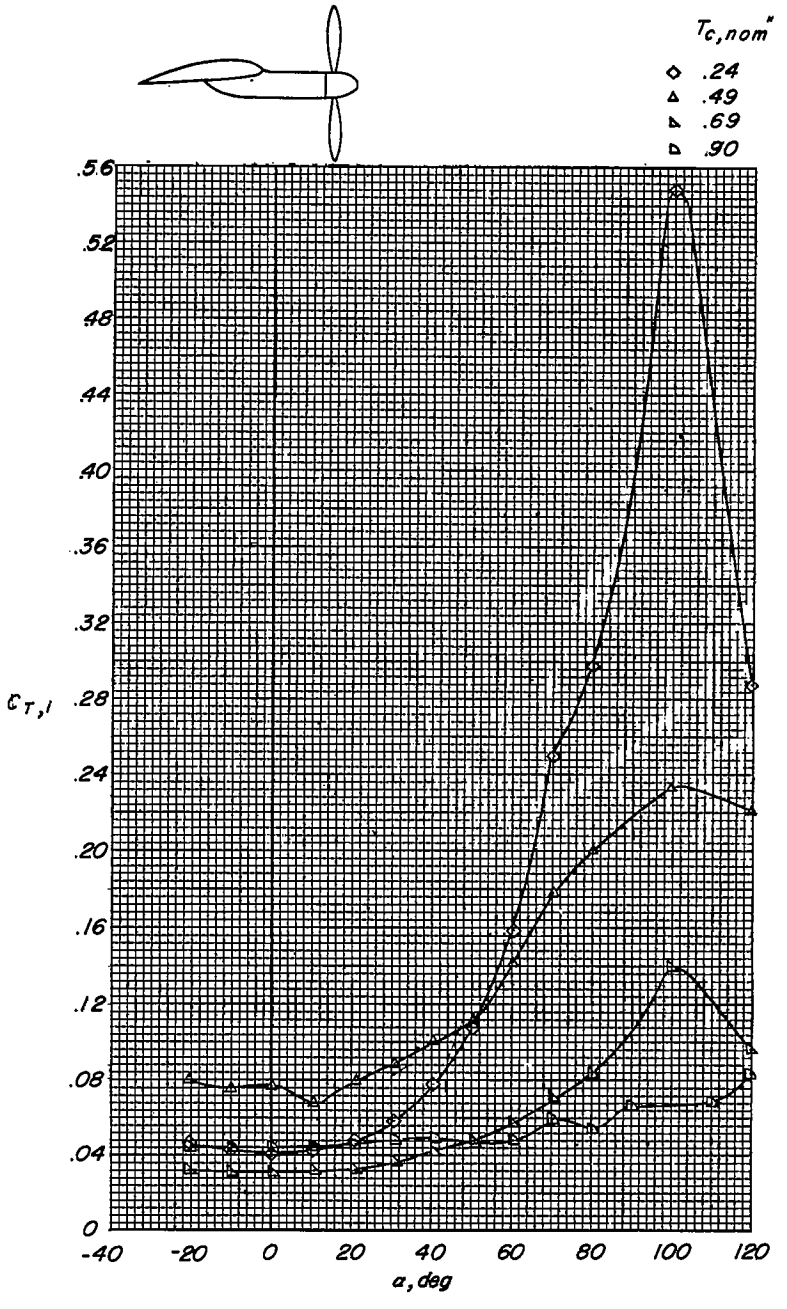

(b) Thrust coefficient. Inboard propeller.

Figure 17.- Continued.

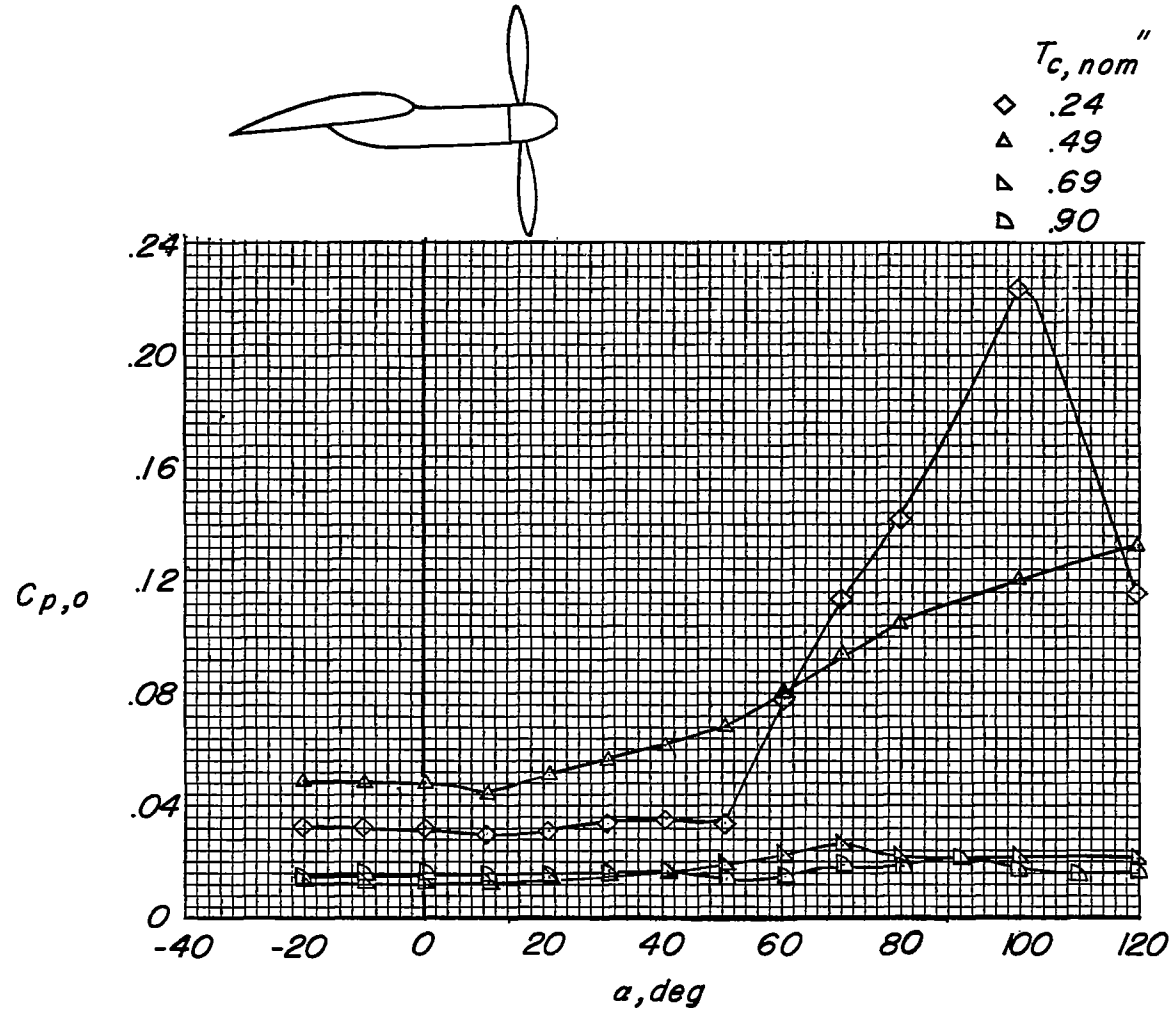

(c) Power coefficient. Outboard propeller.

Figure 17.- Continued.

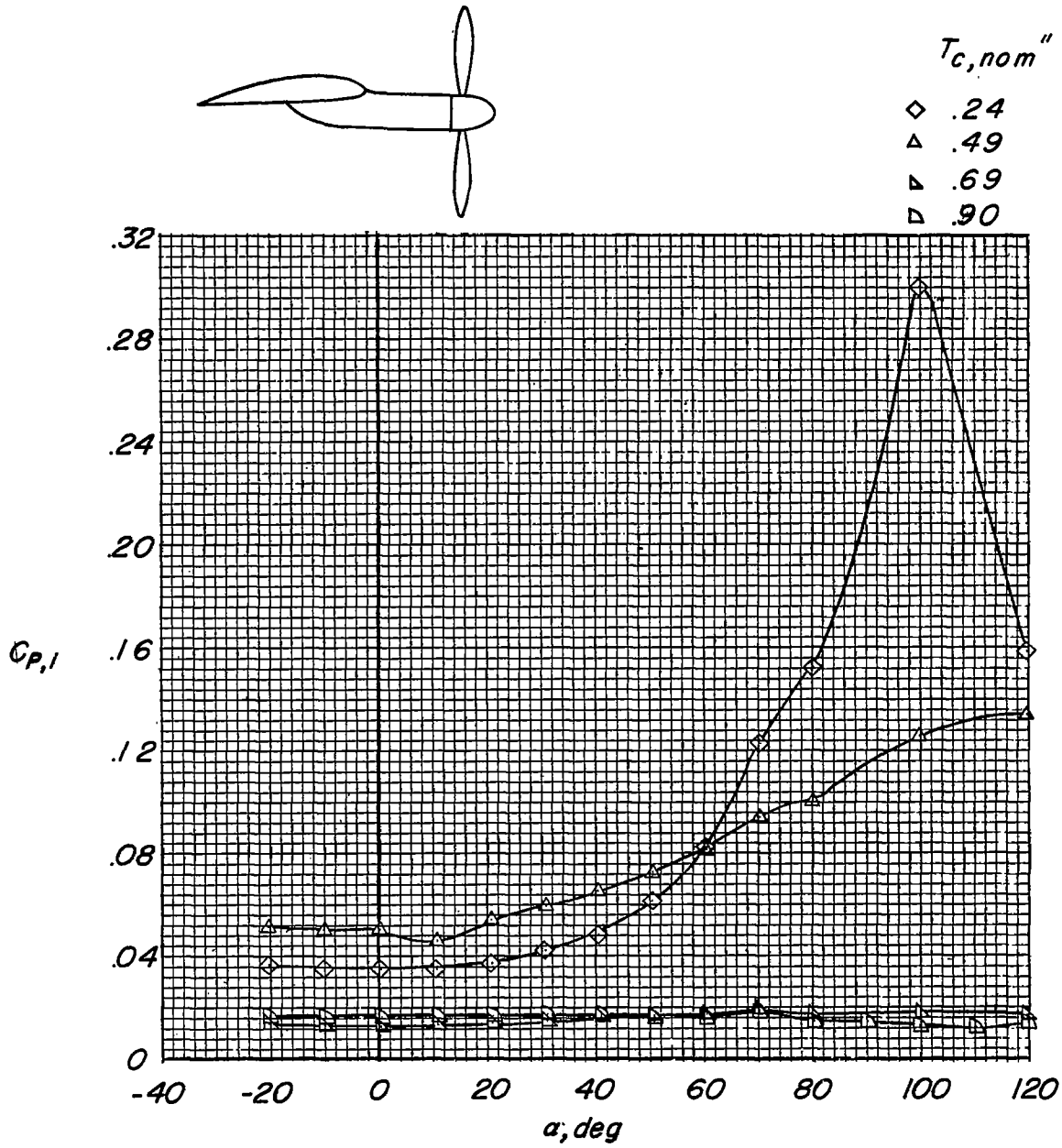

(d) Power coefficient. Inboard propeller.

Figure 17.- Continued.

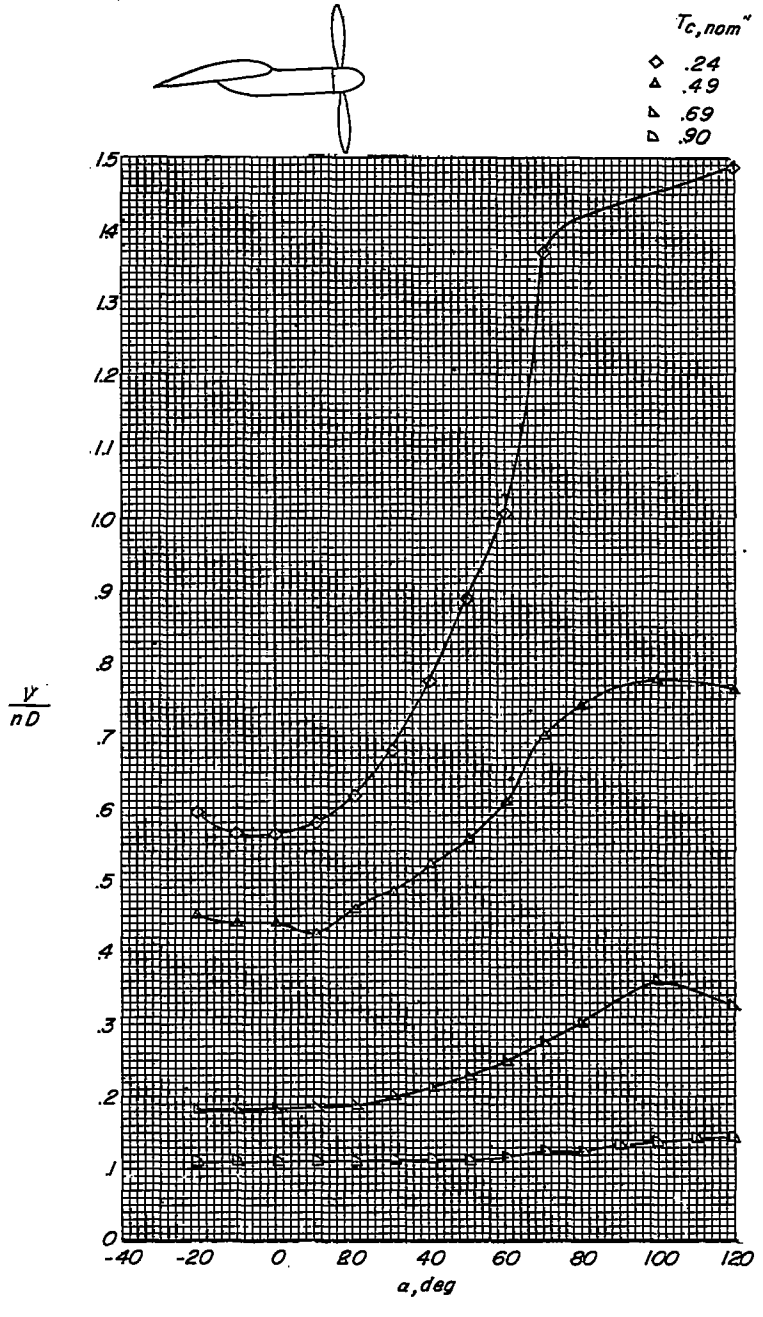

(e) Variation of V/nD with α.

Figure 17.- Concluded.

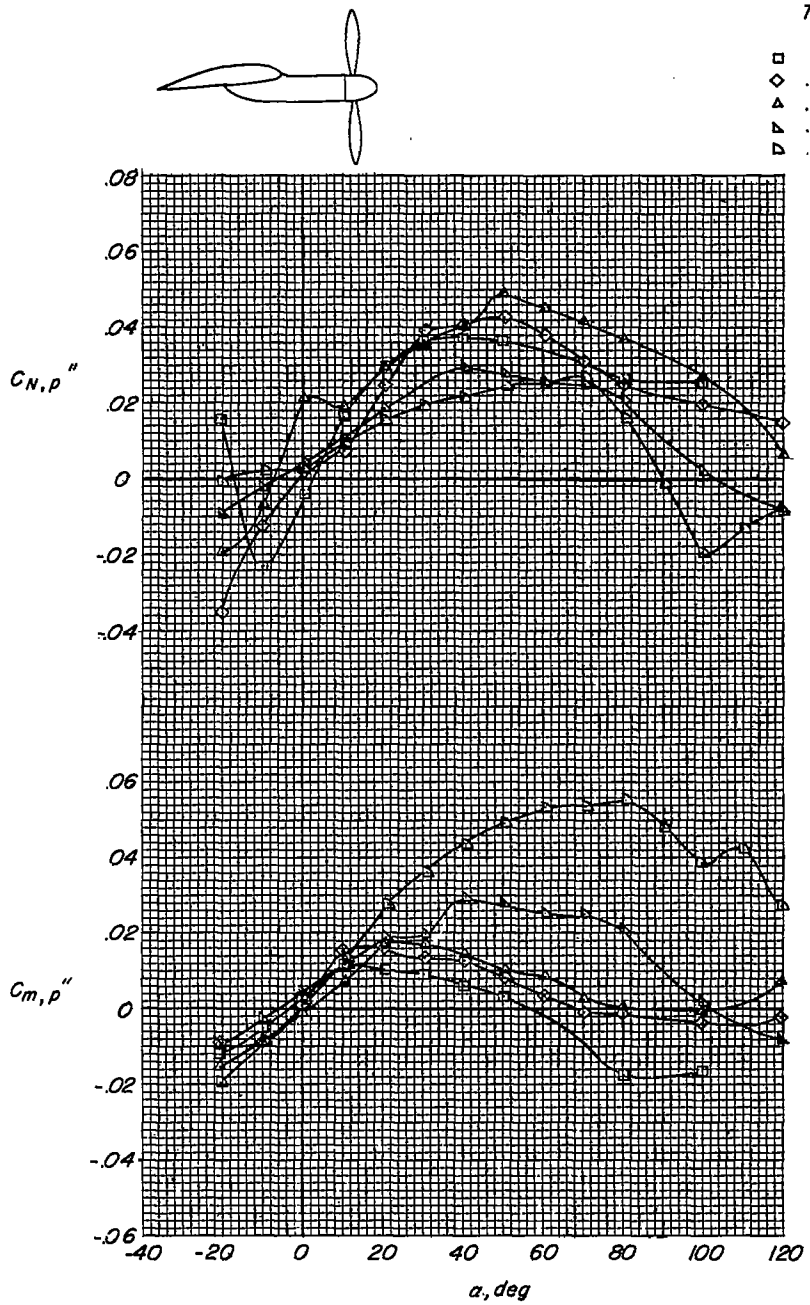

Figure 18.- Propeller normal-force and pitching-moment characteristics. Inboard propeller; $\delta_{f,30} = 0^\circ$; $\delta_{f,50} = 0^\circ$; slat off; stabilizer off.